POLITECNICO DI MILANO

DOCTORAL PROGRAM IN

"ENERGY AND NUCLEAR SCIENCE AND TECHNOLOGY"

XXVI CYCLE

Development of a Model-based approach for studying the system dynamics and control of Gen-IV Lead-cooled Fast Reactors

Supervisor:
Prof. Antonio Cammi

Tutor:
Prof. Lelio Luzzi

Chair of the Doctoral Program
Prof. Carlo Enrico Bottani

Doctoral Dissertation of:

Roberto Ponciroli

FEBRUARY 2014

Table of contents

List of Figures

List of Tables

Acknowledgements

The research activities which constitute the main focus of this thesis work have been carried out in the framework of the LEADER (Lead-cooled European Advanced DEmonstration Reactor) Project, a medium-scale LFR-focused project developed within the 7th Framework Programme "Fission 2009 – Advanced Nuclear Systems for Increased Sustainability", and financed by the European Community, in the years 2010-2013. The Politecnico di Milano was involved in the project within the Work-Package 4 "Plant Operation, instrumentation, control & protection system design". This project has led relevant benefits to my scientific and technical growth since I have had the opportunity to collaborate on the development of the ALFRED reactor, and to present the results of the work at several meetings of the European partners of the project. In particular, being the field of I&C a multidisciplinary area of research, I have had the possibility to interface with experts of neutronics, thermal-hydraulics and system designers, gaining a wide perspective about the design issues and constraints concerning this reactor concept. In this perspective, acknowledgement is due to all the experts of the participant organizations for their contributions in many different topics, in particular to Dr. Alessandro Alemberti and Dr. Luigi Mansani (Ansaldo Nucleare, Italy) for their valuable support and fruitful criticism, besides their constant and accurate monitoring over the performed investigations. In addition, I want to thank Dr. Pierre Sciora (CEA, France) and Dr. Giacomo Grasso (ENEA-Bologna, Italy) for their suggestions and explanations provided about the ALFRED reactivity coefficients, control rods operation and core design issues.

In the last part of my PhD, I have spent a period of research at Argonne National Laboratory (ANL) as Graduate Guest. I acknowledge Dr. Richard Vilim for this opportunity to collaborate with US DOE Advanced SMR researchers. Thanks to this collaboration, I have had the possibility to adopt the modelling techniques developed for ALFRED on another reactor concept, to test innovative control approaches for NPPs, and to develop a perspective about the innovative and promising sodium-cooled SMRs as well. This period was financially supported by Politecnico di Milano via the PhD grant entitled "International Mobility 2012/2013", in the frame of the Doctoral Program in "Energy and Nuclear Science and Technology – 26 cycle".

Abstract

The Lead-cooled Fast Reactor (LFR) is one of the innovative systems envisaged by the Generation IV International Forum in order to provide sustainable, safe and proliferation resistant nuclear energy production. This reactor concept offers a great potential for plant simplifications and higher operating efficiencies, introducing at the same time safety concerns and technological constraints, due to the use of lead as coolant. The subject of this thesis work is the development of an "integrated" methodological approach for the study of dynamics and the definition of suitable control strategies for LFRs, adopting ALFRED (Advanced Lead Fast Reactor European Demonstrator) as a reference reactor.

First of all, the system stability features have been characterized. The root locus method has been adopted so as to demonstrate that no problems arise in plant operation even at reduced load factors. The system stability has been assessed through the calculation of the system eigenvalues and the corresponding trajectories in the Gauss plane. In order to properly characterize the ALFRED governing dynamics, an accurate simulator representing the overall power plant, and integrable with the control system model, has been developed by adopting the object-oriented Modelica language, specifically meant to the validation of the proposed control strategies. The preliminary outcomes of the dynamics simulations have been supported by the RGA (Relative Gain Array) approach, which allows selecting the most efficient control action for each output variable. Once having finalized the control strategy, the control scheme based on feedforward-feedback regulators has been implemented. The control system architecture has been finalized by designing a procedure for the reactor start-up by means of the Petri net approach. By representing the system desired evolution through this logic-mathematical formalism, it has been possible to derive hints for the development of the control scheme, and hence to develop the supervisory control system that rules the operation of the modulating controllers and ensures achieving the power build-up. Finally, the possibility of connecting the ALFRED reactor to the electrical grid so as to perform load-frequency control has been studied. In the proposed strategy, the operation of the balance of plant has been decoupled from the primary circuit so as to meet the grid demands according to the time constants of the conventional part of the plant. As a major outcome of this work, the "integrated" methodological approach, developed for ALFRED in the thesis, reveals to be of more general interest for the Liquid Metal Fast Reactors.

1. Introduction

1.1. Background and introduction to the thesis work

The Lead-cooled Fast Reactor (LFR) is one of the six innovative systems envisaged by the Generation IV International Forum (GIF, 2002) in order to provide sustainable, safe and proliferation resistant nuclear energy production. The LFR system has excellent materials management capabilities since it operates in the fast-neutron spectrum, and employs a closed fuel cycle for efficient conversion of fertile uranium. It can also be used as an incinerator to consume actinides from spent Light Water Reactors (LWRs) fuel or as an "adiabatic reactor" (able to burn the self-generated actinide waste, see Artioli et al., 2010). Moreover, this reactor concept offers a great potential for plant simplifications and higher operating efficiencies, introducing at the same time specific features, safety concerns, design challenges, and technological constraints brought by the use of lead as coolant, different from both water-cooled reactors and other fast systems (e.g., Sodium Fast Reactors, SFRs). In particular, this reactor is characterized by a large thermal inertia and a very corrosive coolant environment that determine strict constraints on the temperature field in the power channels. Such different plant conditions and plant configurations increase the need for enhanced Instrumentation and Control (I&C) capabilities. At the present time, dedicated analyses regarding the control strategies to be applied to this reactor concept are not available in literature, and the procedures currently employed in LWRs cannot be directly adopted. Therefore, in this thesis work, the system governing dynamics of LFRs has been studied and the issues related to the definition of dedicated control strategies have been investigated.

This research activity has been carried out in the framework of an R&D collaboration with the LEADER Project (Alemberti et al., 2010) of the Euratom 7th Framework Program (FP7). The Project efforts have been mainly focused on the resolution of the key issues emerged in the frame of the previous Euratom ELSY Project to reach a new reference reactor configuration, which has been used to design a fully representative scaled-down prototype, i.e., the Advanced Lead Fast Reactor European Demonstrator (ALFRED). The demonstration ALFRED unit will be built at ICN (Institute de Cercetari Nucleare) facility near Pitesti in southern Romania, where a fuel manufacturing plant is in operation for the country two operating CANDU reactors. Construction should begin in 2017 and the unit should start operating in 2025, supplying 120 MWe to Romania electrical grid. In this perspective, the study of the LFR dynamics and a systematic analysis of its control strategy are thought to be fundamental for the midterm development of this reactor technology. The analyses and the investigations described in this thesis work and the implementation of the developed control schemes have been performed adopting ALFRED as a reference reactor configuration.

As far as the control strategy definition is concerned, besides the technological constraints, it is fundamental to account for the differences regarding the operation of the studied Lead-cooled Nuclear Power Plant (NPP). Indeed, ALFRED reactor is a Small sized Modular Reactors (SMR), whose economic competitiveness relies on plant simplification and reduced operational costs, given the disadvantage compared to traditional units in terms of economy of scale. Plant economics is significantly driven in part by plant availability, which can be enhanced by means of innovative strategies that act to avert plant or unit trips. In particular, while the traditional concept of covering base load demand was sound for large units, it is not suitable for the SMRs which are envisaged to operate cooperatively also with Renewable Energy Sources (RES), whose unsteady nature can lead to fluctuations in voltage and frequency on the grid. Therefore, without appropriate and highly reliable automated controls, such fluctuations may result in reactor trips and consequently in a worsening of the plant availability (Holcomb, 2013).

Figure 1.1. Control strategy definition road map.

As shown in the Figure 1.1, the definition of the control strategy for a nuclear reactor is a multi-phase and multi-disciplinary process whose final result is the implementation of dedicated controllers. Indeed, given that for the considered system neither prior experience nor operational data are available, before starting to build up the control system and to implement devices, it is fundamental to have an exhaustive knowledge of the system to be governed. Therefore, a model-based approach has been conceived. In this perspective, the characterization of reactor dynamics is of primary importance for the study of plant global performance and for transient design-basis

analysis since it accounts for the interactions among input and output variables, while providing useful guidelines for the conception of an appropriate control system.

First of all, it is necessary to prove the system stability and robustness not only at nominal power level but also at reduced load factors. Indeed, it is fundamental that no problems arise in operated transients, e.g., during the attainment of the full power condition or following any load variation according to the grid demands. Therefore, an analytical zero-dimensional model of the ALFRED reactor allowing for all the main system feedbacks has been developed. In order to adopt the linear analysis tools, the resulting non-linear model has been linearized and then implemented in MATLAB® (The Mathworks Inc., 2005). In this way, the reactor stability has been verified through the calculation of the system eigenvalues and the corresponding trajectories in the Gauss plane, assessing the robustness of the dynamic system on its entire power range.

Secondly, a sufficiently accurate description of the reactor and of the connected components, such as the turbines, the pumps, and the Steam Generators (SGs), turns out to be necessary. A very flexible, straightforward and fast-running dynamics simulator has been developed by employing the reliable and well-documented Modelica language (Fritzson, 2004). This approach has been specifically addressed to transient analyses, since its more realistic and detailed geometry description ensures more accurate simulations. Such a tool has been specifically conceived for predicting the reactor response to typical transient initiators, and characterizing the system dynamic behaviour. In this way, it is possible to obtain a preliminary evaluation of the inputs effectiveness on the output variables to be controlled.

Starting from the preliminary outcomes both from the stability and free dynamics analyses, the control system issue has been finally dealt with. As far as the regulator configuration is concerned, a decentralized control scheme has been considered in virtue of its simplicity in the implementation, which favours Operation and Maintenance (O&M) of controllers. Given that for the considered system it is not possible to employ the procedure currently adopted in LWRs, dedicated quantitative techniques, which allows developing the most efficient control strategy starting from the constitutive equations that describe the physical system taken into account, have been employed. Therefore, coupling between the control and the controlled variables has been carried out by means of the RGA (Relative Gain Array) method. As far the implemented controllers are concerned, classical feedback regulators have been employed. The regulator parameters have been tuned so as to ensure a sufficient robustness to the control scheme. In this way, the controllers can operate in a wide power range, even very far from nominal conditions. The designed linear control scheme has been tested by simulating controlled operational transients on the Modelica-based simulator, which

has been used both for the realization of the control system and the assessment of the proposed control system.

After having developed a control strategy for the full power mode of the ALFRED reactor, the problem of the reactor start-up has been studied, laying the basis for the preliminary version of the control system architecture. The definition of a viable start-up procedure for a Generation-IV reactor, for which no operational experience is available, may turn out to be quite difficult. In particular, this applies to a LFR demonstrator, which requires dedicated technological solutions with respect to the better-known systems cooled by sodium or water. A synchronization of the different control actions to be taken on the overall plant is then required. For this reason, it has been decided to adopt a formalism widely used in industrial automation as the Petri nets. Generally, the start-up procedure of a NPP is characterized by listing the sequence of operations to be performed. Such a description does not facilitate the coordination of different activities in parallel and does not allow focusing on the key events that rule the switches among the involved controllers. On the other hand, the application of the logical-mathematical approach of Petri nets to describe the reactor start-up procedure has allowed defining the different steps to be taken, and to point out the necessary system conditions so that the scheduled control actions can be performed.

Since the ALFRED reactor constitutes a demonstrator for LFR feasibility, the issue of the load-frequency control (i.e., the operational procedure thanks to which the NPP manage to meet the load demands by modulating the active power production) has been investigated. Therefore, the possibility of connecting the ALFRED reactor to the electrical grid so as to perform automatic generation control in reaction to frequency deviations has been studied. Such aspects are particularly important in view of the increasingly relevant fraction of power plants based on RES. In the perspective of achieving the plant operational flexibility, it has been tried to adapt the procedure employed in PWRs, namely the *reactor follows*. However, because of the time constants ruling the primary circuit dynamics, it has been necessary to decouple the operation of the primary circuit and the Balance of Plant. In this way, it has been possible to meet the grid demands according to the time constants of the conventional part of the plant so as to fulfil the requirements of the primary frequency regulation.

The different steps describing the analysis performed in the definition of an effective control strategy for a LFR constitute an integrated model-based methodological approach. As a major outcome of the work, the developed procedure has the advantage of not being tailored to the ALFRED reactor but it can be extended to other LFR reactor designs or other advanced SMR concepts as well. Indeed, the modelling tools adopted in the thesis work have been employed to the study of the fast-runback operational transient for a Sodium-cooled SMR. Therefore, even though

the features of the studied reactor concept are totally different from the ALFRED reactor ones, the proposed investigation procedure has turned out to be very effective, demonstrating its validity and versatility.

1.2. ALFRED reactor configuration

In this section, the reactor configuration and the parameters employed in this work have been summarized. ALFRED is a small-size (300 MW_{th}) pool-type LFR. Its primary system configuration is depicted in Figure 1.2. All the primary components (e.g., the core, the pumps in the primary circuit and the SGs) are contained within the main reactor vessel, being located in a large lead pool inside the reactor tank. The coolant flow coming from the cold pool enters the core and, once passed through the latter, is collected in a volume (hot collector) to be distributed to eight parallel pipes and delivered to as many SGs. After leaving the SGs, the coolant enters the cold pool through the cold leg and returns to the core.

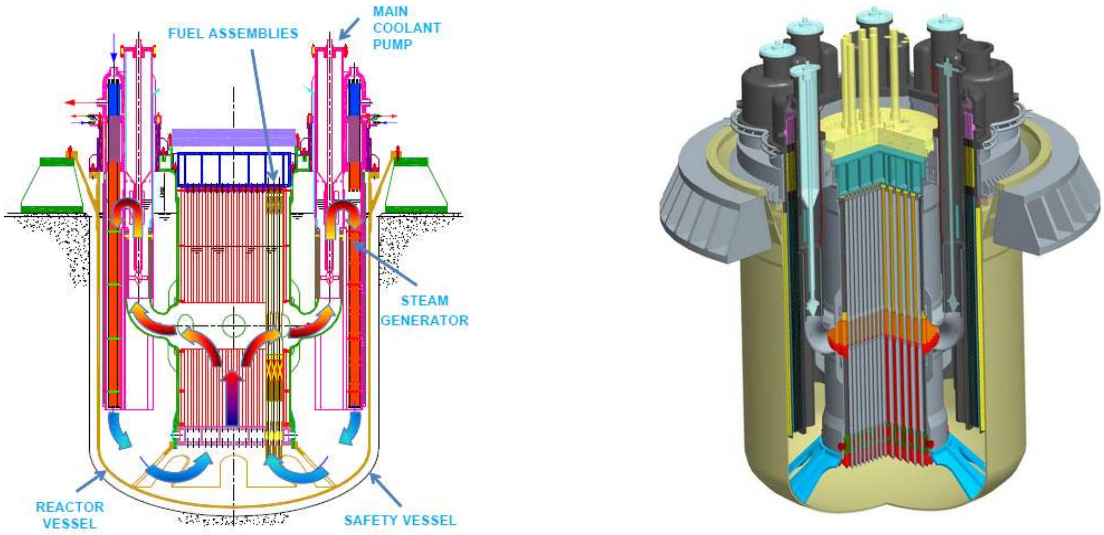

Figure 1.2. ALFRED primary system (Alemberti et al., 2013).

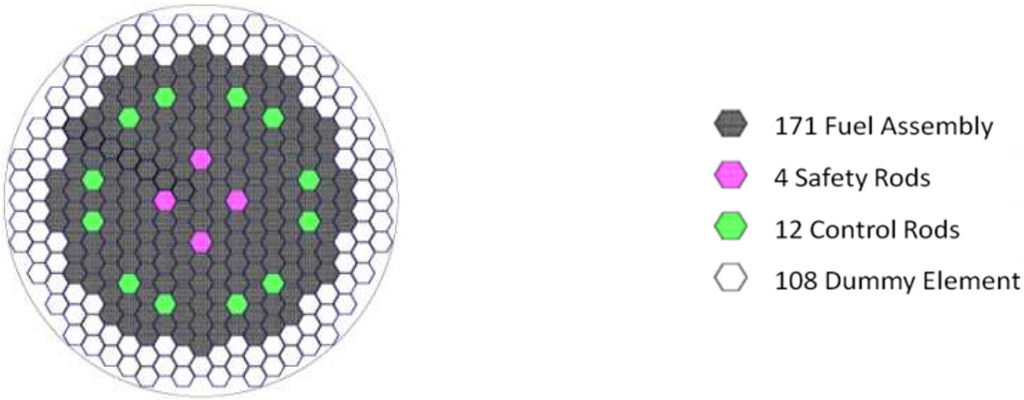

Figure 1.3. ALFRED core layout (Alemberti et al., 2013; Grasso et al., 2013).

The ALFRED core (Figure 1.3) is composed by wrapped hexagonal Fuel Assemblies (FAs) with pins arranged on a triangular lattice (Alemberti et al., 2013). The 171 FAs are subdivided into two radial zones with different plutonium enrichment guaranteeing an effective power flattening, and surrounded by two rows of dummy elements (geometrically identical to the fuel assemblies but not producing thermal power) serving as reflector. Two different and independent control rod systems have been foreseen, namely the Control Rods (CRs) and the Safety Rods (SRs). Power regulation and reactivity swing compensation during the cycle are performed by the former, while the simultaneous use of both is foreseen for scram purposes, assuring the required reliability for a safe shutdown (Grasso et al., 2013). In Table 1.1, the major preliminary nominal parameters employed are presented.

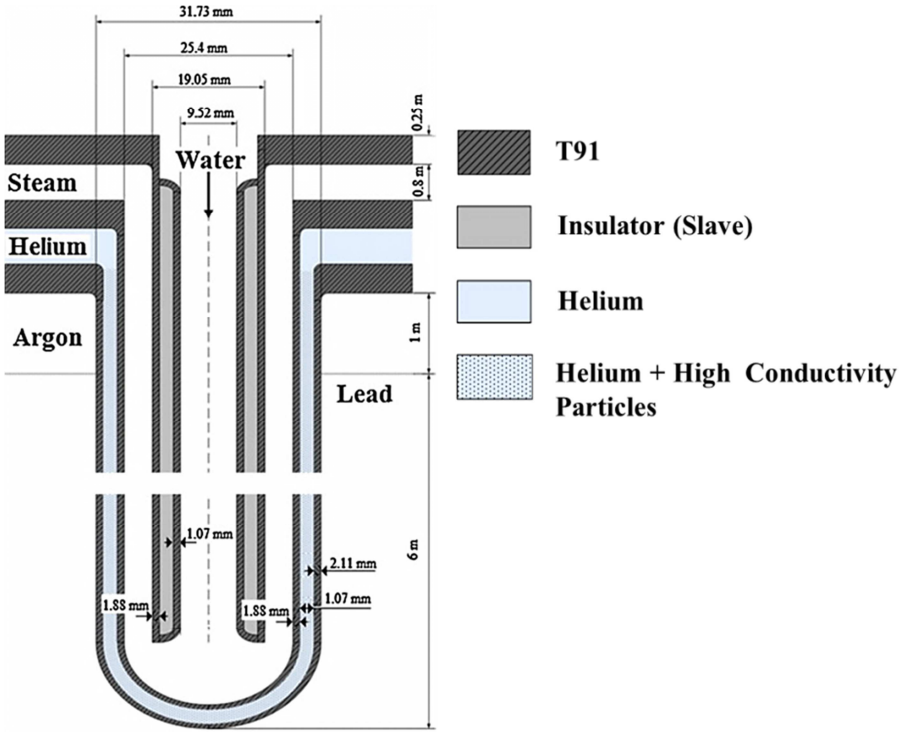

Figure 1.4. ALFRED SG bayonet tube configuration (Alemberti et al., 2013; Damiani et al., 2013).

Each of the eight SGs incorporated in ALFRED (Figure 1.4) consists in bundles of bayonet vertical tubes with external safety tube and internal insulating layer (delimited by a slave tube), which is aimed at ensuring the production of superheated dry steam, since, without a proper insulation, the high temperature difference between the rising steam and the descending feedwater promotes steam condensation in the upper part of the SG (Alemberti et al., 2013). The gap between the outermost and the outer bayonet tube provides mechanical decoupling between the components, and is filled with pressurized helium and high thermal conductivity particles to enhance the heat exchange capability (Damiani et al., 2013). The feedwater from dedicated headers flows in the slave tube and, after reversing the motion at the bottom, rises along the annulus between inner and outer

tubes. On the primary side, lead flows downwards axially along the outermost tube. In Table 1.2, the main SG parameters and specifications are listed.[1]

Table 1.1. ALFRED preliminary core parameters (Alemberti et al., 2013; Grasso et al., 2013).

Parameter	**Value**		**Units**
Core			
Thermal power	300		MW_{th}
Coolant mass flow rate	25,984		kg s^{-1}
Total number of FAs	171		-
Pins per FA	127		-
Coolant inlet temperature	400		°C
Coolant outlet temperature	480		°C
Fuel pin			
Fuel type	MOX		-
Average enrichment as Pu/(Pu+U)	25.77		wt%
Cladding material	Ti 15-15		-
Fill gas	He		-
Pin pitch	$13.86 \cdot 10^{-3}$		m
Cladding outer radius	$5.25 \cdot 10^{-3}$		m
Cladding inner radius	$4.65 \cdot 10^{-3}$		m
Pellet outer radius	$4.50 \cdot 10^{-3}$		m
Pellet inner radius	$1.00 \cdot 10^{-3}$		m
Active height	0.6		m
Reactivity and kinetics coefficients	*BoC*	*EoC*	
Doppler constant	-555	-566	pcm
Lead expansion coefficient	-0.271	-0.268	pcm K^{-1}
Axial clad expansion	0.037	0.039	pcm K^{-1}
Axial wrapper tube expansion	0.022	0.023	pcm K^{-1}
Radial clad expansion	0.008	0.011	pcm K^{-1}
Radial wrapper tube expansion	0.002	0.003	pcm K^{-1}
Axial fuel expansion (linked case)	-0.232	-0.242	pcm K^{-1}
Diagrid expansion	-0.147	-0.152	pcm K^{-1}
Pad expansion	-0.415	-0.430	pcm K^{-1}
Mean Neutron Generation time	$6.116 \cdot 10^{-7}$	$6.296 \cdot 10^{-7}$	s
Delayed neutron fraction	336	335	pcm

[1] The SGs constitute the interface of the primary circuit to the conventional part of the ALFRED reactor, i.e., the Balance of Plant (BoP) designed to implement a Rankine power cycle. As far as its layout is concerned, the design has not been finalized yet. Therefore, in this thesis work, the geometrical and operational data concerning the components downstream the SGs have been taken from a reference configuration, which is expected to be close to the ALFRED layout (Empresarios Agrupados, 2012).

Table 1.2. ALFRED SG major nominal parameter (Alemberti et al., 2013; Damiani et al., 2013).

Parameter	**Value**		**Units**
Single SG parameter			
Power	37.5		MW
Feedwater inlet temperature	335		°C
Steam outlet temperature	450		°C
Steam pressure	180		bar
Length of heat exchange	6		m
Number of tubes	510		-
	Outer diameter	*Thickness*	
Slave tube	$9.52 \cdot 10^{-3}$	$1.07 \cdot 10^{-3}$	m
Inner tube	$19.05 \cdot 10^{-3}$	$1.88 \cdot 10^{-3}$	m
Outer tube	$25.40 \cdot 10^{-3}$	$1.88 \cdot 10^{-3}$	m
Outermost tube	$31.75 \cdot 10^{-3}$	$2.11 \cdot 10^{-3}$	m

2. Governing dynamics and stability analysis

Outline

In the development of an innovative reactor concept, the characterization of the governing dynamics is of primary importance for the study of plant global performance, and for transient design-basis analysis since it accounts for the interactions among input and output variables. As first step, it is necessary to prove the system stability and robustness not only at nominal power level but also at reduced load factors. Therefore, an analytical zero-dimensional model of the ALFRED reactor has been developed. The model incorporates a neutronics description based on point-wise kinetics coupled with a single-channel, average-temperature heat transfer treatment for thermal-hydraulics. It also includes a simplified approach for the simulation of the reactor primary circuit with characteristic time delays and power exchange at the SG. The resulting non-linear model has been linearized so as to verify the reactor stability through the calculation of the system eigenvalues and the corresponding trajectories in the Gauss plane.
In addition, the impact of a fundamental parameter such as the coolant density feedback reactivity coefficient on the system stability has been evaluated by considering both the stand-alone core and the primary circuit configuration. In particular, a dedicated sensitivity analysis has been carried out, thanks to which the fundamental roots of the system have been parameterized as function of the values assumed by the considered reactivity feedback coefficient. In this way, it has been possible to assess how the system stability features change according to the variations of this parameter. In common practice, the reactor control system is developed once the reactor design has been finalized. Otherwise, it would be beneficial that the dynamic response features could be allowed for in the preliminary design procedure. For this purpose, it has been demonstrated that it is possible to obtain for the system key-parameters the admissible range within which they may vary. In this way, it is possible to provide indications to the designers on the optimal system configuration from a control-oriented perspective.

The main results have been published in:

- Bortot, S., Cammi, A., Lorenzi, S., Ponciroli, R., Della Bona, A., Juarez, N.B., 2013. Dynamics and a stability analyses of the European LFR Demonstrator. In: Nuclear Engineering and Design, **265**, 1238-1245.

Introduction

In the development of an innovative reactor concept, the characterization of reactor dynamics is of primary importance for the study of plant global performance, and for transient design-basis analyses since it accounts for the interactions among input and output variables. As first step, it is necessary to prove system stability and robustness not only at nominal power level but also at reduced load factors. Indeed, it is important that no problem arise in currently operated transients (e.g., during the attainment of the full power condition or following any change of load according to the grid demands). In this sense, an analytical treatment of the problem has been opted for by adopting a lumped-parameter simulator based on a system of ODEs (Ordinary Differential Equations). Such a tool has been specifically conceived for evaluating the stability and the robustness of the dynamic system itself on its entire power range thanks to the possibility of linearizing the constitutive equations around different operating conditions. Indeed, the root locus tool has been adopted, so as to express the value of the system eigenvalues as function of the power level. Besides studying the system stability over the operational range, the impact of a neutronics parameter (i.e., the reactivity feedback bond to the lead density) on the system dynamic response has been investigated by considering both a stand-alone core and a closed primary circuit configuration.

2.1. Model development

The analytical model is composed of different subsystems describing the core dynamics (i.e., neutronics, thermal-hydraulics and reactivity), and dedicated blocks representing the SG and the delays related to the hot collectors and the cold pool. In the following, each model with the respective equations employed has been briefly described.

2.1.1. Neutronics

Pointwise kinetics model with one neutron energy group and eight delayed neutron precursor groups has been employed for the core neutronics model, in which the total power is considered as generated only by fission events while the contribution of decay heat being neglected (Hetrick, 1971)

$$\begin{cases} \dfrac{dn}{dt} = \dfrac{\rho - \beta}{\Lambda} n + \displaystyle\sum_{i=1}^{8} \lambda_i c_i + s \\ \dfrac{dc_i}{dt} = \dfrac{\beta_i}{\Lambda} n - \lambda_i c_i \qquad i = 1, \dots, 8 \end{cases} \tag{2.1}$$

The system equation (2.1) represents nine ODEs, i.e., one nonlinear equation for neutron density and eight linear ones for precursor densities. In the present model, a further simplified version has been adopted, in which all the precursor groups have been collapsed into a unique one by means of an abundance-weighted average decay constant (Duderstadt, 1976).

$$\frac{1}{\lambda} = \frac{1}{\beta}\sum_{i=1}^{8}\frac{\beta_i}{\lambda_i} \tag{2.2}$$

2.1.2. Thermal-hydraulics

A zero-dimensional approach has been adopted to describe the system thermal-hydraulics as well. Some simplifying hypotheses have been assumed and a single-node heat transfer model has been implemented by accounting of three distinct temperature regions– corresponding to fuel, coolant and cladding – enabling the reactivity feedback to include all the major contributions as well as the margin against technological limits to be monitored. A separate, multi-zone pin model accounting of the temperature distribution from the fuel centerline to the coolant bulk has been employed to evaluate global heat transfer coefficients, by assuming physical properties and thermal resistances of fuel, gap and cladding to be constant with temperature and time, and neglecting thermal diffusion in the axial direction within the fuel pin. As far as the dynamic variation of the fuel internal and external temperatures is concerned, the heat transfer process has been achieved by taking an energy balance over two fuel zones:

$$M_{f,int}C_f\frac{dT_f{}^{int}(t)}{dt} = q_{int}(t) - k_f(T_f{}^{int}(t) - T_f{}^{ext}(t)) \tag{2.3}$$

$$M_{f,ext}C_f\frac{dT_f{}^{ext}(t)}{dt} = q_{ext}(t) + k_f(T_f{}^{int}(t) - T_f{}^{ext}(t)) - k_{fc}(T_f{}^{ext}(t) - T_c(t)) \tag{2.4}$$

where the fission power generated within the fuel is calculated according to Eq. (2.5) in which the subscript *0* refers to steady-state values, and is treated as an input for the heat transfer dynamic model:

$$n(t)/n_0 = q(t)/q_0 \tag{2.5}$$

As far as the gradient of the cladding surface temperature is concerned, the following energy balance has been applied:

$$M_cC_c\frac{dT_c(t)}{dt} = k_{fc}(T_f{}^{ext}(t) - T_c(t)) - h_{cl}\big(T_c(t) - T_{out}(t)\big) \tag{2.6}$$

Finally, for the energy balance equation within the coolant, the respective temperature at the end of the channel has been assumed as a state variable. Since the coolant inlet temperature has been regarded as a fixed input, the energy balance has been written as:

$$M_l C_l \frac{dT_{out}(t)}{dt} = h_{cl}\big(T_c(t) - T_{out}(t)\big) - \Gamma C_l\big(T_{out}(t) - T_{in}(t)\big) \tag{2.7}$$

Calculations of material properties have been performed in correspondence with the average nominal steady-state temperatures and the parameters obtained have been kept constant for the stability analysis.

2.1.3. Reactivity

Consistently with the lumped-parameter model employed, the reactivity feedbacks have been expressed as functions of the average values of fuel and coolant temperature fields. Moreover, externally induced reactivity has been simulated through a dedicated coefficient associated with the insertion length of a representative control rod, which has been treated as a simple input parameter.

Reactivity effects by coolant density variations, axial and radial expansions, and control rod motion have been accounted by adopting a linear equation with constant coefficients. In particular, axial expansion has been related to the fuel thermal conditions, whereas radial expansion has been considered as governed by the average lead temperature as well as the coolant density feedback.
As far as the Doppler coefficient determination is concerned, an effective average fuel temperature that accounts for resonances broadening, has been calculated at each power level (ranging from 30% to 100%) as indicated by Kozlowski and Downar (2007).

$$T_f{}^{eff} = 0.3 \cdot T_f{}^{int} + 0.7 \cdot T_f{}^{ext} \tag{2.8}$$

where $T_f{}^{int}$ and $T_f{}^{ext}$ indicate the internal and external surface fuel temperatures respectively. The magnitude of the reactivity variation from a generic fuel temperature distribution T_{f1} (with effective average $T_{f1}{}^{eff}$) to a fuel temperature distribution T_{f2} (with effective average $T_{f2}{}^{eff}$) around the steady-state value (Waltar et al., 2011) has been evaluated by

$$\Delta\rho\left[T_{f1} \rightarrow T_{f2}\right] \approx 1.1 \cdot K_D \left(ln \frac{T_{f2}{}^{eff}}{T_{f1}{}^{eff}} \right) \tag{2.9}$$

Therefore, the Doppler coefficient has been defined at each power level as

$$\alpha_D[pcm\ K^{-1}] = \frac{\Delta\rho\left[T_{f1} \rightarrow T_{f2}\right]}{T_{f2}{}^{eff} - T_{f1}{}^{eff}} \tag{2.10}$$

In this work, a linear relation for core expansions (axial and radial) and coolant density reactivity effects has been adopted, leading to the following expression incorporating constant coefficients:

$$\rho = \rho_0 + \alpha_D \cdot \left({T_f}^{eff} - {T_{f,0}}^{eff}\right) + \alpha_Z \cdot \left(T_f - T_{f0}\right) + \alpha_L \cdot \left(T_l - T_{l,0}\right) + \alpha_R \cdot \left(T_l - T_{l,0}\right) + \alpha_H \cdot (H - H_0) \tag{2.11}$$

where stationary average temperatures have been calculated in correspondence with each power level considered. The terms in Eq. (2.11) indicates the reactivity margin stored in the core, the feedbacks induced by fuel temperature changes (i.e., Doppler effect and axial expansion, respectively), the effect due to the coolant temperature variations (i.e., lead density and radial expansion, respectively), and the externally-induced reactivity, respectively.

2.1.4. Primary circuit modelling

In order to evaluate the system stability features when considering the entire primary circuit configuration, a simplified treatment has been adopted to describe the coolant flowing toward the SG after being heated in the core, being cooled while passing through the SG and coming back to the core through the cold pool. In particular, in order to account for the time constants of the system, suitable time delays have been introduced. The power exchange at the SG has been modelled by incorporating an equivalent exchange unit and taking an energy balance as follows:

$$\frac{dT_{l,in\,SG}}{dt} = -\frac{1}{\tau_{HL}} T_{l,in\,SG} + \frac{1}{\tau_{HL}} T_l \tag{2.12}$$

$$\frac{dT_{l,out\,SG}}{dt} = \frac{\Gamma C_l - K_{eq}}{M_{eq} C_{eq}} T_{l,in\,SG} - \frac{\Gamma}{M_{eq}} T_{l,out\,SG} + \frac{K_{eq}}{M_{eq} C_{eq}} T_{sat} \tag{2.13}$$

More specifically, the SG has been modelled so that in nominal conditions the difference between core outlet and inlet coolant temperature is equal to the nominal value (80 °C), whereas in ideal heat exchange conditions the cold leg temperature is kept constant and equal to the saturation temperature of the secondary loop, which depends only on SG pressure, regardless of the power produced in the core. In such a system, the coolant core inlet temperature is no longer an input variable, but a state variable determined by the heat transfer conditions at the SG interface:

$$\frac{dT_{in}}{dt} = -\frac{1}{\tau_{CL}} T_{in} + \frac{1}{\tau_{CL}} T_{l,out\,SG} \tag{2.14}$$

On the other hand, when “ideal heat transfer conditions” are considered, the SG is assumed to be able to remove any power produced in the core, thus keeping the lead temperature in the cold leg always close to the nominal value (i.e., 400 °C).

Table 2.1. Primary circuit characteristic time delays.

Parameter	Value	Units
Coolant flowing time (hot leg)	10	s
Coolant flowing time (SG)	10	s
Coolant flowing time (cold leg and pool)	60	s

2.2. Stability analysis

The analytical zero-dimensional model has been simplified and linearized so as to enable the use of the linear stability theory to study the reactor behaviour over the entire power range at different conditions through calculation of the system eigenvalues (Lyapunov, 1966). The stability analysis has been carried out both for the stand-alone core and the overall primary circuit configuration. Moreover, the impact of the coolant density reactivity coefficient on stability has been evaluated. Such a study has been meant to provide the reactor designer with quantitative feedbacks concerning this key parameter from a safety-oriented perspective. Indeed, being the coefficient tightly dependent on the core arrangement, in terms of both geometrical and material buckling, it is expected that significant differences may occur between the demonstrator and the industrial scale LFR, with consequent impact on the plant dynamics. Therefore, the system stability has been investigated against the lead density reactivity coefficient value in order to assess a theoretical threshold making the reactor unstable, so that the core designer can adopt suitable provisions to ensure the reactor operates under stable conditions in any frame. Finally, in order to evaluate the dynamic characteristics of the system as a function of the core lifetime, calculations have been carried out at BoC (Beginning of Cycle) and EoC (End of Cycle), so as to evaluate the effects of the fuel burn-up.

2.2.1. Method

According to the linear analysis theory, the dynamic behaviour of a linear system depends on the eigenvalues of the state matrix. This principle is still applicable to the linearization of a non-linear system around a certain steady-state condition, given that the imposed are either small or slow compared with the local dynamics. Thus, such linearization has been performed on the set of equations reported in Section 2.1 and it has been possible to express the model in terms of the following matrix system:

$$\begin{cases} \dot{x} = \underline{\underline{A}}x + \underline{\underline{B}}u \\ y = \underline{\underline{C}}x + \underline{\underline{D}}u \end{cases} \tag{2.15}$$

where x is the vector of the state variables, u the input vector, y the output vector, $\underline{\underline{A}}$ the state matrix, $\underline{\underline{B}}$ and $\underline{\underline{C}}$ the corresponding matrices, and $\underline{\underline{D}}$ is an empty matrix since there is no feedthrough between input and output. This allows focusing on the state matrix $\underline{\underline{A}}$ and its eigenvalues which represent the carriers of the dynamic response of the system; the latter, alternatively defined as poles or roots of the system, have been calculated through proper MATLAB® scripts. The position of the poles and their trajectories across the Gauss plane describe the reactor dynamic behaviour. In order for the system to be stable, it is necessary that all poles remain in the left hand side of the plane in any operating condition and following any perturbation of the nominal parameters as discussed in the following case studies.

2.2.2. Lead density reactivity feedback coefficient

The reactivity feedback associated to the coolant density variations is a particularly challenging design parameter for Fast Reactor concepts, especially SFRs. Indeed, reduction of coolant density may lead to relevant positive reactivity insertion, which constitute a serious safety concern. In this perspective, innovative approaches to the core design have mainly focused on limiting the sodium void effect (Sciora et al., 2013). As far as LFR are concerned, in virtue of the higher boiling point of the coolant, such a problem does not constitute a pressing issue. However, having a positive global variation of the reactivity due to the coolant expansion is a problem for safe reactor operation. Therefore, the system stability has been investigated, evaluating the trajectories of the roots at different values of this parameter. The reactivity feedback of coolant density can be evaluated as the reactivity change following a coolant temperature variation:

$$\alpha_L = \frac{\partial \rho}{\partial T_l} \tag{2.16}$$

The coolant temperature increase involves a decrease of its density, and so a decrease of the interactions between neutrons and coolant nucleus. It involves a spectral effect (positive), an effect due to the leakages (negative) and an effect bound to the captures (positive).

Spectral effect

The main physical phenomenon following a coolant density decrease is a spectral hardening due to the decrease of the coolant interactions. It implies effects mostly on fuel, for which the dominant one is the increase of fission probability p_F.

$$p_F = \frac{\Sigma_f \phi}{\Sigma_a^{tot} \phi + F} = \frac{\Sigma_f \phi}{\Sigma_f^{fuel} \phi + \Sigma_c^{fuel} \phi + \Sigma_c^{mat} \phi + F} \tag{2.17}$$

where Σ_f^{fuel} and Σ_c^{fuel} are the capture and fission cross sections occurring in the fuel, Σ_c^{mat} is the absorption cross section in the structural materials and F is the neutron leakage term. The predominant contributions are due to even isotopes, among which ^{238}U plays a major role (even-even isotope), because of their fission cross section high sensitivity to spectral hardening (threshold reactions), despite their modest absolute contribution to the total fissions. Since fission and capture rates depend on neutron flux, the major contribution appears in the inner core zone, decreasing toward the border of the active core, to become almost null in the external zone (Lorenzi, 2011). Therefore, as a consequence of the faster spectrum, the reactivity increases.

Effect bound to the leakages

As there are less interactions with the coolant, there are more available neutrons, and they are more energetic. Although the interaction and absorption probability function of the incoming neutrons energy depends on each isotope, it generally decreases with energy. Therefore, a significant relative increase in leakage probability is observed after a reduction of coolant density. In diffusion theory, leakage can be written as:

$$F = D\nabla^2\phi = \frac{1}{3\Sigma_s}\nabla^2\phi = \frac{1}{3N_l\sigma_s}\nabla^2\phi \tag{2.18}$$

In particular the system is more transparent after a density reduction, so that neutrons can escape more efficiently because of a macroscopic absorption cross section global diminution. This is determined by a decrease of both material density (lack of coolant) and microscopic absorption cross section: neutrons interact with less atoms in the core and less efficiently as well, in absolute terms. It is interesting to note from Eq. (2.18) that the leakage term is strongly dependent on the spatial coordinate through the flux gradient, i.e., in the inner zone of the reactor, the gradient is low and the contribution to leakage is minimum, otherwise in peripheral zones the derivative is high and leakages are relevant.

Capture effect

The decrease of the coolant interactions involves a decrease of the capture by the coolant isotope and so an increase of the available neutrons. This positive effect is however weak. The variation of the core reactivity depends on the competition between these three effects. In case of Fast Reactors, the global variation of the reactivity due to the coolant expansion is generally positive. In ALFRED reactor, the dominant contribution is represented by the leakage term,

whereas the positive ones are less important due to the small dimensions of the reactor. For the calculation of the coolant density coefficient, the entire system has been considered (active core with axial reflector (Sciora, 2011)). The reactivity coefficient remains negative even when considering only the active zone. In larger reactors, such as ELSY, the coefficient is positive when considering a density reduction only in active zone, and slightly negative if the calculations are made on the entire core.

2.2.3. Results

Six different conditions have been considered to draw the roots of the system. First of all, the stand-alone core configuration has been studied, in this case the inlet temperature is considered as a fixed input. In this condition, three major cases have been analysed:

a) power level ranging between zero power and full nominal power at BoC;
b) power level ranging between zero power and full nominal power at EoC;
c) parametric variation of the lead density reactivity coefficient on the entire power range at BoC.

Secondly, the simplified primary system configuration has allowed for, and the effects of closing the loop on stability have been assessed. Similarly to the stand-alone core study, three cases have been considered:

a) power level ranging between zero power and full nominal power at BoC with SG at nominal conditions;
b) power level ranging between zero power and full nominal power at BoC with SG at ideal heat exchange conditions;
c) parametric variation of the lead density reactivity coefficient on the entire power range at BoC with SG at nominal conditions.

Reactor configuration, input data and parameters adopted for the core and SG modelling are resumed in Table 1.1 and Table 1.2.

Stand-alone core analysis

A stand-alone core analysis has been carried out aimed at assessing the core system stability at different power levels at BoC conditions. In particular, the neutronics block has been treated as the open loop, whereas the thermal-hydraulics coupling with its reactivity coefficients constitutes the feedback loop (Figure 2.1).

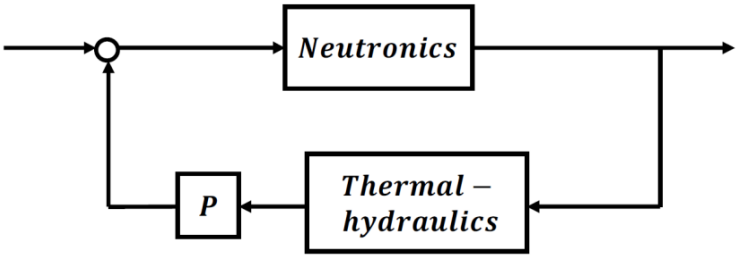

Figure 2.1. Conceptual scheme employed to describe the stand-alone core behaviour.

A 13th order system has been obtained by implementing equations described in Sections 2.1.1, 2.1.2 and 2.1.3. A four roots system has been derived after simplification and linearization, collapsing the neutron precursors groups into a single one whose decay constant is provided by Eq. (2.2), whereas the cladding dynamics has not allowed for.

Observing the roots trajectories as function of the operating power level, it can be seen that all the system roots lay on the left hand side of the Gauss plane, confirming that the core is stable on the entire power range[2]. In particular, the neutronics-related pole is located in the origin when the reactor is at zero power conditions and, because of the increasing effect of the temperature-induced reactivity feedbacks, moves to the left as the power rises, granting a higher margin of stability to the system. At a certain power level, the dominant poles become complex conjugated (Figure 2.2) indicating that power fluctuations begin occurring. In particular, the imaginary part of the poles increases along with the rising power level meaning that the frequency of the oscillations increases too. Despite the increase of the imaginary part of the poles, the magnitude of the real negative part grants the damping of such oscillations. This trend ensues from the fact that in the linearized model the gain of the thermal feedback is proportional to the power level. Thus, for equal variations of reactivity, the oscillation frequency grows as the power increases.

An analogous behaviour is found at EoC, whose root locus is shown on the right side of Figure 2.2. In this case, the core exhibits the same stability characteristics at BoC, coherently with the very slight differences between the respective reactivity coefficients and kinetic parameters. As a consequence of such minor discrepancies, it can be concluded that the influence of the fuel burn-up is definitely negligible as far as the system stability is concerned.

[2] Poles at -4700 rad s^{-1} and -2.5 rad s^{-1} are not shown and discussed in this analysis since they do not change their position significantly with varying power and lead coefficient, resulting in an almost constant contribution to the system behaviour.

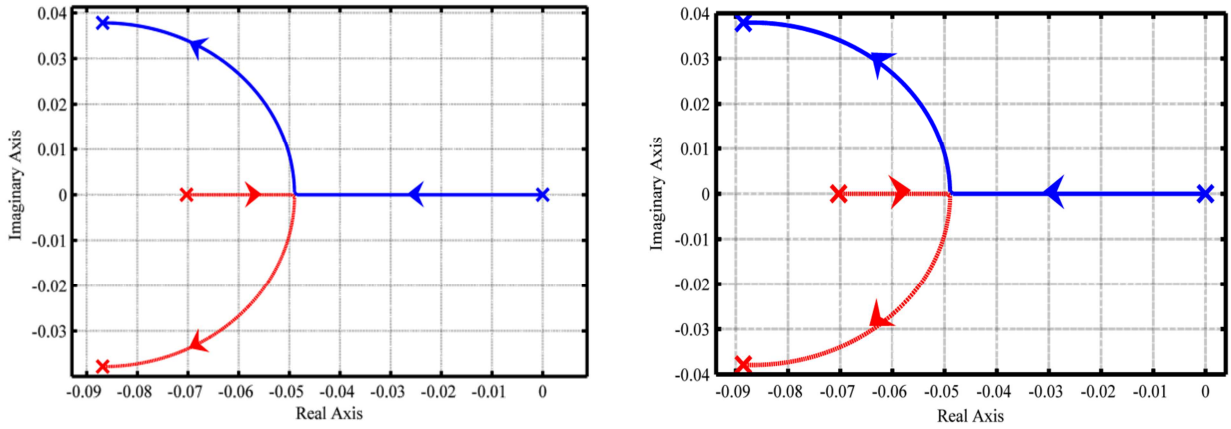

(a) (b)

Figure 2.2. Root locus detailed view for the core as a function of power level (a) at BoC and (b) at EoC.

Furthermore, the core system stability has been investigated when the coolant density reactivity coefficient (indicated as α_L) parametrically varies from its nominal value to large positive figures so as to determine a critical threshold causing the system to be unstable. As shown in Figure 2.3 and Figure 2.4, the blue track represents the poles trajectory as a function of power level (from 0 to 300 MW_{th}) with α_L kept constant at its nominal value. The red lines represent the poles trajectories evaluated at discrete power levels (from 30% to nominal power, with 10% steps) as a function of α_L continuously varying from 0 to 12 $pcm \cdot K^{-1}$. In this latter case, for increasing values of the lead density coefficient, the roots move to the right, becoming first real and then also positive at a certain critical value around 12 $pcm \cdot K^{-1}$. Such a trend is not always the same since the critical value depends on the considered power level. Indeed, the system at nominal power becomes unstable for the lowest lead density coefficient (as described in Figure 2.3 and Figure 2.4, black track). This trend is mainly due to the amplified feedback effects at higher power. Indeed, if the action of a feedback is destabilizing (i.e., the corresponding reactivity coefficient is positive), its impact is first noticed at high power, where its magnitude is larger because more amplified. In addition, the Doppler effect is more strongly perceived at low power levels, and decreases along with the power level increase. Therefore, at low power levels there is a more relevant counteraction by the Doppler effect, which counterbalances the lead density coefficient positive action. In other words, the core behaviour is more sensitive to this design parameter variation at nominal power, and thus it may be concluded that, at low power levels, the system is more robust to uncertainties affecting its value. In any case, it has been seen that the system becomes unstable only for extremely high values of α_L, in a clearly unrealistic condition. Therefore, it can be stated that the system is inherently stable, both at low power levels and in the case of positive coolant density reactivity coefficients.

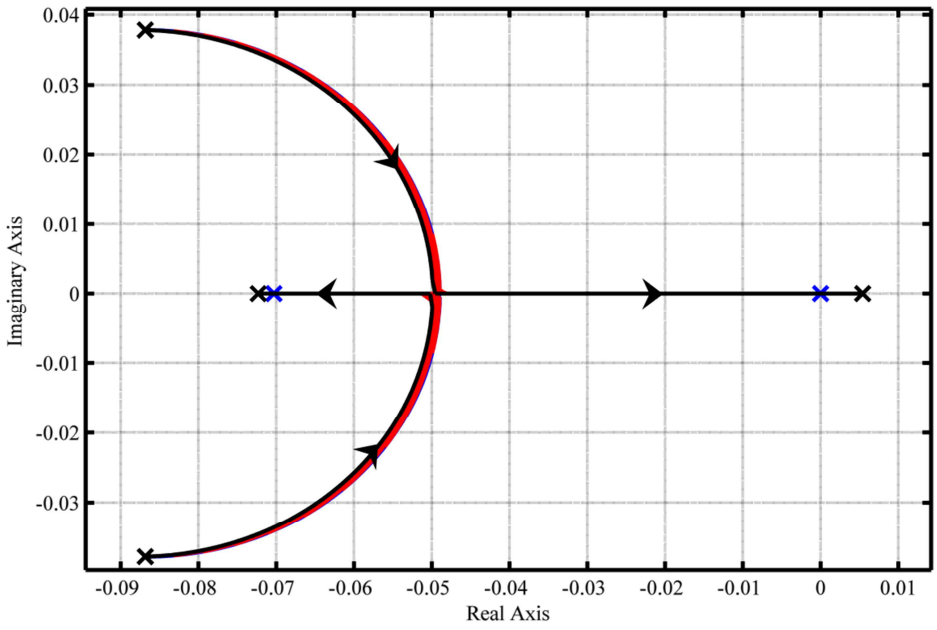

Figure 2.3. Root locus for the core system as a function of power level with $0 < \alpha_L < 12$ pcm·K^{-1} at BoC.

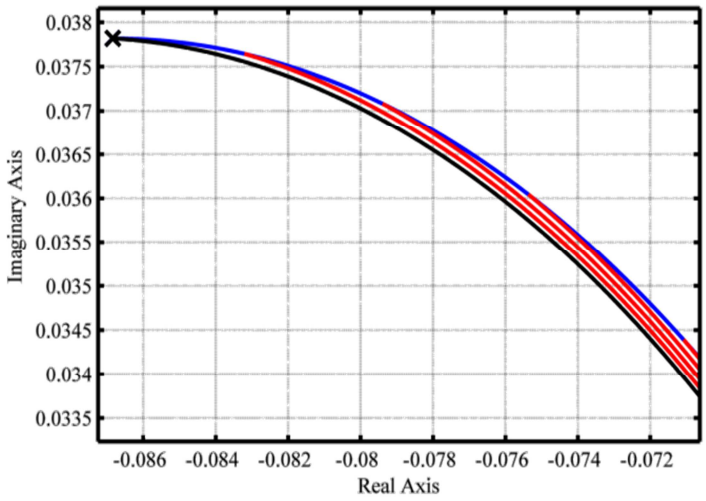

Figure 2.4. Zoom of Figure 2.3.

Primary circuit analysis

A stability analysis has been carried out allowing for the overall primary circuit configuration so as to consider a more realistic configuration in which the SG feedback action on the core dynamics is accounted for (Figure 2.5). In addition to the previous set of equations, Eqs. (2.12)-(2.13) have been added to take into account the influence of the SG and the closure of the primary circuit, obtaining a total of 16 equations. Also in this case, model simplification and linearization have allowed reducing the dimension of the equations set. Finally, a seven roots system has been derived.

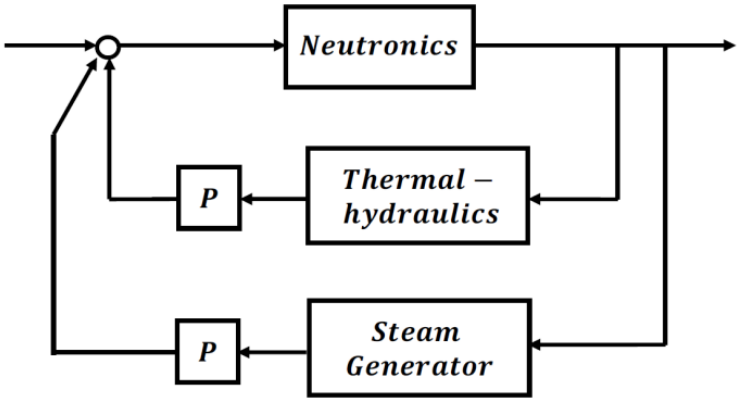

Figure 2.5. Conceptual feedback scheme employed to point out the primary circuit dynamics.

As shown in Figure 2.6, the system is stable at each power level, but compared to the previous case, additional complex conjugate poles appear in the plots. A new dynamics has been found on the right of the trajectories representative of the stand-alone core. These new tracks are closer to the origin and complex conjugate for low power levels, suggesting that the dynamics they describe is slower and with damped oscillations. In this case, only one pole remains close to the origin even at high power levels, whereas in the stand-alone core analysis both the roots move to the left. As mentioned previously, when coupling the core with the SG, the coolant core inlet temperature is no longer a fixed input, becoming instead a state variable depending on the power exchange conditions at the interface with the secondary circuit. This induces a feedback on the core behaviour whose neutronics is influenced by the reactivity effects related to the temperature variations.

When the SG is operated at nominal conditions, any reactor power variation causes the core inlet temperature to change affecting the system reactivity (mainly through the coolant temperature variation with a consequent additional lead density and radial expansion feedback), differently than in the stand-alone core case, in which the inlet temperature is a fixed input. Such phenomena explain the system new oscillatory behaviour at low power shown in Figure 2.6a.

In particular, the situation of ideal heat exchange conditions on the SG side have been considered (Figure 2.6b). Indeed, it is supposed that the SG manages to dispose any thermal power produced in the reactor core, ensuring that the coolant temperature at the core inlet remains close to its nominal value. Therefore, for increasing exchange capabilities, the circle moves to the left and reduces its dimensions meaning that oscillations progressively damp as the stand-alone core case is asymptotically approached (i.e., the inlet core temperature independent of the SG heat exchange capabilities).

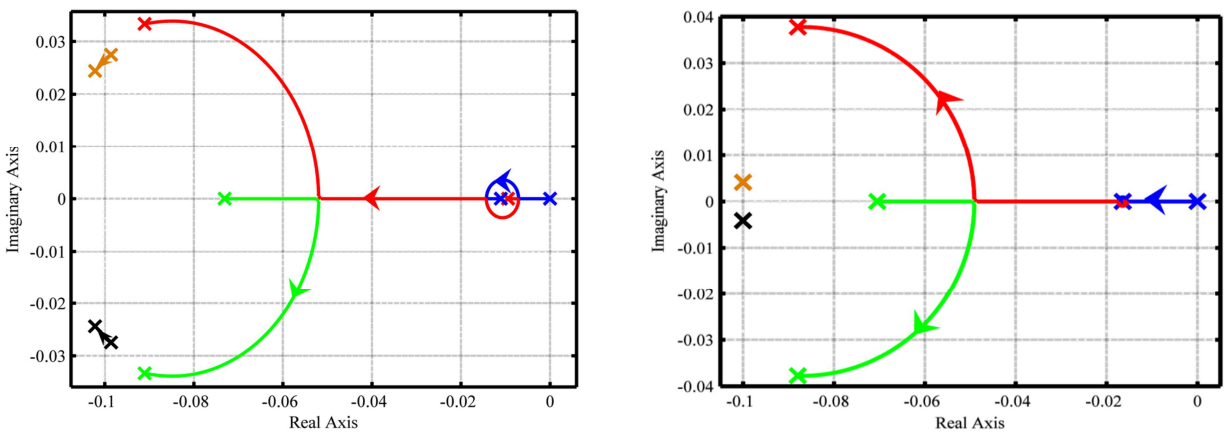

Figure 2.6. Root locus for the primary circuit as a function of power level, BoC conditions, considering (a) nominal SG conditions and (b) ideal exchange conditions.

In both the above mentioned situations, the primary circuit pole trajectories have been examined again as a function of the lead density coefficient variation (Figure 2.7). As in the previous plots, the blue track constitutes the roots trajectories when the power varies and α_L is equal to its nominal value, whereas red tracks represent the poles motion induced by continuous variations of α_L from 0 to 7 pcm·K^{-1} at each power level (the trajectory referred to the nominal power level is depicted with black track).

By comparing Figure 2.7 with Figure 2.3, it can be inferred that the primary circuit behaves qualitatively as the stand-alone core one, but the instability threshold is reached earlier in the former case. For increasing values of the lead density coefficient, the poles move to the right and become real positive when α_L is between 6 and 7 pcm·K^{-1}, focusing the "destabilizing" effect due to the SG. In confirmation of this, the system stability has been analysed by connecting a progressively more performing SG to the core, and it appears very clearly that the closer the heat exchange conditions are to the ideal ones, the higher is the margin of stability of the reactor system, since the core is less and less influenced by the secondary side dynamics. Indeed, when considering an ideal SG (Figure 2.9), the poles never reach a positive real part for the considered range of α_L, implying that greater values of the reactivity coefficient are needed for the system to become unstable. Anyway, even when considering the closed system configuration with nominal SG conditions, the reactor becomes unstable only for very high values of α_L, which are still non-realistic. Therefore, it can be definitely concluded that the overall system is indeed inherently stable, and consequently safe.

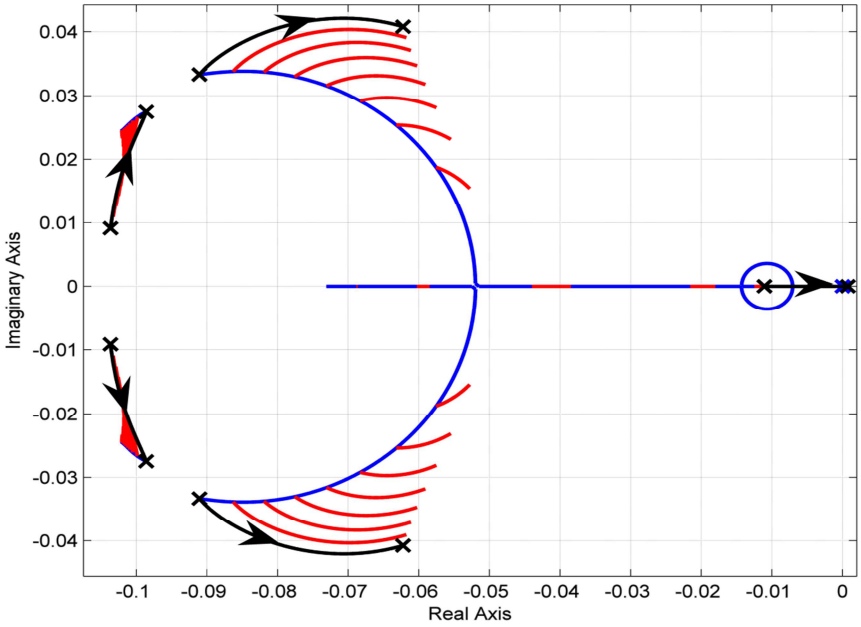

Figure 2.7. Root locus for the primary system as a function of power level with $0 < \alpha_L < 7$ pcm·K^{-1} at BoC, nominal SG conditions.

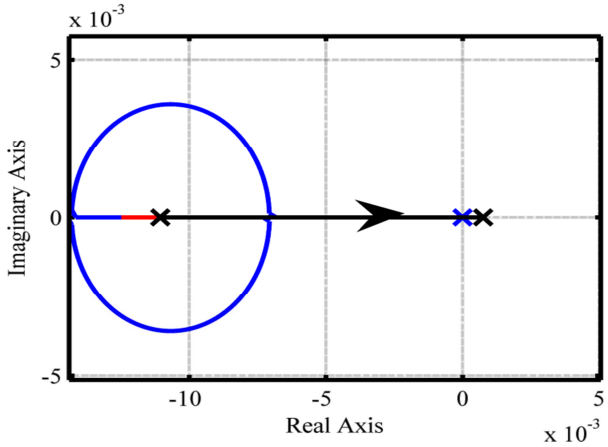

Figure 2.8. Detailed view of Figure 2.7.

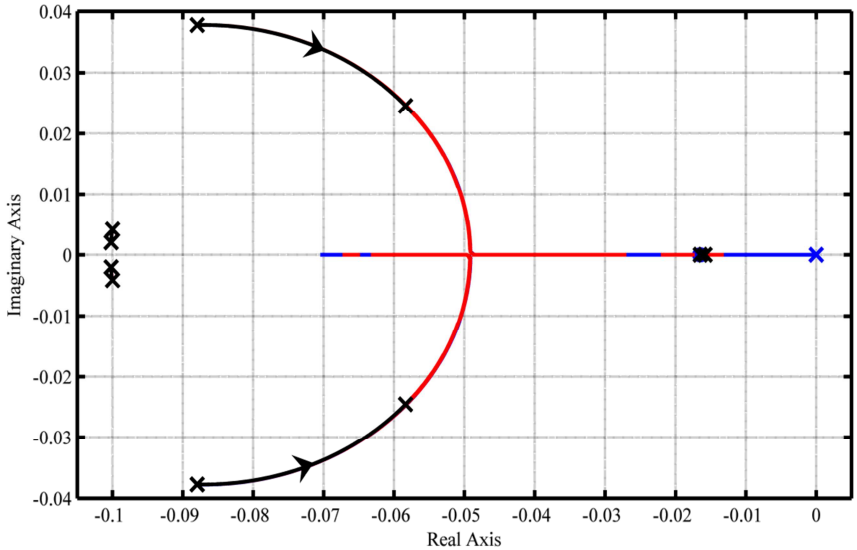

Figure 2.9. Root locus for the primary system as a function of power level with $0 < \alpha_L < 7$ pcm K^{-1} at BoC, ideal exchange conditions.

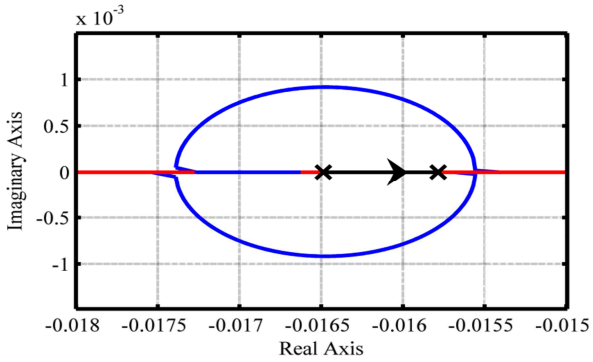

Figure 2.10. Detailed view of Figure 2.9.

2.3. Concluding remarks

In this Chapter, the stability analysis of the ALFRED reactor has been performed in order to study the governing dynamics of the system as well as the stability features, with the main purpose of providing the system designers with fundamental feedbacks useful to improve or even finalize the system layout. In this perspective, a simulation tool has been developed expressly meant for such an early phase of the reactor design. Both a stand-alone core case and a simplified primary system configuration have been considered for the analysis. In the former scenario, the core inlet temperature has been considered as a fixed input, while the power varies between zero and the full nominal figure at both BoC and EoC, in order to evaluate the stability of the system as a function of power level and stage of the fuel cycle. Analogous studies have been carried out on the entire primary circuit, considering a more realistic situation in which the SG feedback action on the core dynamics is allowed for. In both configurations, a parametric variation of the lead density reactivity coefficient (from its actual negative value to large positive figures making the reactor unstable) has been investigated. The system has turned out to be inherently stable at all design-basis power levels, independently of the value of the coolant density coefficient, which should reach unrealistic high values (nearly 6 pcm K^{-1}) to make the reactor unstable even when introducing the destabilizing action of the SG on the core.

As a major outcome, the performed investigation has assessed the possibility of adopting such a tool to provide useful hints for the plant design. Indeed, in common practice, the analyses oriented to the control system design are carried out once the reactor design has been finalized. Otherwise, it would be beneficial that the outcomes of the system dynamic response characterization could be allowed for in the preliminary design procedure. In this perspective, it has been demonstrated that it is possible to obtain for the system key-parameters (such as the feedback coefficients) the admissible range within which they may vary. In this way, it is possible to provide indications to the designers on the optimal system configuration from a control-oriented perspective as well.

3. Object-oriented modelling of the ALFRED reactor

Outline

In order to properly characterize the ALFRED governing dynamics, it has been necessary to develop an accurate simulation tool. In this perspective, the model must be conceived to be modular (in order to enhance the reusability of pre-existing and validated components), open, since the equations implemented have to be clearly readable, efficient (meaning that the simulation code should be fast running), and integrable with the control system model. Recent advances in object-oriented modelling, and in particular the development of the Modelica language, represent a viable path to achieve the above-mentioned goals. Therefore, an a-causal object-oriented one-dimensional model has been developed, specifically meant for

- *Evaluation of the system governing dynamics;*
- *Definition of full power control mode with simulation of ALFRED controlled operational transients;*
- *Validation of the proposed control strategy.*

The overall plant model has been built and implemented in Dymola environment by assembling both component models already available in a specific thermal-hydraulic library, named Thermopower, and specific nuclear component models taken from the NuKomp library, suitably modified according to the ALFRED specification to provide the required capabilities for the analysis.
The primary circuit model has been built by connecting the above-mentioned components, taking into account suitable time delays, and incorporating the cold pool, which has revealed to be fundamental to allow for the system characteristic time constants. The plant simulator has been finalized by connecting standard turbine, condenser and other components of the Balance of Plant. This approach has been specifically addressed to transient analyses, since its more detailed geometry characterization ensures more accurate simulation outcomes. Different design-basis transient scenarios have been simulated to characterize the system free dynamics. In this way, the physical bonds among input and output variables have been highlighted, providing useful guidelines for the control strategy definition.

The main results have been published in:

- Ponciroli, R., Bigoni, A., Cammi, A., Lorenzi, S., Luzzi, L, 2014. Object-oriented modelling and simulation for the ALFRED dynamics. In: Progress in Nuclear Energy, **71**, 15-29.

Introduction

In order to study and characterize the ALFRED plant dynamics, a control-oriented modelling and simulation tool for has been developed to perform design-basis transient analyses with the main purpose of laying the foundations of the control strategy, besides providing useful feedbacks for the system design finalization. In particular, the simulator is devoted to

- predicting the reactor response to typical transient initiators and thus obtaining more detailed information about its dynamic behaviour;
- favouring the control system design for both its realization (linear model) and its validation (non-linear model).

A flexible, straightforward and fast-running (i.e., without significant computational burden and implementation-related efforts) dynamics simulator has been sought for this early phase of the reactor conceptual design, in which all the system specifications are still considered open design parameters and thus may be subject to frequent modifications. In a control-oriented perspective, the most important features (Cammi and Luzzi, 2008) required to the modelling tool are the following: (i) *modularity*, in order to enhance the reusability of pre-existing and validated components; (ii) *openness*, since the equations implemented have to be clearly readable; (iii) *efficiency*, meaning that the simulation code should be fast running; and (iv) *integrability* with the control system model.

A viable path to achieve the above-mentioned goals is constituted by the adoption of the Modelica language (Fritzson, 2004; Modelica, 2011). Introduced in 1997, Modelica is a modelling language which allows an object-oriented approach specifically designed for the study of engineering system dynamics. In this perspective, Modelica facilitates the system description in terms of physical and engineering principles, i.e., mass, energy and momentum balance equations. Modelica is employed for the modelling of general physical phenomena described by sets of Differential Algebraic Equations (DAEs), supporting a declarative language. Modelica is open-source and it has already been successfully adopted in different fields, such as automotive, robotics, thermo-hydraulic and mechatronic systems, but also in nuclear simulation field (Cammi et al., 2005; Souyri et al., 2006).

As a consequence of the above mentioned considerations, a dynamic simulator of the ALFRED reactor has been realized by adopting the Modelica object-oriented language. The primary and secondary systems have been modelled and implemented in Modelica by assembling conventional component models already available in a specific thermal-hydraulic library, named *Thermopower* (Casella et al., 2006), and specifically developed nuclear component models, taken from the *NuKomp* library (Cammi et al., 2005), modified in order to provide the required capabilities for the analysis. The resulting overall plant simulator, incorporating also the BoP, consists of the following essential parts: core, steam generator, primary and secondary pumps, cold and hot legs, cold pool,

turbine, and condenser. The realization of a preliminary "engineering simulator" may allow to predict the reactor responses to typical transient initiators, involving not only the primary circuit, but also considering the BoP and eventually the electrical grid interaction.

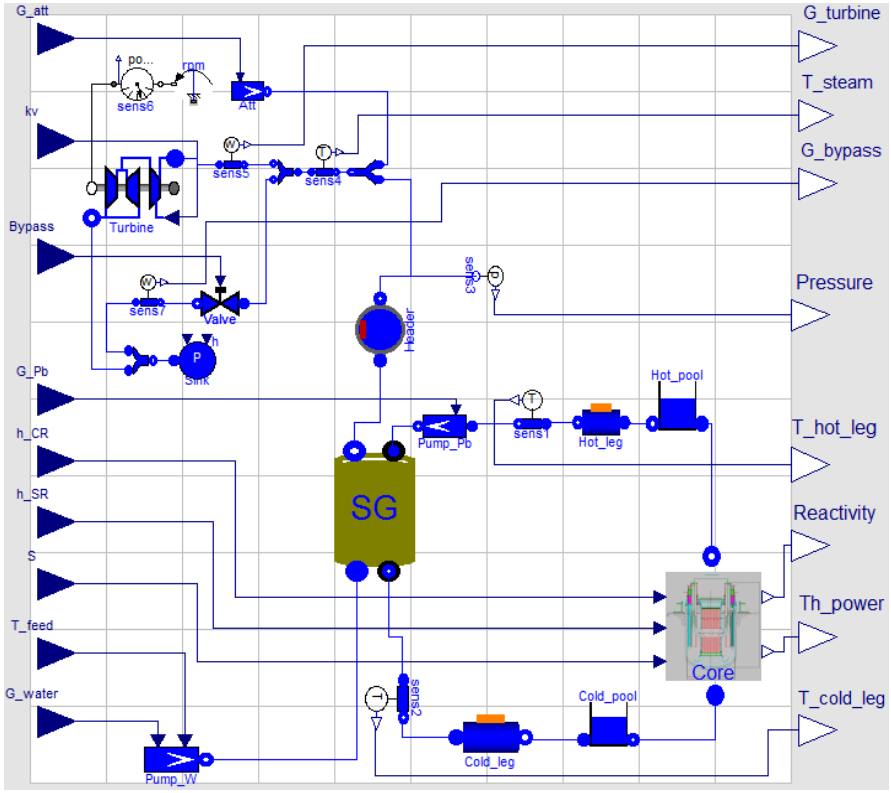

Component	Description
Core	Reactor core
Cold_pool	Pool collecting the lead coming from the SG outlet
Cold_leg	Collector between the SG outlet and the core inlet
Hot_pool	Pool collecting the lead coming from the core outlet
Hot_leg	Collector between the core outlet and the SG inlet
sens	Temperature and pressure sensor
Pump_Pb	Lead pump
SG	Steam Generator
Header	Volume collecting the produced steam
Pump_W	Water pump
Turbine	Steam turbine unit
Sink	Condenser
Att	Attemperator

Input variable	Definition
G_att	Attemperator mass flow rate
kv	Turbine admission valve coefficient
Bypass	Bypass valve coefficient
G_Pb	Primary circuit mass flow rate
h_CR	Control rod height
h_SR	Safety rod height
S	Neutron source
T_feed	Feedwater inlet temperature
G_water	Feedwater mass flow rate

Output variable	Definition
G_turbine	Turbine admitted mass flow rate
T_steam	Turbine inlet steam temperature
G_bypass	Bypass discharged mass flow rate
Pressure	SG pressure
T_hot_leg	Core outlet temperature
Reactivity	System reactivity
Th_power	Thermal power
T_cold_leg	Core inlet temperature

Figure 3.1. Representation of the ALFRED object-oriented model. In the legend, the input and output variables are reported in order to allow the comprehension of the graphical interface.

3.1. Object-oriented simulator development

A nonlinear one-dimensional model of the ALFRED preliminary configuration has been developed by adopting an object-oriented approach based on the Modelica language. The overall system model has been built by connecting the different components (*objects*) through rigorously defined interfaces (*connectors*) corresponding to specific physical interactions occurring with the relative external environment. One of the main advantages of employing the Modelica language is the possibility of performing *acausal modelling*, i.e., the direct use of equations without imposing

the classic input/output declaration, granting a more flexible and efficient data flow (Fritzson, 2011). The system behaviour is described in terms of conservation laws that, combined with components constitutive equations, determine the overall system of equations to be solved. Thanks to the a-causal formulation of the problem, the equations describing each component model are written independently of the actual boundary conditions and it is not necessary to establish a priori which variables will work as inputs and which as outputs. Model causality of the model is determined automatically by the Modelica model interpreter or compiler at the aggregate level when a system model is assembled out of elementary ones. In this way, models are much easier to write and reuse, while the burden of determining the actual sequence of computations required for the simulation is entirely left to the compiler. In the common practice, most of the present simulators are based on causal modelling, whose main features are reported in Table 3.1.

Table 3.1. A-causal vs. causal approach.

Causal approach	A-causal approach
System input and output variables have to be established at the beginning	It is not necessary to establish *a priori* input and output variables
Equations have to be rewritten for each specific application in state space representation	Causality remains unspecified as long as equations have to be solved
Low flexibility in changing the model configuration	More realistic description of components and modularity
Low reusability of previous work. Problem formulation in a series of operations has to be performed by the user, according to the particular applicative context	Possibility of easily reusing previously developed models. Components models are defined independently of the context they are used
Block diagram representation (physics-oriented)	Plant representation (component-oriented)
Integration algorithm for ordinary differential equations (lower computational cost)	Integration algorithm for differential algebraic equations (higher computational cost)
Low order modelling, easy to linearize	Potentially high number of equations involved

In addition, the multiphysics approach of the Modelica language provides modelling primitives such as generic algebraic, differential and difference equations, and it is not tied to any specific physical or engineering domain such as mechanics, electrical engineering, or thermodynamics. Thus, it is quite straightforward to model multi-disciplinary systems as the reactor core, where several physics (i.e., neutronics, heat exchange, and fluid dynamics) interact with each other. Furthermore, a more realistic plant representation is made possible by the component-based description. As simulation environment, *Dymola* (Dynamic Modelling Laboratory) (DYNASIM, 2006) has been adopted as it allows the hierarchical composition of models and offers wide libraries of pre-defined components. Dymola compilers incorporate sophisticated symbolic manipulation algorithms, which allow to

obtain index-1 systems of differential-algebraic equations from higher-index ones, to symbolically solve both linear and nonlinear model equations (Fritzson, 2004). The resulting code is then linked to state-of-the-art numerical integration codes such as DASSL (Brenan et al., 1989). As shown in Figure 3.1, the ALFRED object-oriented model has been built by connecting the plant components. In the following sub-sections, the components specifically modelled in this work (i.e., core, SG, turbine) will be described in detail, whereas for the most conventional ones the reader can refer to Casella and Leva, 2006.

3.*1.1. Core*

As far as the core is concerned, point reactor kinetics and one-dimensional heat transfer models have been implemented coherently with the ALFRED specifications by incorporating suitable geometry, material properties and correlations, neutronic feedback coefficients and kinetic parameters.

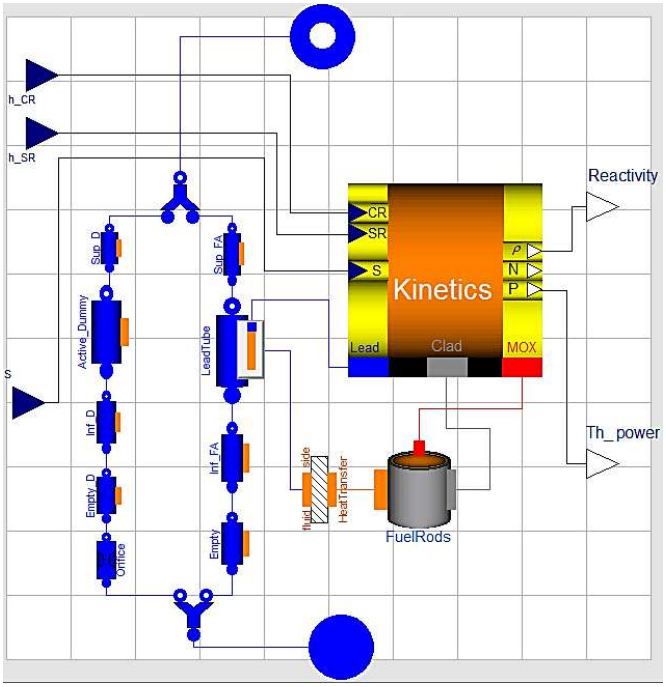

Figure 3.2. Object-oriented model of the ALFRED core.

The component-based core model (Figure 3.2) is composed by four sub-systems. The component *Kinetics* employs a point reactor kinetics model, with one neutron energy group and eight delayed precursor groups, which has been presented in Section 2.1.1. In particular, two different relationships were also adopted to describe the effective fuel temperature. ${T_f}^D$ expresses the average temperature taking into account the broadening of resonances, whereas ${T_f}^{eff}$ represents the temperature range that allows to evaluate quantitatively the deformation of the pellet due to the field of thermal. As far as the Doppler coefficient is concerned, the approach previously used in the

stability analysis has been adopted, implementing Eq. (2.8) for the effective Doppler temperature and Eq. (2.9) for the magnitude of the actual reactivity variation following a generic fuel temperature change. Conversely, in Eq. (3.1), weights have been used in order to reproduce the parabolic trend of the temperature field within the fuel pellets, to provide an estimate of the volume-weighted average behaviour.

$$T_f^{\,eff} = (1/2) \cdot T_f^{\,ext} + (1/2) \cdot T_f^{\,int} \tag{3.1}$$

Reactivity effects due to the coolant density variations, as well as to the axial and radial expansions, have been taken into account by adopting linear equations with constant coefficients. In particular, axial and radial cladding expansions have been related to the average cladding thermal conditions, while axial and radial wrapper expansions have been considered governed by the lead temperature. On the other hand, the grid expansion effect concerns the increase of the core radius due to the incoming coolant temperature enhancement. Therefore, the coolant volume inside core increases as well as the core volume and, in turn, the leakages. These combined effects determine an overall negative contribution. The pad effect (also called "flowering") is determined by the differential radial expansion between the bottom of the subassemblies at the incoming coolant temperature and their top at the outlet coolant temperature. However, this reactivity contribution is not particularly relevant (Sciora, 2011).

As far as the CRs are concerned, a reactivity differential curve has been adopted based on the reactivity worth of the 12 rods at different insertion lengths (Figure 3.3). On the other hand, SRs worth characterization does not require such an accuracy, because this kind of rods are extracted during start-up phase and then they remain outside the core while the reactor is operating at rated power conditions. Consequently, a linear dependence of the handled reactivity as function of position is sufficient to describe the SRs reactivity contribution. Consequently, the overall system reactivity is given by the sum of the various contributes, as follows:

$$\begin{aligned}\rho(t) = \rho_0 + \ & Lead\ density + Doppler\ effect + Axial\ cladding\ expansion + \\ & Axial\ wrapper\ expansion + \ Radial\ cladding\ expansion + \\ & Radial\ wrapper\ expansion \ + Axial\ fuel\ expansion + \\ & Diagrid\ expansion + Pad\ expansion + CRs + SRs\end{aligned} \tag{3.2}$$

where

$$
\begin{aligned}
Reactivity\ margin &= \rho_0 \\
Lead\ density &= \alpha_L \cdot (T_l - T_{l,0}) \\
Doppler\ effect &= 1.1 \cdot K_D \cdot log\left({T_f}^D / {T_{f,0}}^D\right) \\
Axial\ cladding\ expansion &= \alpha_{CZ} \cdot (T_C - T_{C,0}) \\
Axial\ wrapper\ expansion &= \alpha_{WZ} \cdot (T_l - T_{l,0}) \\
Radial\ cladding\ expansion &= \alpha_{CR} \cdot (T_C - T_{C,0}) \\
Radial\ wrapper\ expansion &= \alpha_{WR} \cdot (T_l - T_{l,0}) \\
Axial\ fuel\ expansion &= \alpha_{FZ} \cdot (T_C - T_{C,0}) \\
Diagrid\ expansion &= \alpha_{Dia} \cdot (T_{l,in} - T_{l,in}) \\
Pad\ expansion &= \alpha_{Pad} \cdot (T_{l,out} - T_{l,out}) \\
Control\ Rods &= A_{CR} \cdot sen(B_{CR} \cdot h_{CR} + C_{CR}) + D_{CR} \\
Safety\ Rods &= A_{SR} \cdot (h_{SR} - x_{SR})/L_{SR}
\end{aligned}
\tag{3.3}
$$

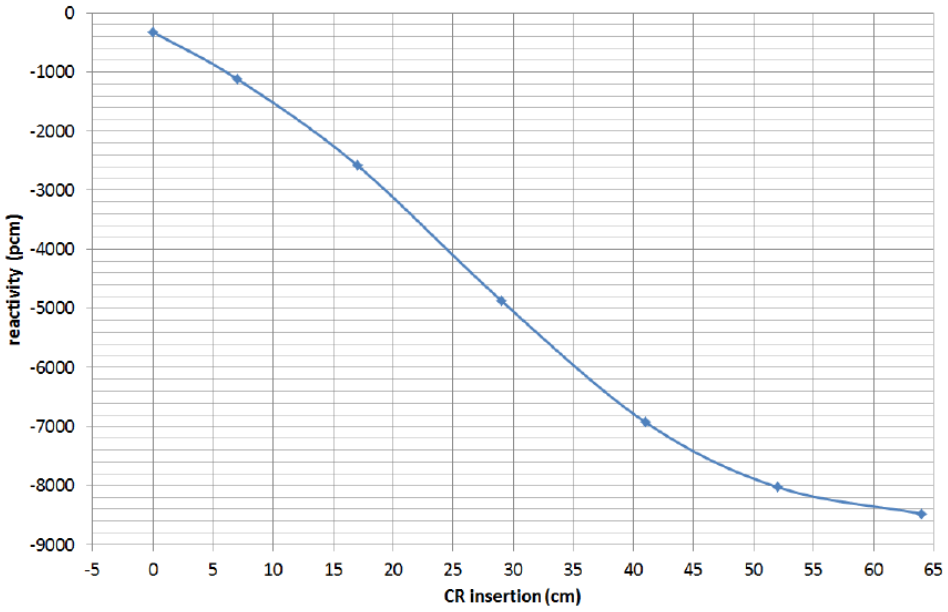

Figure 3.3. Calibration curve of Control Rods.

The component *FuelRods* describes the thermal behaviour of the fuel pins by adopting five radial regions within the element (i.e., cladding, gaseous gap and three concentric zones within the pellet). The time-dependent Fourier equation is applied considering only the radial heat transfer, thus disregarding both the axial and the circumferential thermal diffusion. Fourier equation has been radially discretized in five zones and longitudinally in a user-defined number (*N*) of nodes.

$$
d_f c_f \frac{\partial T_f}{\partial t} = \frac{1}{r}\frac{\partial}{\partial r}\left(r k_f \frac{\partial T_f}{\partial r}\right) + q'' \tag{3.4}
$$

$$
\frac{\partial}{\partial r}\left(r k_g \frac{\partial T_g}{\partial r}\right) = 0 \tag{3.5}
$$

$$d_c c_c \frac{\partial T_c}{\partial t} = \frac{1}{r}\frac{\partial}{\partial r}\left(r k_c \frac{\partial T_c}{\partial r}\right) \tag{3.6}$$

The component *LeadTube* models the coolant flowing through the core channels represented ad cylindrical conduits. It simulates a one-dimensional single-phase fluid flow with heat transfer from the fuel boundary and with temperature-dependent physical properties (OECD-NEA, 2007). This approach is based on distributed-parameter mass, momentum, and energy conservation equations discretized by employing a finite-volume method.

$$A\frac{\partial d}{\partial t} + \frac{\partial w}{\partial x_s} = 0 \tag{3.7}$$

$$\frac{\partial w}{\partial t} + A\frac{\partial p}{\partial x_s} + dgA\frac{\partial z}{\partial x_s} + \frac{C_f \omega}{2dA^2} w|w| = 0 \tag{3.8}$$

$$dA\frac{\partial h}{\partial t} + dAu\frac{\partial h}{\partial x_s} - A\frac{\partial p}{\partial t} = \omega\varphi \tag{3.9}$$

In Eqs. (3.7) - (3.8) the fast pressure and mass flow rate waves dynamics are modelled, while Eq. (3.9) describes the slower dynamics of heat transport and the fluid velocity.

The component *HeatTransfer* allows evaluating the heat flux exchanged between two one-dimensional interacting objects (e.g., the fluid flow and metal wall) as a function of the corresponding surface temperatures. Since the fuel pins are arranged on a triangular lattice, the Ibragimove-Subbotine-Ushakov correlation (Cheng and Tak, 2006) has been implemented in Eq. (3.10) to properly estimate the convective heat transfer coefficient. Moreover, among the possible correlations, it is the most conservative one since gives the lowest value of the Nusselt number.

$$Nu = 4.5 + 0.014 \cdot Pe^{0.8} \tag{3.10}$$

In the ALFRED primary circuit, it has been envisaged the presence of a *bypass mass flow rate*, i.e., a part of the coolant passes through the fuel elements and removes heat from the fuel elements, while a reduced fraction passes through the interstices between the wrappers, through the dummy element, the cases of the CRs and the SRs. Indeed, the thermal power is deposited not only in the fuel, but in the other materials, mainly due to the γ emission, as well. For these reasons, the lead mass flow rate devoted to the bypass has been fixed at the 3% of the one that circulates in the primary circuit. In a preliminary description, in order to represent the evolution of the temperature fields of the main components of the core, the presence of the bypass mass flow rate can be neglected. This approach can be suitable if the system is studied only in nominal operating conditions. Nevertheless, in accidental scenarios or in operating conditions in which the lead mass flow rate is not kept constant at the nominal value (e.g., during the reactor start-up), a more accurate

characterization of the pressure field is essential. In particular, in the core thermal-hydraulics description, two types of channels, which represent the fuel elements and the dummy elements, have been allowed for. Therefore, in order to refine the description of the thermal-hydraulics of the primary circuit, it has been decided to consider the presence of the bypass, providing it with two types of channels, which represent the fuel elements and the dummy elements.

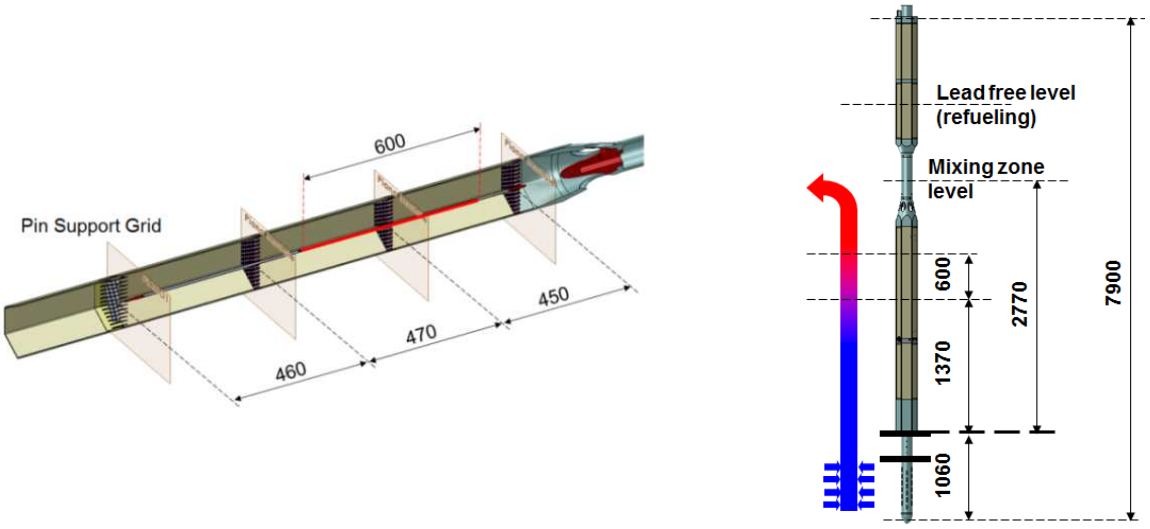

Figure 3.4. Fuel assembly geometry.

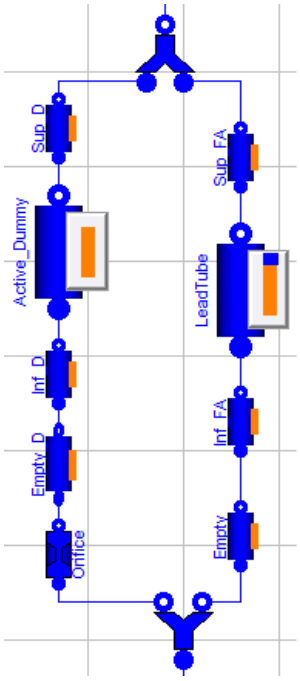

Component	Description
Sup D	Upper region of dummy elements
Active_Dummy	Region of dummy elements corresponding to the active zone of fuel assemblies
Inf D	Lower region of dummy elements
Empty D	Empty region of dummy elements
Orifice	Form pressure drop which allow to achieve the real pressure field
Sup FA	Upper region of fuel assemblies
LeadTube	Active region of fuel assemblies
Inf FA	Lower region of fuel assemblies
Empty	Empty region of fuel assemblies

Figure 3.5. Representation of the coolant channels in the ALFRED core model.

In the modelling of the channels, in order to reproduce the layout of the assemblies (Figure 3.4), different types of components (Figure 3.5) have been employed. In particular, a component which allows setting additional pressure losses has been added to the dummy elements model. Since the channels are subjected to the same pressure drop, hydraulic resistance at the entrance of dummy

elements has been suitably tuned so as to achieve the desired pressure field. As far as the distributed losses within the coolant channels are concerned, they have been preliminarily estimated adopting the Mc-Adams correlation (Todreas and Kazimi, 2012) for the Fanning friction factor.

$$f_{Fanning} = 0.046 \cdot Re^{-0.2} \tag{3.11}$$

On the other hand, the modelling of the form losses has turned out to be difficult since the dimensional specifications concerning the spacers have not been assessed yet. At this point, since the total pressure losses are specified in the core design and the distributed ones have been evaluated, it has been easy to obtain the contribution of the form losses, representing the influence of the spacers in the core thermal-hydraulics by using the dedicated component (*Orifice*), which allows implementing a suitable hydraulic resistance.

All the several core subsystems have been eventually connected. In particular, the mutual influences between neutronics and thermal-hydraulics have been taken into account by means of the above mentioned feedback reactivity coefficients represented in the Modelica language through dedicated connectors. As shown in Figure 3.2, blue, grey and red connectors allow carrying the information about lead, cladding and fuel thermal behaviour in order to allow for their influence on the neutronics.

3.1.2. Hot and cold pool

The coolant hot and cold pool models (named *Hot_pool* and *Cold_pool*) have been implemented by employing suitable components describing free-surface cylindrical lead tank (responsible for most of the large thermal inertia characterizing the overall system), on which mass and energy balances have been taken, assuming that no heat transfer occurs, except through the inlet and outlet boundaries.

3.1.3. Hot and cold legs

In order to represent the hot and cold connectors, simple one-phase *LeadTube* components have been employed (named *Hot_leg* and *Cold_leg*). One-dimensional flow models have been implemented, neglecting thermal dispersion, to properly consider the time delays due to transport phenomena between the core and the SG, and between the SG and the cold pool.

3.1.4. Pumps

As far as the primary and secondary pumps are concerned, ideal flow rate regulators have been employed.

3.1.5. Steam generator

Due to its non-conventional bayonet-tube design, an effort has been spent to develop a specific component representing the ALFRED SGs (Figure 3.6). A simplified treatment has been opted for, based on a rigorous one-dimensional description of the actual geometry, which has been reproduced by adopting different tube models connected together. In such a way, the relevant feature of reusability in the Modelica language has been exploited. Indeed, a-causal modeling and encapsulation are a strong incentive towards the development of libraries of general-purpose reusable models. For this reason, the same tube, based on a certain set of equations, can be employed in several contexts and extended through *inheritance* by adding further equations. After entering the SG, water flows down in the slave tube (Figure 1.4) and there is no heat exchange neither thermal dispersion, thanks to the effective insulation provided. Thus, water conditions at the SG inlet and at the bottom of the tube are the same. For this reason, the transport phenomena in the first part have been neglected and the feedwater has been simulated to flow directly in a counter-current configuration, exchanging thermal power with the external lead. The component geometry has been substituted with concentric tube bundles in a counter-current flow configuration where the pressure drops are concentrated at the bottom of the bayonet tube (i.e., where the fluid flow reverses). A turbulent, lumped pressure drop model has been assumed, proportional to the kinetic pressure. As far as the water side is concerned, a tube allowing to describe a two-phase fluid has been selected, adopting averaged densities in the neighbourhood of phase changes so as to avoid non-physical simulation artefacts due to phase change discontinuities at the model nodes. A two-phase homogeneous model (i.e., with the same velocity for the liquid and vapour phases) has been adopted. Waterside convective heat transfer coefficients have been evaluated by implementing the Dittus-Boelter correlation for one-phase regions, and the Kandlikar correlation for the boiling region (Todreas and Kazimi, 2012). According to the latter correlation, the two-phase heat transfer coefficient, h_{TP} , is equal to the larger of $h_{TP,NBD}$ and $h_{TP,CBD}$, i.e., the two-phase heat transfer coefficients in the nucleate boiling dominant and convective boiling dominant regions, respectively. These coefficients are given by the following equations:

$$h_{TP,NBD} = 0.6683 \cdot Co^{-0.2}(1-x_v)^{0.8} f(Fr_{LO}) h_{LO} + 1058.0 Bo^{0.7}(1-x_v)^{0.8} F_{Fl} h_{LO} \quad (3.12)$$

$$h_{TP,CBD} = 1.136 \cdot Co^{-0.9}(1-x_v)^{0.8} f(Fr_{LO}) h_{LO} + 667.2 Bo^{0.7}(1-x_v)^{0.8} F_{Fl} h_{LO} \quad (3.13)$$

where $Co = (d_L/d_V)^{0.5}[(1-x_v)/x_v]^{0.8}$ and $Bo = q"/w \cdot i_{LG}$ are the convection and boiling numbers, respectively. F_{Fl} is the fluid surface parameter that incorporates the effect of surface and fluid properties, and allows to take into account differences in nucleating characteristics. h_{LO} is the single-phase heat transfer coefficient with all flow as liquid. The function $f(Fr_{LO})$ is a Froude

number with all flow as liquid. This parameter addresses the stratified flow region. On the lead side, the component describing the behaviour of a single-phase fluid, previously used for the core model, has been adopted. Convective heat transfer coefficients have been evaluated by implementing the Ibragimov-Subbotin-Ushakov correlation as well.

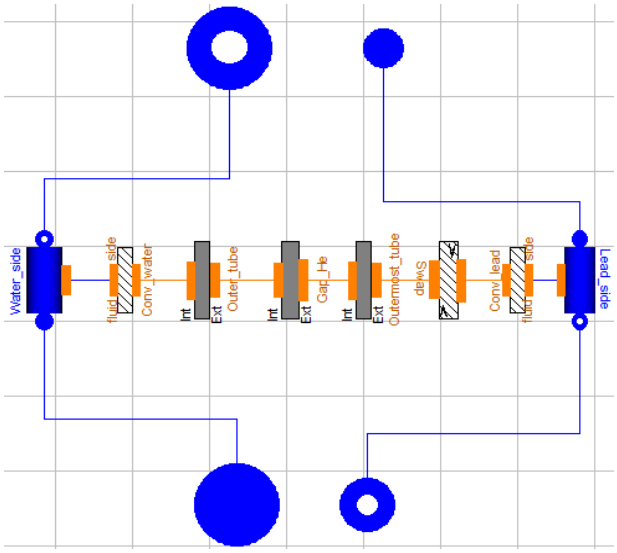

Component	Description
Water_side	Tube model describing the water flowing
Conv_water	Component that describes the convective heat transfer on water side
Gap_He, *Outer_tube*, *Outermost_tube*	Components allowing for the conduction phenomena within the different interfaces
Swap	Component that allows to reproduce the counter-current configuration.
Conv_lead	Component that describes the convective heat transfer on lead side
Lead_side	Tube model that describes the lead flowing

Figure 3.6. ALFRED SG object-oriented model.

The multiple wall interfaces have been modelled by adopting different conductive-exchange elements, in which thermal resistance is computed according to the formulation of Fourier equation in cylindrical coordinates, while the heat capacity is lumped in the middle of the tube thickness. Dedicated components have been implemented to represent each interface constitutive layer (i.e., insulating layer, outer tube, helium gap, outermost tube). Besides, the *HeatTransfer* component has been used to evaluate the convective heat exchange on both water and lead sides, a Swap component has been adopted to allow for the counter-current configuration. In this way, temperature and flux vectors on one side are swapped with respect to the ones on the other side. Furthermore, only one SG with a suitably rescaled number of tubes guaranteeing a thermal power of 300 MW_{th} (instead of the actual eight 37.5 MW_{th} SGs) has been considered.

3.1.6 Outlet header

The steam coming out from the SG is suitably collected in a header, i.e., a well-mixed chamber having no pressure drop and no energy exchange with the environment which allows to dampen any pressure transient limiting their impact on the conditions of the steam that flows into the turbine.

3.1.7 Attemperator

An attemperator has been foreseen between the outlet header and turbine, i.e., a reduced water mass flow rate at saturation conditions which is added to the steam flow. In this way, it is possible

to promptly limit the steam temperature at the turbine inlet keeping this variable of interest as close as possible to its nominal value (450 °C).

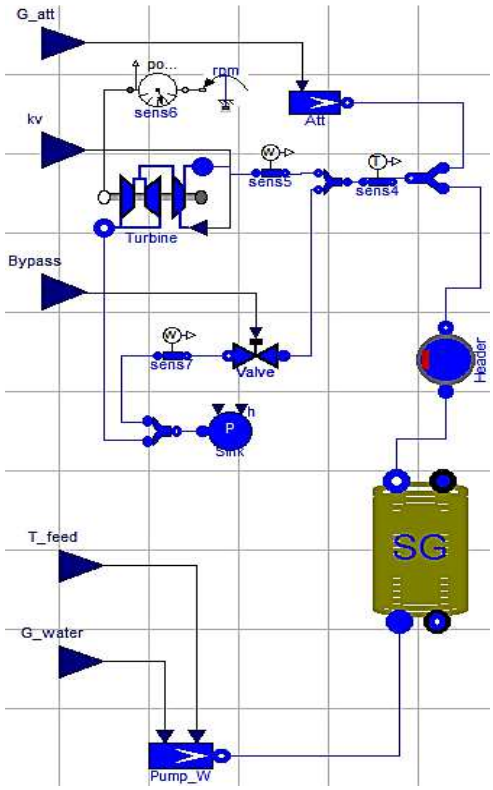

Figure 3.7. ALFRED reactor secondary side.

3.1.8 Turbine

Particular attention has been paid to this component, which is fundamental to properly account for the actual electrical power provided to the grid, as it constitutes a crucial parameter in a control perspective. The component selected for the turbine model describes a simplified steam turbine unit, in which a fraction of the available enthalpy drop is disposed by the High Pressure (HP) stage, whereas the remaining part by the Low Pressure (LP) one, with different time constants. A valve governs the overheated steam mass flow rate passing through the turbine. By adopting a simplified approach, choke flow conditions have been imposed. If the ratio of upstream pressure to downstream pressure is higher than the critical ratio ($x_c \approx 0.5$), in the section of maximum damping of the fluid vein a sonic shock wave is produced (Dolezal and Varcop, 1970). In this way, the inlet steam mass flow rate does not depend on the downstream pressure:

$$\frac{p_{\mathrm{up}} - p_{\mathrm{down}}}{p_{\mathrm{up}}} > x_c \quad \Longrightarrow \quad w_v = A_v \lambda_c \sqrt{d_{\mathrm{up}} p_{\mathrm{up}}} \tag{3.14}$$

Given that for the superheated steam is possible to adopt the approximation,

$$d_{sv}(p)p \cong Kp^2 \tag{3.15}$$

It is obtained

$$w_v \cong k_v p \tag{3.16}$$

Accordingly, the steam mass flow rate is regarded proportional to the inlet pressure and governed by operating the turbine valve admission (system input), not by throttling (i.e., no loss of thermodynamic efficiency occurs).

3.1.9 Bypass

After having passed through the SG, downstream of the temperature sensor, the steam mass flow rate can be subdivided into two ways (Figure 3.7). The former is a pipe that leads to the turbine, whereas the latter constitutes a bypass that directly leads to the condenser. This "alternative way" performs a very important function in particular operative conditions of the secondary side, when the reactor is operating at very low power levels, such as during the start-up phase. Indeed, when the thermal power from the primary circuit is not sufficient to ensure the steam nominal conditions, the flow is directly disposed to the condenser to avoid jeopardizing the integrity of the turbine, which cannot process an incoming fluid in such conditions. On the other hand, when the power level allows to obtain overheated steam, it is possible to let it flow to the turbine, while the bypass way is progressively closed.

3.2. Simulations and results

The reactor response to typical transient initiators has been investigated. In particular, three scenarios have been simulated, i.e., feedwater mass flow rate reduction, turbine admission valve coefficient variation, and Unprotected Transient of OverPower (UTOP), starting from nominal full power steady-state operating conditions. The tool developed in the present work allows simulating a transient of 2500 s requiring a computational time of less than 30 s (2.20 GHz with 8 GB memory), hence turning out to be suitable for control-oriented purposes.

3.2.1. Feedwater mass flow rate reduction

The dynamic response of the system to a 20% step reduction of the feedwater mass flow rate has been investigated. This transient is particularly relevant in a control perspective since the feedwater mass flow rate may be considered as one of the most promising control variables for the regulation of the lead temperature in the cold pool. In particular, this variable of interest has to be kept as close as possible to its nominal value. The main outcomes of this simulation scenario are the assessment of: (i) the dynamics of the transients, (ii) the influence of the feedwater mass flow rate on the lead

temperature in the cold pool; (iii) the compliance of the other variables of interest with the operational or safety limits; (iv) the coupling between the primary and the secondary circuit. Indeed, the feedwater mass flow variation affects the secondary circuit, the steam generation and the electrical power production as well. Moreover, in the common practice for nuclear reactor control, after an enhancement of the power request by the electrical grid, the feedwater mass flow rate is usually enhanced to fulfill the load demand. For these reasons, it is relevant to investigate the plant dynamic behaviour, following a feedwater mass flow rate variation.

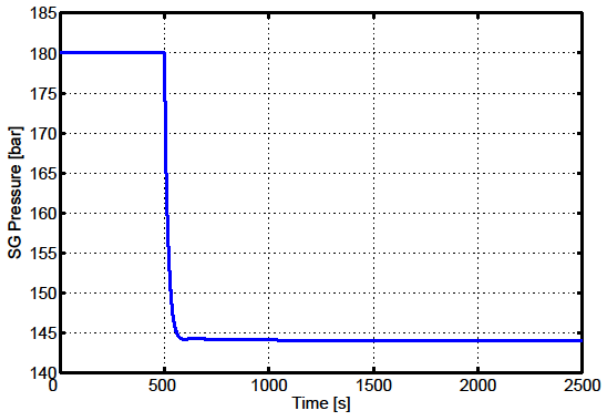

(a)

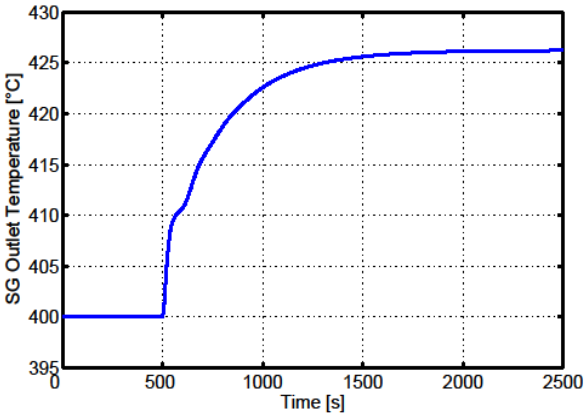

(b)

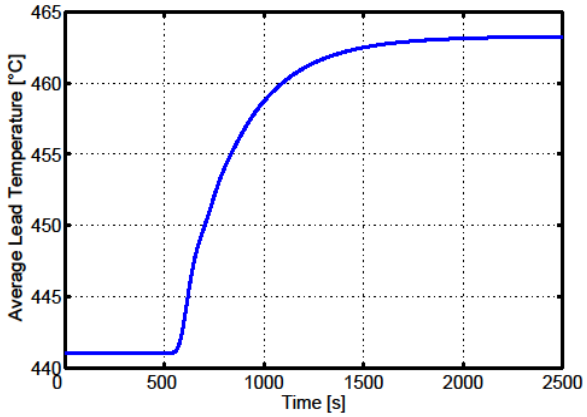

(c)

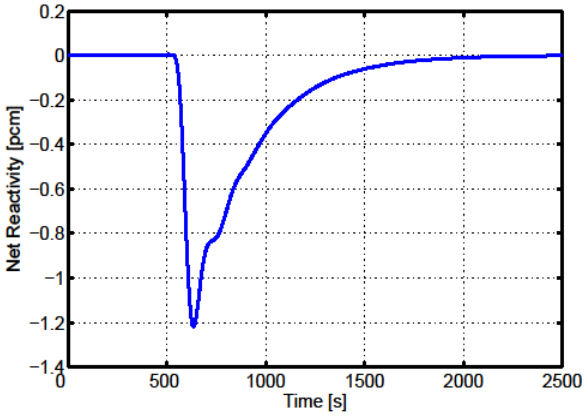

(d)

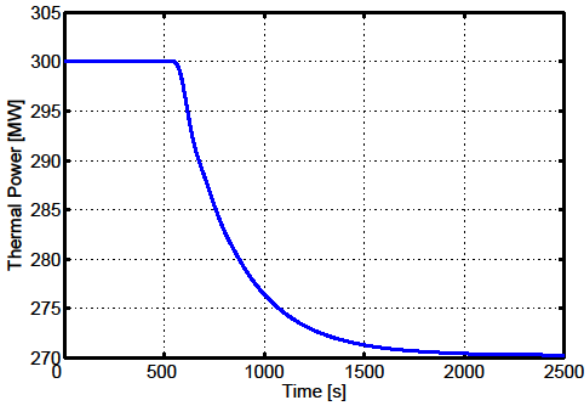

(e)

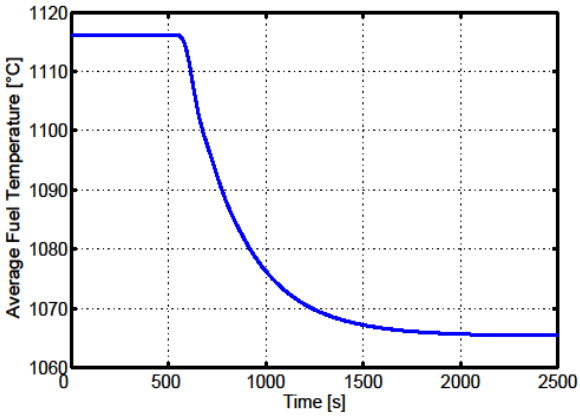

(f)

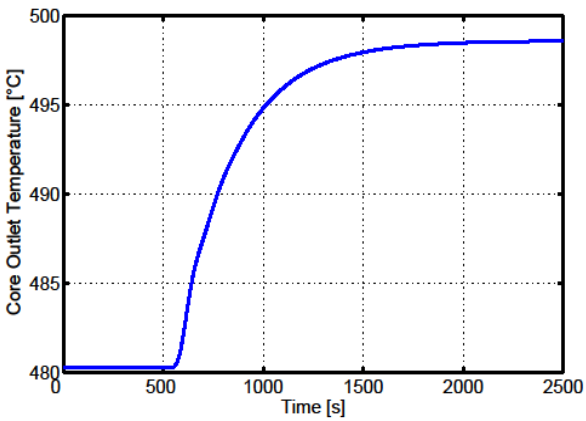

(g)

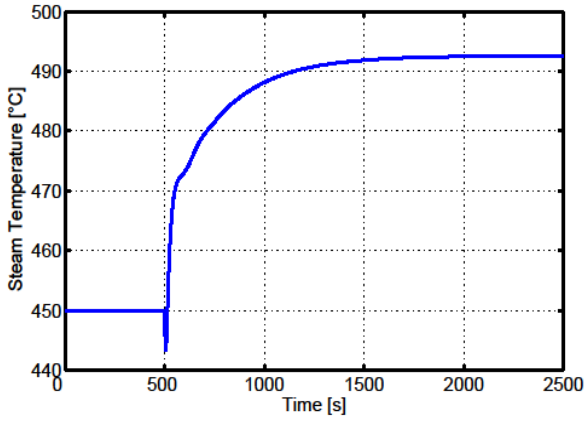

(h)

Figure 3.8. Output variables evolution after a feedwater mass flow rate reduction: (a) SG pressure variation; (b) lead SG outlet temperature variation; (c) average lead temperature variation; (d) net reactivity variation; (e) core thermal power variation; (f) average fuel temperature variation; (g) core outlet temperature variation; (h) steam temperature variation.

For the first 70 s, the only component affected by the perturbation is the SG itself, while in the second part of the transient SG and core are strongly coupled in virtue of reciprocal feedbacks. Since the other operating conditions are not modified (the turbine admission valve is not operated), the first consequences are a nearly step-wise pressure reduction in the SG (Figure 3.8a), a global worsening of the heat exchange conditions because of the combined effects of a reduced mass flow rate and a narrower temperature difference between primary and secondary fluids. Therefore, an increase of the lead temperature at the SG outlet occurs (Figure 3.8b). When the hotter coolant begins to flow into the core, the average lead temperature increases (Figure 3.8c), inducing a negative reactivity insertion (Figure 3.8d) that leads to a reduction of both core power and fuel temperature (Figure 3.8e -Figure 3.8f). Nevertheless, the coolant core outlet temperature (Figure 3.8g) undergoes an increase, even if smaller than the inlet perturbation, and consequently hotter lead flows towards the SG inlet. The feedback to the BoP is evident when examining the steam outlet temperature evolution (Figure 3.8h). Indeed, it rises almost instantaneously after the perturbation and, when the core power starts decreasing, it continues increasing but exhibiting a smaller and smaller gradient, consistently with the progressive thermal power reduction, to the final steady-state condition. As far as the system dynamic response is concerned, it is possible to assess the time constants characterizing this plant, which are key parameters for the development of the reactor control. In addition, relevant outcomes concerning the control action necessary to satisfy the operational constraints are highlighted. In particular, a strong control action has to be carried out in order to keep the SG pressure as close as possible to its nominal value (180 bar) avoiding depressurization. The same attention has to be paid to the steam temperature since hotter (or colder) vapour condition can jeopardize the turbine stages.

3.2.2. Turbine admission valve coefficient variation

In order to study the system behaviour after a change of the grid request, the system response after a 10% reduction of the turbine admission valve flow coefficient has been simulated. This is another fundamental transient for the control design since it allows evaluating the possibility of performing load-frequency regulation according to the grid demands by adopting this kind of reactor. In particular, in case of power decrease, the power regulation is achieved by closing the turbine admission valve. In this way, a lower steam mass flow rate circulates in the turbine and a lower mechanical power is available to the alternator. As far as the SGs are concerned, the pressure increase following the valve closing is compensated by a simultaneous control action performed both on feedwater mass flow rate and control rods in order to balance the power produced. This transient is relevant in the control strategy definition and characterization because of ALFRED is meant to be employed as a NPP connected to the electrical grid.

The first consequence of the performed perturbation is an instantaneous pressure rise within the SG (Figure 3.9a) since in the simulated transient a coordinated control strategy is not carried out. Because of the secondary fluid sudden compression, the temperature difference between primary and secondary fluids decreases and a lower power transfer occurs, inducing a lead temperature enhancement at the SG outlet (Figure 3.9b). The ensuing negative reactivity insertion (Figure 3.9c) determines a core power reduction (Figure 3.9d). As to the coolant core outlet temperature (Figure 3.9e), an increase is observed even though slighter than the one at the core inlet.

It is worthwhile discussing the behaviour of the steam temperature (Figure 3.9f). In the first part of the transient, its evolution is characterized by the typical dynamics of a stand-alone SG. The initial sudden rise is due to the fact that the turbine admission variation causes a mass flow rate reduction and, at constant thermal power exchanged, the steam gets hotter and hotter. Nevertheless, the overall tube is immediately affected by the pressure change and by the consequent saturation temperature increase, and therefore the overheated region within the tube gets shorter and the steam temperature decreases. After 70 s, the SG begins perceiving the effects ensuing from the core evolution and then, according to the core outlet lead temperature, the steam temperature increases until the system settles at a higher new steady-state value. The main outcome of this simulation is that, in virtue of the values assumed by the reactivity feedback coefficients, the ALFRED reactor response following the turbine admission valve variation can be considered similar to that of PWRs (“reactor follows turbine”), though the characteristic time constants are definitely longer. It is worthwhile to remind that, even this similarity with the classic and well-known PWR concept, the control scheme developed for the PWRs cannot be applied “as it is” to the LFRs due to the different

constraints to be fulfilled (e.g., the lead temperature in the cold pool has to be kept as close as possible to 400 °C).

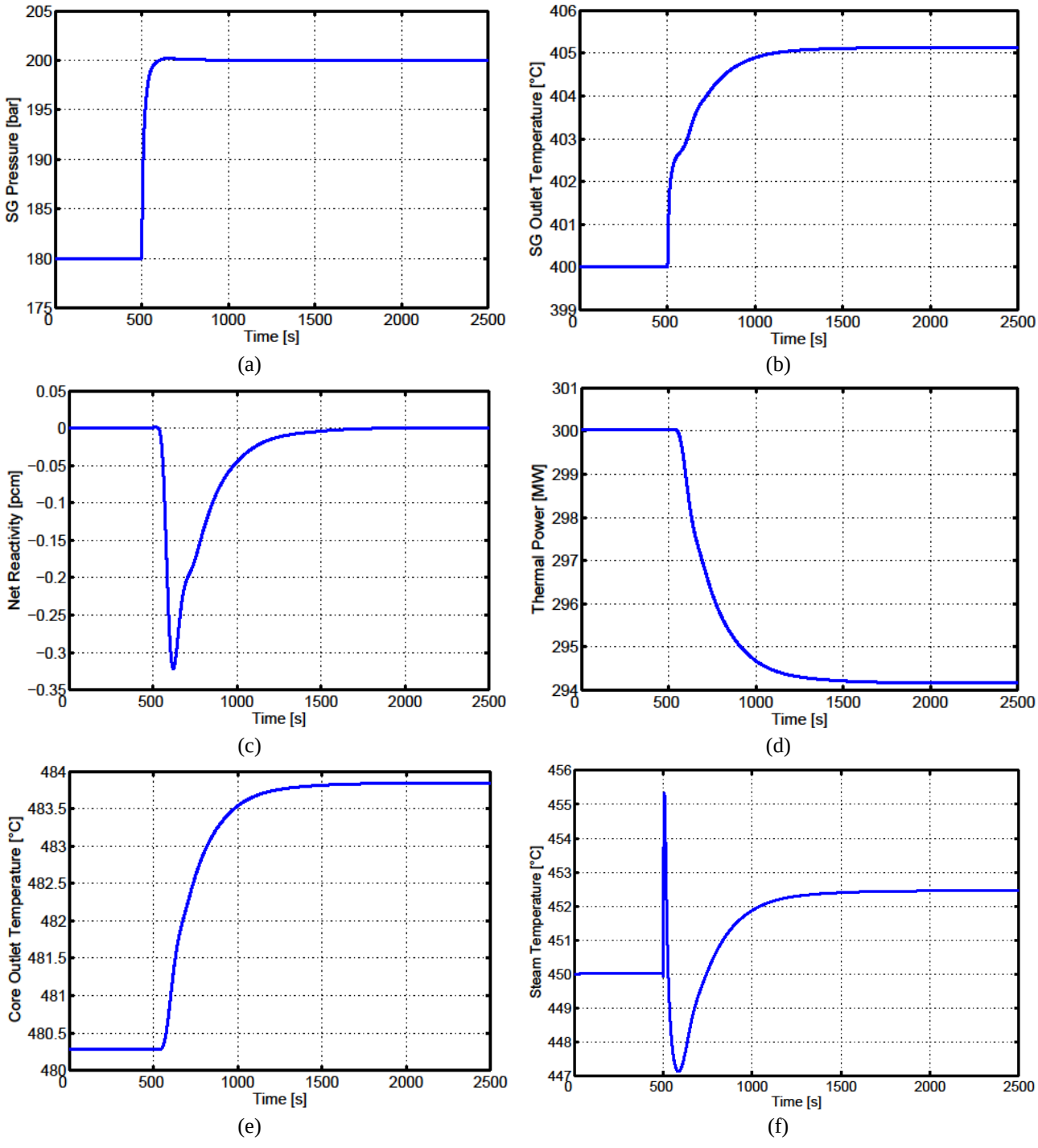

Figure 3.9. Output variables evolution after a variation of the turbine admission valve coefficient: (a) SG pressure variation; (b) lead SG outlet temperature variation; (c) net reactivity variation; (d) core thermal power variation; (e) core outlet temperature; (f) steam temperature variation.

3.2.3. UTOP

A control rods extraction corresponding to a 20 pcm step reactivity variation (Figure 3.10a) has been simulated. This is an interesting operational transient to be evaluated since it involves the dynamics associated to the handling of the control rods, and how this kind of perturbation has effect on the rest of the plant. This core-driven simulation determines an immediate feedback to the SG due to the coolant core outlet temperature enhancement. Thanks to the presence of the pool, the action of the SG on the core, consisting in an increase of the coolant core inlet temperature, is delayed and softened.

As far as the first part of transient is concerned, the behaviour of the system is the same as if a stand-alone core simulation were performed. Indeed, after the step-wise insertion of reactivity given by control rods the power suddenly increases exhibiting the typical prompt jump behaviour and, after a small decrease, reaches the steady state (Figure 3.10b). The reactivity insertion in the core affects the SG as a temperature enhancement of the lead coming from the core (Figure 3.10c). As a direct consequence of the improved heat exchange conditions due to the hotter primary fluid, the steam temperature increases (Figure 3.10d). The abrupt change of the steam density determines a perturbation in the SG pressure (Figure 3.10e), which ends when the primary circuit reaches a new equilibrium condition. The higher thermal power level promotes an enhancement of the lead SG outlet temperature (Figure 3.10f). As far as the core behaviour is concerned, the MOX-based fuel elements, because of the low thermal conductivity, cause a stepwise increase of fuel temperature and, consequently, of the coolant average temperatures (Figure 3.10g-h), after the reactivity insertion. This response produces an immediate feedback on the system due to the Doppler effect and to lead density contribution, which cause an abrupt inversion of the reactivity evolution that quickly gets back to zero.

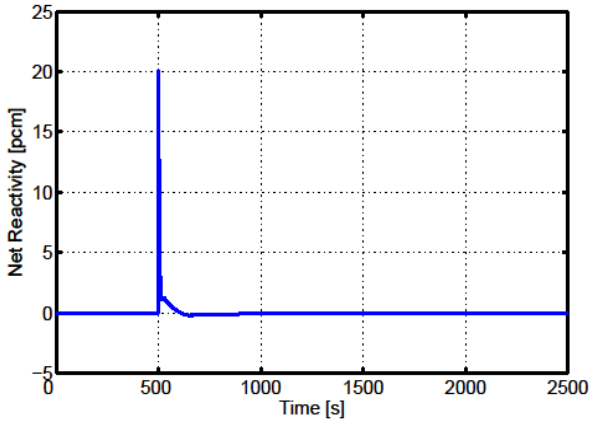

(a)

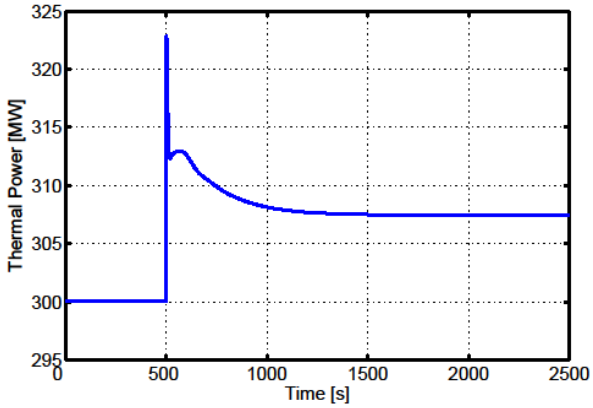

(b)

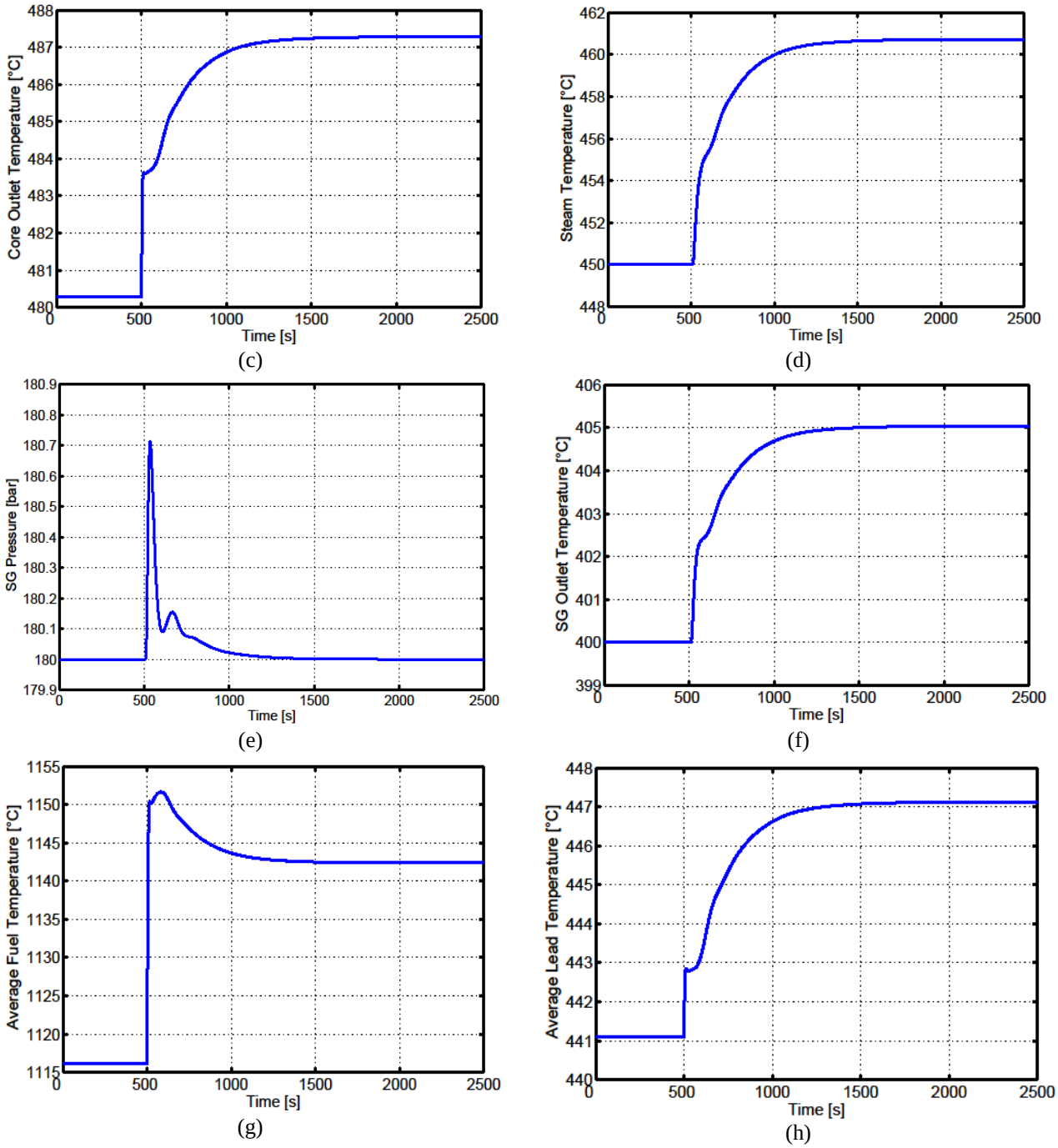

Figure 3.10. Output variables evolution after a step reactivity variation, (a) net reactivity variation; (b) core thermal power variation; (c) core outlet temperature variation; (d) steam temperature variation; (e) SG pressure variation; (f) lead SG outlet temperature variation; (g) average fuel temperature variation; (h) average lead temperature variation.

3.3. Concluding remarks

In this Chapter, the development of the overall plant dynamics simulator oriented to the design of the ALFRED reactor has been presented. The features of the object-oriented modelling language Modelica have been exploited in order to obtain a very flexible, straightforward, and fast-running simulator aimed at performing dynamics analyses and testing in prospect of the control strategies proposed for ALFRED. The simulator has been built by assembling different components from

available libraries, and some of them have been specifically set up to describe the ALFRED reactor configuration. Particular attention has been paid to the assessment of the reactivity feedback and to the bypass way with the purpose to use the simulator also for reproducing the system behaviour during other operational modes (e.g., the reactor start-up). The transport delays and the thermal inertia typical of LFRs have been allowed for through the adoption of dedicated components. In addition, the innovative SG bayonet tube and the BoP up to the turbines have been modelled. After having described the main system components and modelling assumptions, the reactor response to typical transient initiators has been investigated. As a major outcome of the dynamics analyses, the coolant cold pool and the time delays have turned out to play an essential role in determining the system characteristic time constants due to its fundamental delaying and smoothing action on the lead core inlet temperature. Results confirm the strong coupling between core and SG, pointing out the characteristic time constants of the various component responses. The simulator has allowed obtaining accurate information on both transient behaviour and new equilibrium values following any perturbation concerning the main control variables. The outcomes of the free dynamics simulations will turn out to be useful to develop plant control strategies. In this prospect, thanks to the possibility of linearizing the constitutive equations of the model ensured by the Dymola simulation environment, it is possible to get the corresponding transfer functions necessary for the tuning of controllers (i.e., a classic proportional-integral-derivative). Secondly, this reliable tool will be employed to assess the validity and the feasibility of the proposed model-based control strategies through the simulation of controlled operational transients (see Chapter 4 and Chapter 5).

4. Full power mode control scheme definition

Outline

The preliminary investigations on plant dynamics constitute a reliable basis for the definition of suitable control strategies. As far as the regulator configuration is concerned, a decentralized control scheme has been considered in virtue of its simplicity of implementation, and of its robustness towards single control loop malfunctions. In order to select the most effective pairings (given that for the considered system neither prior experience nor operational data are available and it was not possible to adopt the LWR procedure), well-proven investigation tools have been employed. In particular, preliminary indications concerning the interactions between system variables have been supported by the outcomes of the Relative Gain Array (RGA). Diffusely employed in industrial applications, this approach has been applied to verify the most efficient control action for each process variable of interest, dealing with an issue that for LFRs has never been studied yet. The performed analysis has shown the importance of adopting the lead mass flow rate in the primary circuit to regulate the lead temperature in the cold leg, allowing to decouple the safety concerns of the primary circuit from the BoP demands. However, for the ALFRED reactor, it has been decided to have the lead mass flow rate fixed to its nominal value. Indeed, operating the reactor with nominal mass flow rate also at reduced power levels ensures benefits to the structural materials, since they would operate at lower temperatures with consequent positive effect on corrosion concerns.
As a last step, the ALFRED control system configuration has been finalized. The regulator design has been developed based on a feedforward-feedback scheme, i.e., four closed feedback loops with implemented Proportional-Integral (PI) controllers and a feedforward action involving the feedwater mass flow rate which allows a more effective lead temperature control in the cold leg, supporting the control action performed by the dedicated PI.

The main results have been published in:

- Ponciroli, R., A., Cammi, A., Lorenzi, S., Luzzi, L, 2014. *A preliminary approach to the ALFRED reactor control strategy*. In: Progress in Nuclear Energy, http://dx.doi.org/10.1016/j.pnucene.2014.01.016 (In press).
- Ponciroli, R., A., Cammi, A., Della Bona, A., Lorenzi, S., Luzzi, L, 2014. *Development of the ALFRED reactor full power mode control system*. In: Progress in Nuclear Energy (submitted).

Introduction

The design of a NPP control system is a multi-step process whose final result is the implementation and the assessment of the dedicated controllers. In this perspective, as a first step, the asymptotic system stability of the ALFRED reactor has been proven and the system robustness at different operational conditions has been assessed (Chapter 2). Secondly, the reactor dynamics has been deeply investigated since these aspects are fundamental for the study of the overall plant performance. A one-dimensional, object-oriented simulator has been developed by adopting the reliable, tested, and well-documented Modelica language (Chapter 3). Different design-basis transient scenarios have been simulated to characterize the system dynamic response and to evaluate the most effective inputs and their influence on the output variables to be controlled, obtaining useful guidelines for the control system definition. These preliminary investigations constitute a reliable basis to develop suitable control strategies.

As far as LFRs are concerned, the control approach adopted in acknowledged reactor concepts, such as LWRs and SFRs, cannot be immediately applied due to the different features related to the use of lead as coolant, and resulting in several constraints on control and controlled variables. Given that for the considered system neither prior experience nor operational data are available, it has been considered necessary to adopt a quantitative well-proven tool. Therefore, the indications provided by the simulation of the system governing dynamics have been supported by a quantitative technique such as the Relative Gain Array (RGA) method (Bristol, 1966). This tool allows deriving the most efficient control strategy starting from the constitutive equations of the physical system. Through the RGA approach, it has been possible to evaluate the impact and the effectiveness of two different control strategies, based on different control variables, and to compare the performance of the proposed control solutions.

4.1. Pairing selection among control and controlled variables

Generally, most of the physical systems may be modelled as Multiple Inputs Multiple Outputs (MIMO) systems. Since each input performs an influence on the output variables, systems are usually regarded as coupled. These physical bonds strictly limit the direct application of the control techniques developed for Single Input Single Output (SISO) systems (Skogestad and Postlethwaite, 2005). There are two main approaches for controlling multivariable systems. A possible solution is represented by the *centralized scheme* shown in Figure 4.1a. A dedicated block (indicated with $\Delta(s)$) allows treating the MIMO system as if it were constituted by several uncoupled SISO systems, balancing the undesired cross influences between inputs and outputs. Nevertheless, such an option cannot be adopted if the system presents non-minimum phase behaviour and/or pure time

delays as in the case of ALFRED reactor (Chapter 2). In many cases, these severe limitations suggest to employ a different approach, known as *decentralized control* (Figure 4.1b), hence the undesired couplings between input and output cannot be compensated. In such a scheme, the selection of the most effective input (u) to control a specific output variable (y) are performed according to the level of interaction (*pairings selection*). Even if the performance of a decentralized scheme is poorer than the one of a centralized scheme, this configuration allows overcoming many limitations. In particular, the operation and maintenance of controllers are favoured by the simplicity of their implementation, and the resulting system is robust with respect to malfunctioning of the single control loops.

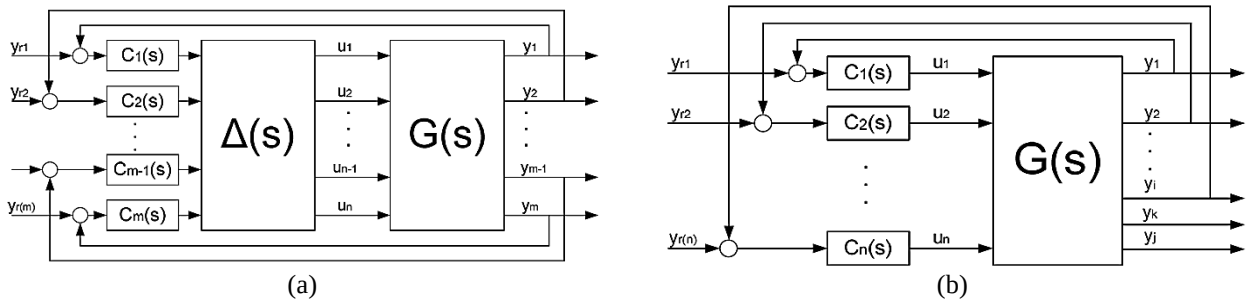

Figure 4.1. Representation of a centralized control scheme (a), and of a decentralized control scheme (b). In particular, the physical process to be controlled (*G(s)*), the several implemented controllers ($C_i(s)$), the system output variables (y_i), the corresponding set-points (y_{ri}), and the system input variables (u_i) are shown.

4.1.1. Relative Gain Array matrix pairing technique

In a decentralized control scheme, the first step is constituted by the selection of the most effective pairings between control and controlled variables. Accordingly, the input showing the most relevant interaction with a certain output, and at the same time not significantly affecting the behaviour of other variables of interest, constitutes the ideal candidate to achieve a feedback control loop. Interactions among variables constitute a structural feature of the system, and the best hints for the coupling can be derived by analysing the free dynamics response of the plant. These indications can be supported by dedicated techniques, such as the RGA (Bristol, 1966), which has been widely used in several industrial fields including chemical processes and power production (Papadourakis et al., 1987), and recently adopted in nuclear applications as well (Guerrieri et al., 2013). It is a heuristic approach which allows determining the most efficient input to control each process variable of interest. In addition, it provides useful suggestions about how the decentralized control system has to be structured. The RGA method is initially considered as a quantitative measure interaction at zero frequency for asymptotically stable processes, represented through a square transfer matrix (e.g., the number of inputs is equal to the number of outputs). The information provided by this measure may be adopted in nuclear plant control system since the characteristic bandwidth is usually composed of very low frequencies.

The effectiveness of a feedback control loop can be assessed by characterizing the MIMO system behaviour both in *open loop* and *closed loop* conditions. As far as the open loop gain is concerned, considering the system at equilibrium condition for fixed constant values of control variables, a step variation of amplitude δu_i on a certain input u_i is carried out, causing a variation of the quantity δy_{jOL} of each output variable y_j (Figure 4.2a). The open loop gain is defined as

$$g_{ji} = G_{ji}(0) = \frac{\delta y_{jOL}}{\delta u_i} \tag{4.1}$$

where $G_{ji}(0)$ is regarded as the gain of the transfer function between u_i and y_j. Instead, for the closed loop gain, it is assumed that, against the same variation of δu_i, an action is performed on all the other input variables in order to keep all the other outputs fixed, except for y_j, thanks to the action carried out by the other inputs (Figure 4.2b). If the variation of y_j in closed loop configuration is indicated with δy_{jCL} , the closed loop gain between u_i and y_j can be defined as

$$h_{ji} = \frac{\delta y_{jCL}}{\delta u_i} \tag{4.2}$$

If the static gain for the open loop (g_{ji}) and for the closed loop (h_{ji}) are evaluated for all the input-output pairs, the matrix of relative gains Λ, the RGA matrix, can be derived. This matrix can be regarded as a quantitative measure of the input-output interaction at zero frequency for asymptotically stable processes. In particular, the elements λ_{ji} of this matrix, namely the relative gain of the pair (u_i, y_j), are defined as:

$$\lambda_{ji} = \frac{g_{ji}}{h_{ji}} \tag{4.3}$$

In a control system design perspective, when the value of a λ_{ji} element approaches unity, there is a fair interaction that can be exploited, whereas if the value of a λ_{ji} element approaches zero the involved variables can be considered uncoupled. If the matrix element λ_{ji} is negative, it means that the control action may produce opposite effects to the desired ones on the controlled variable, depending on whether feedback control loops involve other output variables or not (Skogestad and Postlethwaite, 2005). It is possible to demonstrate that the calculation of Λ can be made adopting the relation

$$\Lambda\big(\mathrm{G}(0)\big) = \mathrm{G}(0) \otimes (\mathrm{G}(0)^{-1})^T \tag{4.4}$$

where ⊗ represents the Schur product and T stands for the operation of matrix transposition. One of the main practical advantages of the RGA matrix is that it produces acceptable results even if it is evaluated from the static transfer matrix of the system. Despite the RGA is derived from $G_{ji}(0)$, its outcomes provide satisfying results for system dynamic response as well, characterizing its non-zero frequency behaviour.

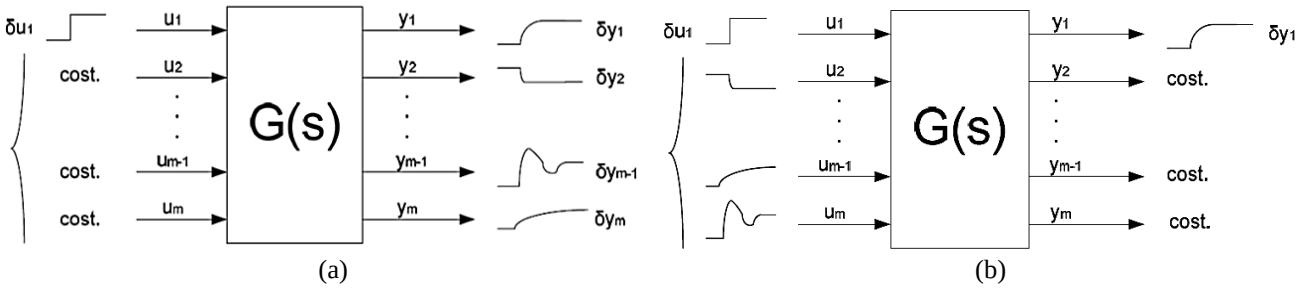

Figure 4.2. Representation of an open loop response (a), and of a closed loop response (b). In particular, the physical process to be controlled (*G(s)*), the system output variables (y_j), the corresponding variation (δy_j), the system input variables (u_i), and the corresponding variation (δu_i) are shown.

4.1.2. Non-square Relative Gain matrix pairing technique

In common applications, the RGA matrix cannot always be applied since the physical system must have the same number of inputs and outputs. Indeed, most of the systems present a number of outputs which is higher than the number of inputs, and thus it is necessary to redefine a formal procedure so as to perform the pairing selection. Such a method allows obtaining a relative gain matrix for non-square systems (i.e., *Non-square Relative Gain array*, NRG) (Chang and Yu, 1990), which is indicated with $\Lambda^{\dagger}$, and can be evaluated through the following relation:

$$\Lambda^{\dagger}\left(\mathrm{G}(\mathrm{j}\bar{\omega})\right) = \mathrm{G}(\mathrm{j}\bar{\omega}) \otimes \left(\mathrm{G}(\mathrm{j}\bar{\omega})^{\dagger}\right)^{\mathrm{T}} \tag{4.5}$$

where $\mathrm{G}(\mathrm{j}\bar{\omega})^{\dagger}$ is the Moore-Penrose pseudo-inverse of $\mathrm{G}(\mathrm{j}\bar{\omega})$. In this case, the pairing process is performed in two phases:

- squaring down of the original system (i.e., disregarding the less relevant outputs in order to obtain a square input-output matrix)
- choice of the input-output pairs.

The squaring down is performed by computing the sum of the elements on each row of the NRG matrix which produces the Row Sum (RS) vector. The outputs associated to the largest figures of the RS vector are the most influenced ones by the inputs variation and thus the most relevant in a control perspective. At this point, the choice of the pairs can be made either through the RGA matrix of the reduced system or through the NRG matrix after having removed the rows

related to the outputs considered useless for the control adopting the same selection criterion used in the RGA approach.

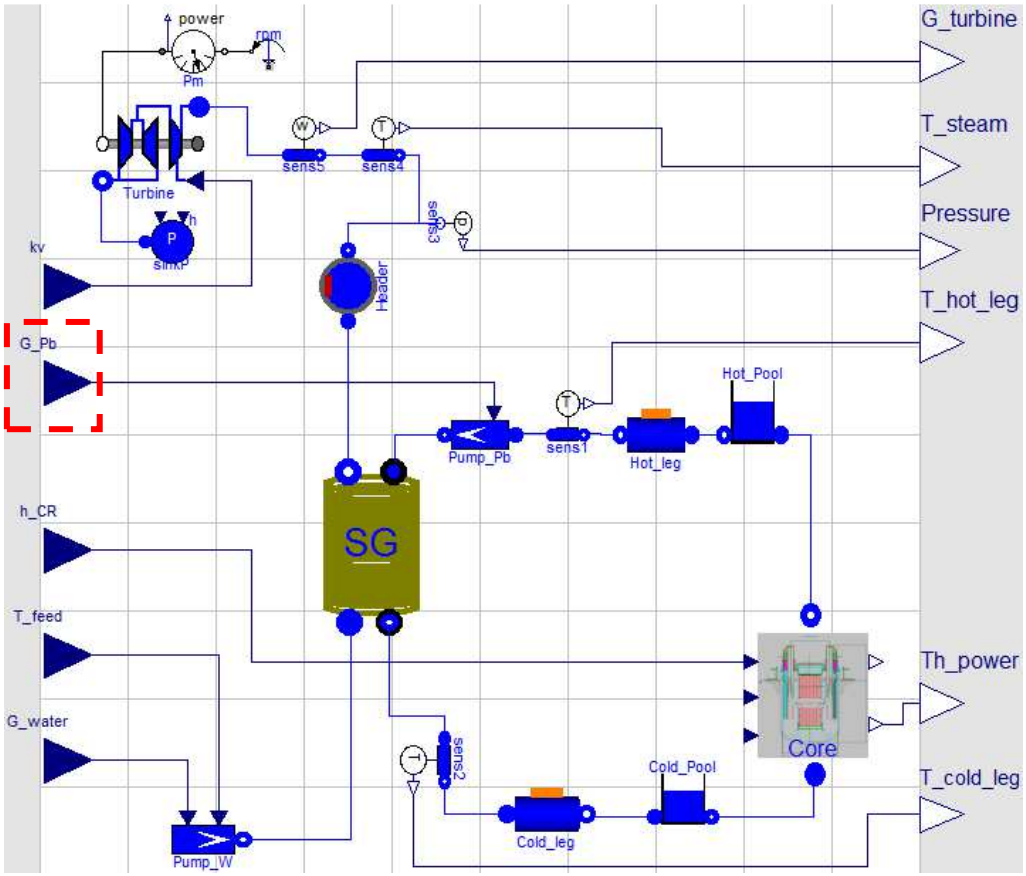

Figure 4.3. ALFRED reactor model configuration. In particular, the primary circuit lead mass flow rate is either considered as a control variable or as a system parameter.

4.2. ALFRED control strategy definition

In a NPP, the most important variable to be controlled is the thermal power produced within the core. As far as the conventional part of the plant is concerned, the other controlled variables are the SG pressure and the steam temperature at the turbine inlet, which should be kept as close as possible to their respective nominal values. The main advantages of running the SG at constant pressure (i.e., the current procedure in the Rankine cycle-based power plants) is the possibility of quickly varying the power produced so as to be adapted to the load demands, and the possibility to avoid thermo-mechanical stresses in the SG at load variations.

As far as the ALFRED primary loop is concerned, the controlled variable which is subject to the most severe constraints is the lead temperature at the SG outlet, called also *cold leg temperature*. Indeed, the control of this variable of interest is particularly concerning, since it has to be set in a narrow range. Low temperatures may lead to a degradation of structural steels due to the embrittlement enhanced by fast neutron irradiation (380 °C, lower limit). On the other hand, if the

lead temperature rises too much, the reactor vessel may overcome the design limits concerning thermal creep (420 °C, upper limit).

As common in the NPP experience, the system has turned out to be *underactuated*, i.e., the manageable inputs are fewer than the variables to be controlled. Among the possible control variables, the coolant mass flow rate in the primary loop constitutes a key-issue in the definition of the control strategy for the ALFRED reactor. One of the major efforts in the development of LFR concept is the design of pumps which operate in highly aggressive lead environment. In the reactor layout, the coolant is currently envisaged to be driven by axial pumps requiring a constant number of revolutions per minute. Moreover, working at nominal mass flow rate also at lower power levels than the nominal one brings benefits as far as structural materials are concerned, since they would operate at reduced temperatures with consequent positive effects on corrosion. Despite these considerations, it may be worthwhile considering the possibility of adopting the lead mass flow rate in the primary loop as a control variable to ensure a more flexible reactor operation. Therefore, two control schemes have been studied in order to evaluate the consequences on the control system definition of considering it either as a system input, or as a parameter which remains fixed at different operating conditions.

In order to develop a control system for the ALFRED reactor, the object-oriented model of the entire plant has been linearized around nominal condition, and then the NRG method has been applied. Based on both the outcomes of the ALFRED free dynamics investigations (Chapter 3) and the results of the NRG analysis, a decentralized control scheme has been chosen because of the presence of non-minimum phases and pure time delays mainly due to the reactor pool-type configuration. Two control strategies have been proposed and discussed depending on whether the lead mass flow rate is considered or not as a control variable.

4.2.1. System model linearization

In order to adopt the NRG tool, the object-oriented model has been linearized in the neighbourhood of the nominal power conditions by means of a useful feature of the Dymola simulation environment. As a result of this operation, the resulting model has been expressed by adopting the matrix-based form of the Linear Time-Invariant (LTI) systems

$$\begin{cases} \delta\dot{x}(t) = A\delta x(t) + B\delta u(t) \\ \delta y(t) = C\delta x(t) + D\delta u(t) \end{cases} \tag{4.6}$$

Once obtained a 194th order system, it is necessary to reduce the system to a more suitable and manageable size. There are several procedures that can be implemented to achieve a satisfactory order reduction and there are several examples in literature (Moore, 1981; Van Dooren, 2000).

Hereafter, the methodology adopted by MATLAB® will be referred, which provides precompiled functions to reduce LTI models. It consists in an appropriate coordinate transformation, which allows obtaining a balanced and equivalent representation, in terms of system state variables, so that observability and reachability Gramians result to be equal and diagonal (Moore, 1981). The balanced model that is obtained is then defined by

$$\begin{cases} \delta\tilde{\dot{x}}(t) = \tilde{A}\delta\tilde{x}(t) + \tilde{B}\delta\tilde{u}(t) \\ \delta\tilde{y}(t) = \tilde{C}\delta\tilde{x}(t) + \tilde{D}\delta\tilde{u}(t) \end{cases} \tag{4.7}$$

where

$$\tilde{A} = {T_L}^{-1} A T_L$$
$$\tilde{B} = {T_L}^{-1} B$$
$$\tilde{C} = C T_L$$
$$\tilde{D} = D$$

The matrix that realizes the change of coordinates (indicated with T_L) can be derived according to the procedure indicated by Laub (Laub et al., 1987). By removing the undesired states, a 43th order reduced balanced system has been derived. At this point, it is necessary to assess this approximation verifying that the linearized reduced order model ensures to effectively reproduce the system response during operational transients. In Figure 4.4, the same transients have been performed both on the non-linear model and the reduced linear model. The comparison of the respective results for the variables of interest has confirmed the accuracy of the approximation. The variables of the resulting model are quite heterogeneous and include variables such as temperature, position, pressure, normalized turbine admittance, etc. The system turns out to be ill-conditioned and it is necessary to scale all the involved variables in order to get the different variations to have the same order of magnitude. After having normalized the LTI model, the NRG method has been adopted so as to verify the level of decoupling of the selected pairings.

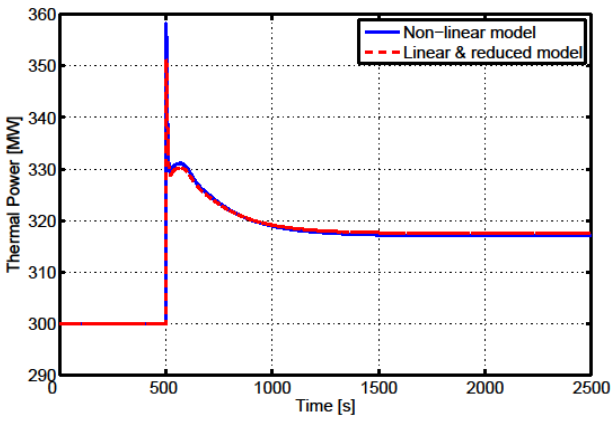

(a)

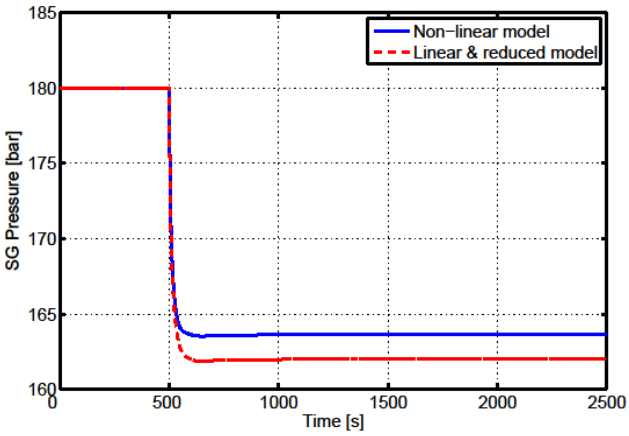

(b)

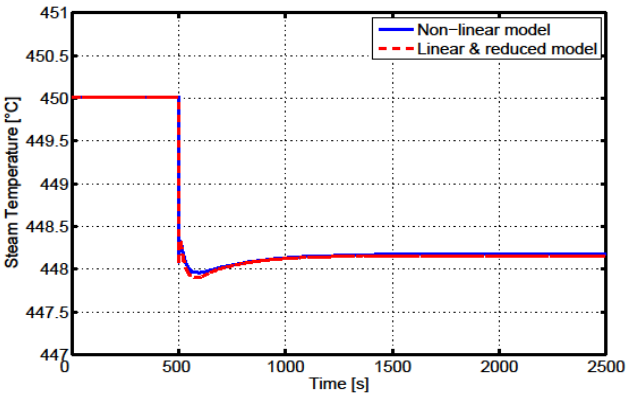

(c)

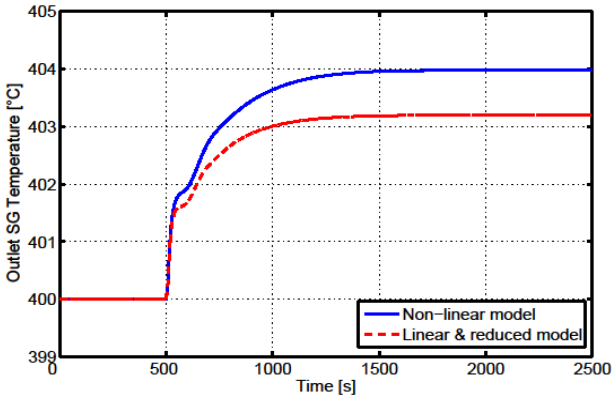

(d)

Figure 4.4. Comparison between linearized model and non-linear model responses: (a) power transient following a step input given on the control rods position (-3mm), (b) pressure transient following a step input given on the turbine admission (+0.1), (c) steam temperature transient following a step input given on the attemperator mass flow rate (+1kg/s), (d) temperature in the cold leg transient following a step input given on the water mass flow rate (-5%).

4.2.2. Five input control strategy

As shown in Figure 4.3, the lead mass flow rate (*G_Pb*) is operated as a system input in the 5-input control strategy. The outcomes achieved by means of the NRG method, shown in Table 4.1, suggest to use this control variable to maintain the lead temperature in the cold leg (*T_cold_leg*) close to its nominal value. In addition, the values representing the interactions between lead mass flow rate and other outputs are sufficiently low so as to allow the closure of a feedback control loop without problematic interactions with other output variables.

Table 4.1. Pairing selection performed by means of the NRG method (5-input control strategy). The rows in grey represent the outputs that have been discarded for control purposes, whereas red values represent the elements corresponding to the selected input/output pairs.

OUTPUTS	INPUTS				
	T_feed	***G_water***	***h_CR***	***G_Pb***	***kv***
T_steam	**0.4169**	0.0082	0.1729	0.0274	-0.0006
T_fuel	0.0478	0.0003	0.2683	-0.0008	-0.0002
Pressure	0.0000	-0.0021	-0.0000	-0.0000	**0.9989**
G_turbine	-0.0000	**0.9986**	-0.0000	-0.0000	-0.0000
T_cold_leg	0.1597	-0.0019	0.0741	**0.5911**	0.0007
Th_power	0.2757	-0.0007	**0.4267**	-0.0018	0.0004
T_hot_leg	0.1000	-0.0024	0.0581	0.3841	0.0009

As far as the remaining control loops are concerned, it appears clear that the steam temperature (*T_steam*) and mass flow rate (*G_turbine*) can be governed by the feedwater temperature (*T_feed*) and mass flow rate (*G_water*), respectively. On the other hand, the core power (*Th_power*) and the SG pressure (*Pressure*) can be regulated by adjusting the CR position (*h_CR*) and the turbine admission valve opening (*kv*), respectively. Finally, two outputs out of seven have been necessarily excluded in order to control the remaining variables of interest with the available five inputs. In particular, the fuel (*T_fuel*) and the hot leg (*T_hot_leg*) temperatures have been left out since they

are of secondary importance compared to the other output variables in the perspective of controlling the power plant. Moreover, the poor value of the feasible pairings induces to eliminate them since their control would not be very effective in any case.

4.2.3. Four input control strategy

In the 4-input control strategy, the lead mass flow rate (*G_Pb*) is kept fixed at its nominal value, hence it does not constitute an input. The lead temperature in the cold leg (*T_cold_leg*) must be governed by adopting another input, and the NRG outcomes suggest to use the feedwater temperature (*T_feed*), as shown in Table 4.2. This coupling, despite being the only way to regulate the SG outlet lead temperature, determines a series of issues which complicate the control scheme design making the system less flexible. First of all, when the lead mass flow rate is a system input (5-input control scheme), the feedwater temperature is the second choice, indicating that the pairing (*T_feed*, *T_cold_leg*) is less efficient. Moreover, there are technological constraints strictly limiting the feedwater temperature range. In particular, the feedwater temperature at the SG inlet cannot exceed 355 °C (i.e., water saturation temperature at the SG nominal pressure) because this eventuality would produce severe damages to the pumps. In addition, there is a lower constraint given by the temperature of lead melting as well. In order to avoid local solidification, the feedwater temperature must always be kept higher than 327 °C. These bounds determine strict restrictions on the use of this input, which can vary between -8 °C and +20 °C with respect to its nominal conditions.

Table 4.2. Pairing selection performed by means of the NRG method (4-input control strategy). The rows in grey represent the outputs that have been discarded for control purposes, whereas red values represent the elements that correspond to the selected input/output pairs.

OUTPUTS	INPUTS			
	T_feed	***G_water***	***h_CR***	***kv***
T_steam	0.3966	**0.0080**	0.2098	-0.0007
Pressure	0.0000	-0.0021	0.0000	**0.9987**
G_turbine	-0.0000	0.9987	0.0000	-0.0000
T_cold_leg	**0.1623**	-0.0027	0.0586	0.0012
Th_power	0.3529	-0.0002	**0.6407**	0.0000
T_hot_leg	0.0881	-0.0018	0.0908	0.0008

As far as the remaining control loops are concerned, the core power can be controlled by regulating the CRs position (*h_CR*), and the pressure within the SG (*Pressure*) can be governed by adjusting the turbine admission valve (*kv*). Differently from the 5-input case, the fuel temperature (*T_fuel*) does not appear among the outputs since this variable cannot be efficiently controlled by acting on the employed inputs (Table 4.2). For what the feedwater mass flow rate (*G_water*) is concerned, this input has been employed to control the steam temperature at the turbine inlet (*T_steam*). However, as indicated in the NRG outcomes, the level of interaction does not allow

creating an effective control loop. For this reason, an additional feedforward control action has been performed, as it will be described in sub-section 4.2.5.

4.2.4. Definitive ALFRED reactor control scheme

The presented investigations have focused the importance of adopting the lead mass flow rate in the primary circuit to regulate the lead temperature at the SG outlet. In a control-oriented perspective, this possibility would bring relevant benefits to the control of the NPP. First of all, observing the outcomes of the NRG matrix, such a pairing is more effective since it ensures a better decoupling with the other outputs. Moreover, adopting a primary circuit control variable to govern the cold leg temperature would avoid the necessity of employing the BoP control variables. Finally, since lead mass flow rate variations are not restricted by so severe constraints, the system would present a higher level of flexibility during operational transients. However, as it has been mentioned before, for the ALFRED reactor, it has been decided to keep fixed the lead mass flow rate to its nominal value, and then it cannot be operated as it were a system input.

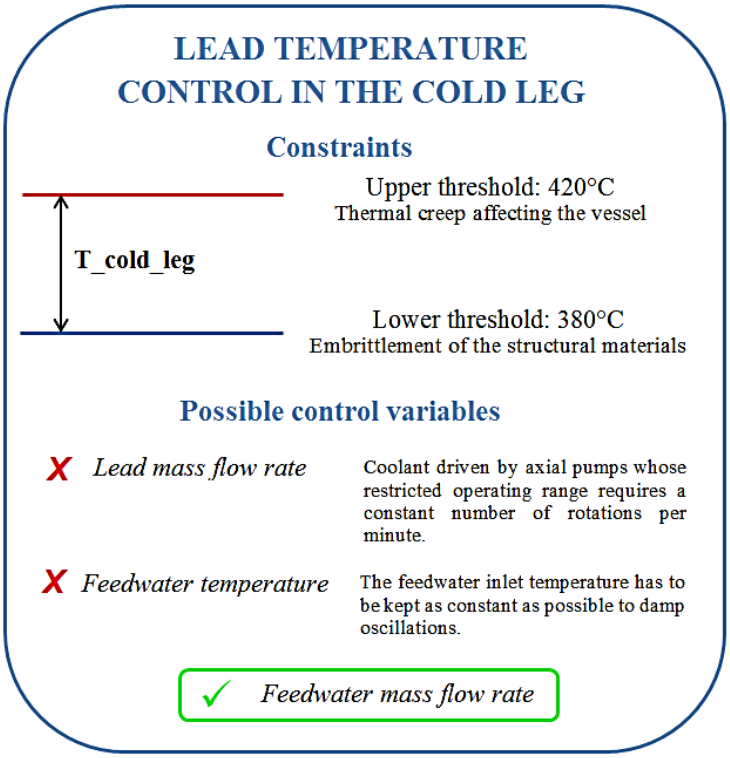

Figure 4.5. Scheme indicating the concerns related to the lead temperature control in the cold leg.

During the project, the necessity of damping possible feedwater inlet temperature variations during operational transients has emerged. Otherwise, the feedwater might flow in the SG inlet at too high temperature (compromising the centrifugal pumps integrity or causing a thermal crisis), or at a too low one (leading to a local coolant solidification at the SG outlet). Therefore, a dedicated device to maintain the feedwater inlet temperature close to its nominal value (335 °C) has been

foreseen. Accordingly, since both the lead mass flow rate in the primary circuit and the feedwater temperature cannot be adopted to govern the lead temperature in the cold leg, despite the lower effectiveness shown by the NRG method outcomes, the water mass flow rate has been employed.

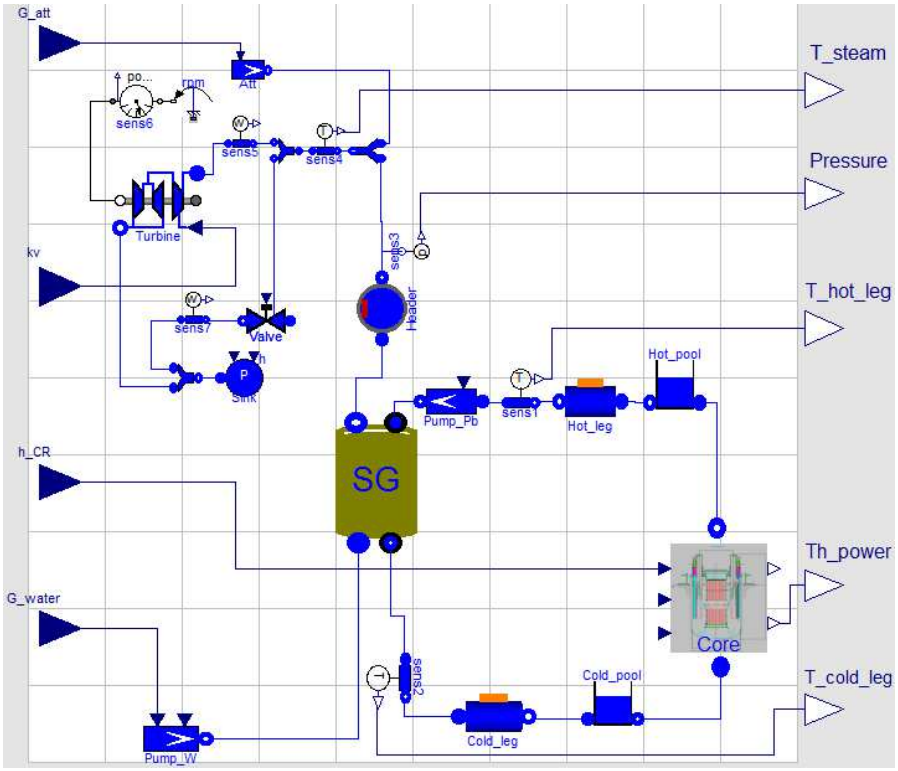

Input variables	Definition
G_att	Attemperator mass flow rate
kv	Turbine admission valve coefficient
h_CR	Control rod position
G_water	Feedwater mass flow rate

Output variables	Definition
T_steam	Turbine inlet steam temperature
Pressure	SG pressure
T_hot_leg	Temperature of lead flowing out the core
Th_power	Thermal power produced within the core
T_cold_leg	Temperature of lead flowing into the core

Figure 4.6. Object-oriented model of the ALFRED reactor. In particular, it is possible to observe the input/output variables employed in the definitive control scheme configuration.

The definitive configuration for the full power mode control scheme foresees four control loops (Figure 4.7). In particular, the thermal power is controlled through the handling of the CRs, the SG pressure is controlled by operating on the turbine admission valve, and the steam temperature is controlled by adding a suitable saturated water mass flow rate to the steam that flows in the turbine (*attemperator*). As far as the lead temperature in the cold leg is concerned, it has been decided to adopt a combined feedforward-feedback scheme, in which the more relevant control action is performed by determining the water mass flow rate to the power level at which the plant is working through an algebraic relationship, whereas the accurate control action is performed by the feedback control loop, always acting on the feedwater mass flow rate. The controller block has been implemented in Simulink® and connected to the nonlinear model exported from Dymola®.

Table 4.3. Full power control loops.

Control variable	Controlled variable	
Control rods height (*h_CR*)	Thermal power (*Th_power*)	Feedback
Turbine admission valve (*kv*)	SG Pressure (*Pressure*)	Feedback
Attemperator mass flow rate (*G_att*)	Turbine inlet temperature (*T_steam*)	Feedback
Feedwater mass flow rate (*G_water*)	Cold leg lead temperature (*T_cold_leg*)	Feedback + Feedforward

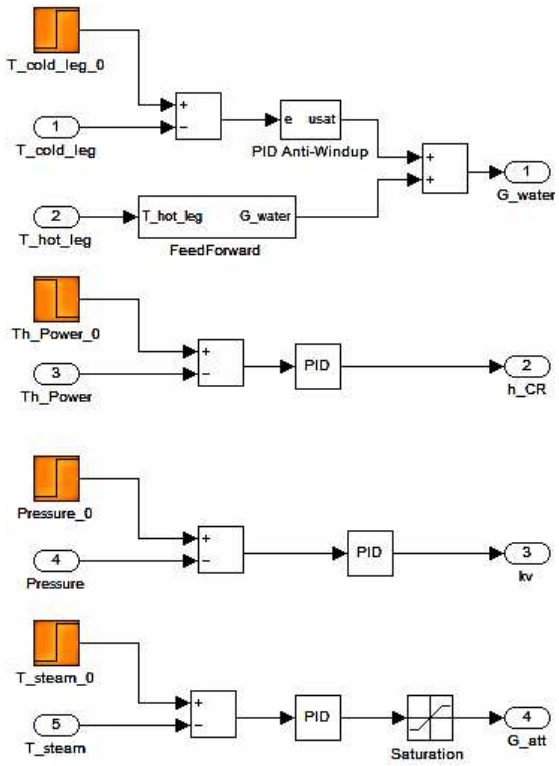

Figure 4.7. Definitive configuration of the control scheme for the full power mode.

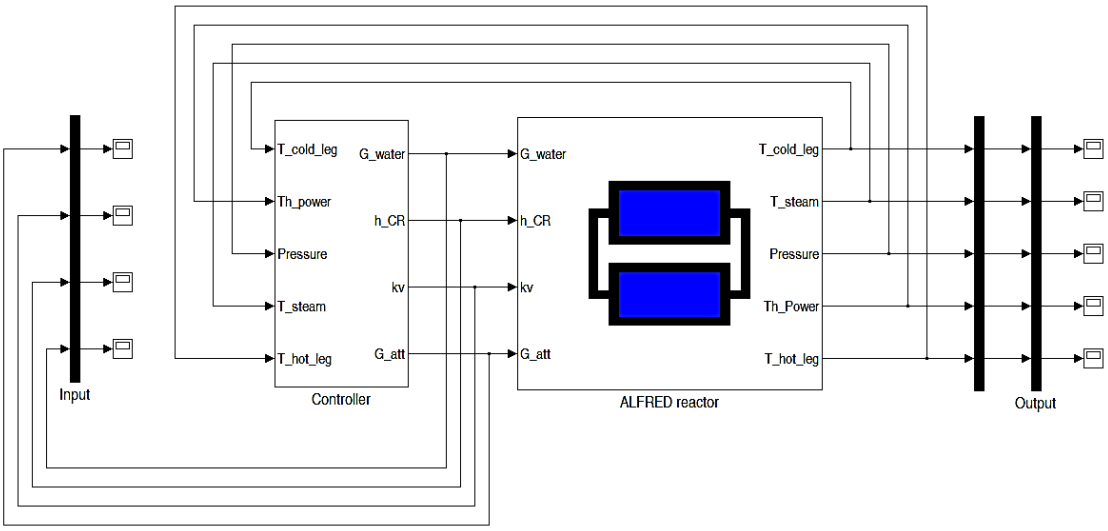

Figure 4.8. Decentralized control scheme adopted for ALFRED reactor control.

Observing the values in Table 4.4, it can be concluded that the *h_CR/Th_power*, *kv/Pressure* and *G_att/T_steam* control loops are scarcely affected by the influences due to control actions performed on other loops. On the other hand, the loop devoted to govern the lead temperature in the cold leg shows non-negligible interactions with other inputs. In this case, the influence of the thermal power has been exploited in the implemented feedforward scheme, whereas the influence produced by the *G_att* and *kv* on *T_cold_leg* must be evaluated and quantified in order to demonstrate that they do not constitute a problem in the control of this output variable.

Table 4.4. Interaction level evaluation performed through the RGA method.

OUTPUTS	INPUTS			
	h_CR	***G_water***	***kv***	***G_att***
T_cold_leg	0.3565	**0.3571**	-0.0401	0.3265
T_steam	0.0002	-0.0002	0.0778	**0.9221**
Pressure	0.0000	0.4456	**0.8045**	-0.2501
Th_power	**0.6433**	0.1975	0.1578	0.0014

4.2.5. Controllers design procedure

As mentioned before, for the proposed control scheme, a decentralized control scheme has been adopted, i.e., the overall MIMO system can be seen as a set of SISO control loops independent of each other. This assumption allows studying separately the different control loops neglecting the inevitable interactions due to control actions performed on other inputs. In order to govern the evolution of the thermal power produced within the core, the lead temperature in the cold leg, the pressure in the SG and the temperature at the turbine inlet, the classic control approach based on a battery of PI (Proportional-Integral) controllers in a decentralized control scheme has been adopted. The control law for PI regulators is given by

$$u(t) = K_p e(t) + K_i \int_0^t e(t)dt \tag{4.8}$$

where $u(t)$ represents the action of the controller, $e(t)$ is the difference between the reference signal and the instantaneous value of the output, K_p is the proportional gain and K_i is the integrator gain. K_p and K_i have been tuned on the linearized system and then it has been verified that performance were satisfying in the nonlinear model as well. These PI regulators are used when the integral action is essential to provide good static performance, but, at the same time, the presence of a zero in the corresponding transfer function is necessary to grant a wider bandwidth compared with the one obtainable by adopting a simple integral action. Moreover, it is important that the error between the set-point signal (e.g., the power requested) and the instantaneous value of the output

(e.g., the power produced within the core) vanishes at the end of the transients (Åstrom and Hagglund, 1995).

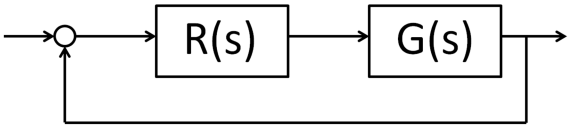

Figure 4.9. Regulator and process transfer functions.

The tuning of PI parameters has been performed by studying the respective transfer functions neglecting the actuators dynamics, according to the desired features for the controlled system response. The overshooting which may jeopardize the components integrity in some cases (e.g., the SG pressure) and the time requested by the controlled variable to reach the new equilibrium condition set constraints on the values of the phase margin (φ_m) and the cut-off frequency (ω_c) of the loop transfer function $L(s)$

$$L(s) = R(s) \cdot G(s) \tag{4.9}$$

where $R(s)$ and $G(s)$ are the transfer functions representing, respectively, the regulator and the process to be controlled (Figure 4.9). In this context, the implemented PI controllers can be calibrated using the procedures commonly employed in the study of the SISO systems. In particular, for each control loop, the tuning has been carried out by adopting the Bode criterion (Levine, 1996). Generally, it is necessary to trace the Nyquist diagram of the loop function to verify the asymptotic stability of the feedback system. On the other hand, when $L(s)$ does not have positive real part poles, the condition expressed by the Nyquist criterion can be verified, taking advantage of the analysis of the Bode diagrams. After having assessed the applicability of the Bode criterion for each control loop, the controllers parameters have been tuned so as to ensure the loop asymptotic stability.

Since the controllers properties in terms of phase and gain margin have been evaluated from the transfer functions of the linearized model around the nominal conditions, the control actions have been optimized for the full power mode. Consequently, the controllers performance will get worse as the system operates at conditions different from the considered ones. In particular, operating the system at reduced loads, the phase margin may turn out to be critically reduced, leading the overall system to become unstable. Therefore, the performed tuning of the regulators parameters ensures large phase margins so as to get satisfying performance even in operational conditions quite different from the nominal ones. In addition, because of the tight connection between the phase margin and the damping, the choice of adopting a considerable phase margin permits to avoid excessive overshooting during transients. Finally, considering the previous constraints, the cut-off

frequencies have been optimized so as to reduce the transient time of the controlled transients. The characteristic times of the PIs have been considered less relevant in the tuning process since the stability, the robustness, and the damping of oscillations in the system controlled response have been favoured in the control design.

In NPPs, manual control is usually adopted while the plant is shut-down and during start-up. Conversely, after having achieved 40% power level automatic control may be initiated. Thanks to the adopted tuning, the system can be properly controlled from 40% to the rated power by adopting the same controllers and there is no need of tuning again the employed PI during the automatic full-power mode operation (i.e., updating the values chosen for K_p and K_i).

Table 4.5. PI controllers parameters.

Control loop		**Controller gain**		**Controller performance**	
Controlled variable	*Control variable*	K_p	K_i	*Phase Margin [°]*	*Cut-off frequency [rad s^{-1}]*
T_cold_leg [°C]	G_water [kg s^{-1}]	$-6\cdot10^{-1}$	$-5\cdot10^{-4}$	99	$3.37\cdot10^{-3}$
Th_Power [W]	h_CR [cm]	$-4\cdot10^{-11}$	$-1\cdot10^{-13}$	110	$3.32\cdot10^{-3}$
Pressure [Pa]	kv [-]	$-3\cdot10^{-7}$	$-1\cdot10^{-8}$	104	0.5418
T_steam [°C]	G_att [kg s^{-1}]	$-1\cdot10^{-1}$	$-5\cdot10^{-2}$	93	0.0833

4.3. Interactions among control loops in the decentralized scheme

The outcomes of the heuristic criterion based on the NRG method allows adopting a decentralized control scheme constituted by four SISO feedback control loops. Interactions among the different control loops can be treated as disturbances, which can modify the output value otherwise determined by the corresponding loop function. In this sense, as shown in Table 4.4, the most problematic loop is the *G_water/T_cold_leg* because of the not negligible interferences. Nevertheless, the impact of the control rods (via the thermal power) on the lead temperature in the cold leg has turn out to be useful, since it has been employed in the feedforward control scheme.

4.3.1. Feedforward control action

The developed scheme has been improved by adding a feedforward control action, in which the water mass flow rate depends on the value of the power exchanged at the SG interface. In order to point out the importance of this control action, it is worthwhile considering the control scheme in which the only feedback action is performed by PI regulators. In this case, when the thermal power produced increases, a lead mass flow rate at higher temperature (i.e., *T_hot_leg* increasing) would flow to the SG. When the hotter lead reaches the SG inlet, the heat transfer conditions are not updated to the new level of thermal power to be disposed. Accordingly, the cold leg temperature tends to rise up, and only then the PI controller increases the water mass flow rate. Therefore, as

long as the hotter lead has not passed through the SG and the lead temperature in the cold leg does not rise up, the PI controller does not perform any control action. This is not an effective way to regulate lead temperature, since the control action is carried out too late. On the other hand, by adopting the feedforward scheme, as soon as the lead flows into the hot leg, the value of the water flow is updated, allowing to establish more effective cooling conditions before hotter lead flows at the SG inlet. Moreover, the proposed combined scheme ensures a more limited use by the PI controller and a non-negligible improvement on the phase margin as well. Indeed, in a NPP a feed-forward logic is often adopted instead of a derivative in order to correct the output for large variations. The expression of the feedforward control action can be obtained from the following equation

$$\Delta h^{ref} \cdot G\_water = \left(T\_hot\_leg - T\_cold\_leg^{ref}\right) \cdot c_p \cdot G\_Pb \tag{4.10}$$

where Δh^{ref} is the reference value for the enthalpy drop along the SG, $T\_cold\_leg^{ref}$ is the reference value for the lead temperature in the cold leg, and c_p is the specific heat of the coolant. It is worth noting that the SG heat transfer conditions are not updated according to the variation of the thermal power produced in the reactor core. The value of the water mass flow rate that allows governing the lead temperature in the cold leg has been obtained from the measurement carried out on *T_hot_leg*, rather than on the core power (Figure 4.10). Indeed, in the latter case, there would be the risk of producing an overcooling of the lead mass flow rate with consequent increase of reactivity and troubling oscillations of the system.

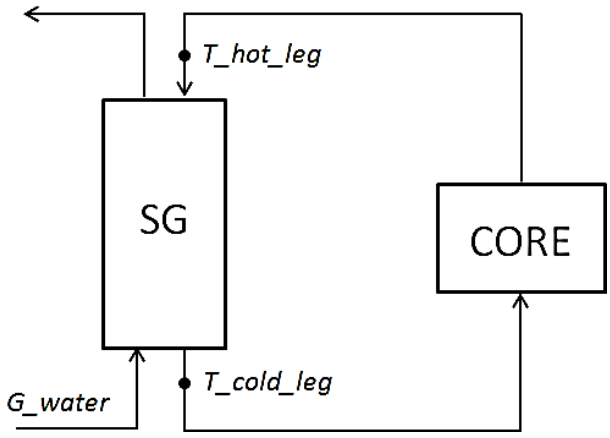

Figure 4.10. Schematic view of the plant.

4.3.2. Evaluation of disturbances on lead temperature in the cold leg control loop

The action of the other inputs on *T_cold_leg* can be regarded as interferences affecting the value of the controlled variable and degrading the performance of the control loop. In order to evaluate the incidence of these effects, the *principle of superposition* has been adopted, assuming

that the disturbance overlaps the undisturbed value of the output variable. In particular, the impact carried out on *T_cold_leg* by the control actions performed on one of the other closed loops have been evaluated. In this perspective, dedicated transfer functions which allow for the interactions between the control loops and evaluate the damping effect ensured by the controllers implemented, have been introduced.

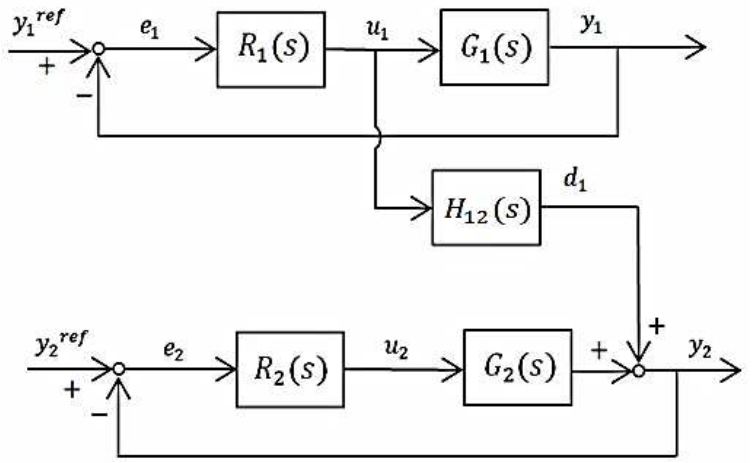

R(s)	Controller transfer function
G(s)	Process transfer function
H(s)	"Cross" transfer function
y^{ref}	Set-point of the control loop
y	Controlled variable
e	Error between y^{ref} and y
u	Control variable
d	Disturbance

Figure 4.11. SISO control loops and representation of the mutual interactions.

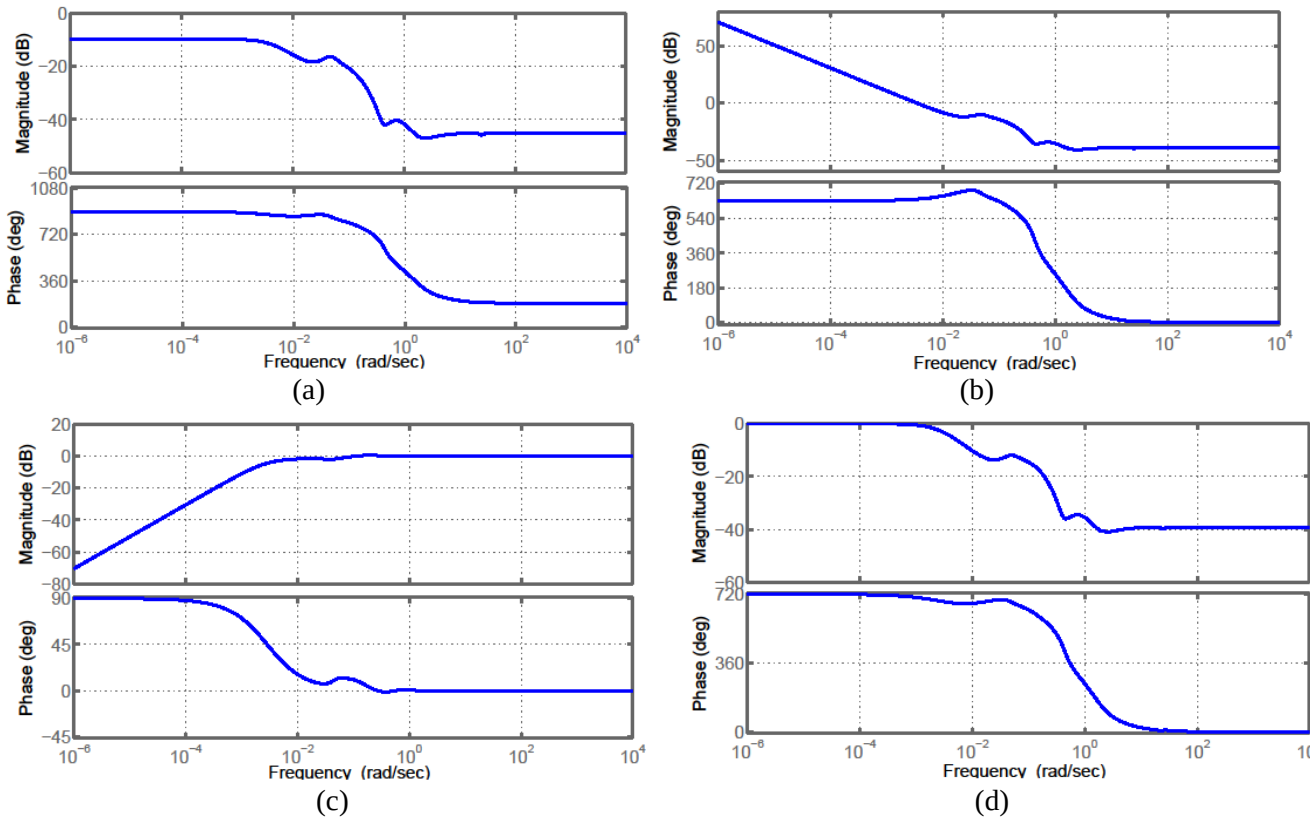

Figure 4.12. Bode diagrams of the different transfer functions, (a) Bode diagram of the *G_water /T_cold_leg* transfer function, $G_2(s)$, which describe the process to be controlled, (b) Bode diagram of the closed loop transfer function, $L_2(s)$, for the *T_cold_leg* control, (c) Bode diagram of the sensitivity function, $S_2(s)$, of the *G_water / T_cold_leg* control loop, (d) Bode diagram of the complementary sensitivity function, $F_2(s)$, of the *G_water / T_cold_leg* control loop.

In Figure 4.11, a representation of two generic control loops is provided, with the disturbance performed by the control variable of the first loop to the controlled variable of the second loop. In particular, the impact of these interferences can be evaluated as follows. Denoted by $H_{12}(s)$, the cross transfer function is defined as

$$H_{12}(s) = \frac{d_1(s)}{u_1(s)} \tag{4.11}$$

The sensitivity function $S_2(s)$ constitutes the transfer function between the noise d_1 and the output y_2, besides representing the transfer function between the set-point ${y_2}^{ref}$ and the error e_2. It accounts for the filtering action performed by the dedicated control loop, indicated with the loop function $L_2(s) = R_2(s) \cdot G_2(s)$. Indeed, under the hypothesis of asymptotic stability, the feedback control loop performs a damping effect on the noise components at lower pulsation than the cut-off frequency.

$$S_2(s) = \frac{1}{1 + R_2(s)G_2(s)} = \frac{1}{1 + L_2(s)} = \frac{{y_2}^{ref}(s)}{e_2(s)} = \frac{y_2(s)}{d_1(s)} \tag{4.12}$$

Another relevant transfer function is the complementary sensitivity function $F_1(s)$, defined as

$$F_1(s) = \frac{R_1(s)G_1(s)}{1 + R_1(s)G_1(s)} = \frac{L_1(s)}{1 + L_1(s)} = \frac{y_1(s)}{{y_1}^{ref}(s)} \tag{4.13}$$

which represents the transfer function between the set-point and the corresponding controlled variable. Finally, the relationship between the reference signal input for the controlled variable 1 (i.e., ${y_1}^{ref}$) and the resulting control action determined by the regulator (i.e., u_1) has been considered. Dividing $F_1(s)$ by the transfer function which describes the characteristic process of the loop 1, $G_1(s)$, the transfer function between the set-point of the control loop 1 and the corresponding input variable is obtained

$$\frac{F_1(s)}{G_1(s)} = \frac{L_1(s)}{1 + L_1(s)} \cdot \frac{1}{G_1(s)} = \frac{R_1(s)}{1 + L_1(s)} = \frac{y_1(s)}{{y_1}^{ref}(s)} \cdot \frac{u_1(s)}{y_1(s)} = \frac{u_1(s)}{{y_1}^{ref}(s)} \tag{4.14}$$

Multiplying this expression by the "cross" transfer function, $H_{21}(s)$, and weighting the result for the sensitivity function of the control loop 2, $S_2(s)$, the overall transfer function $A(s)$ is derived

$$A(s) = \frac{R_1(s)}{1 + L_1(s)} \cdot H_{21}(s) \cdot S_2(s) = \frac{u_1(s)}{{y_1}^{ref}(s)} \cdot \frac{d_1(s)}{u_1(s)} \cdot \frac{y_2(s)}{d_1(s)} = \frac{y_2(s)}{{y_1}^{ref}(s)} \tag{4.15}$$

In particular, the maximum value assumed by $|A(j\omega)|$ over the pulsation range of interest has been considered. This value represents the numerical factor for which the value of the set-point for

the control loop 1, $y_1{}^{ref}$, must be multiplied in order to get the disturbances performed on the controlled variable of the control loop 2, y_2, net of the filtering actions performed by the involved control loops.

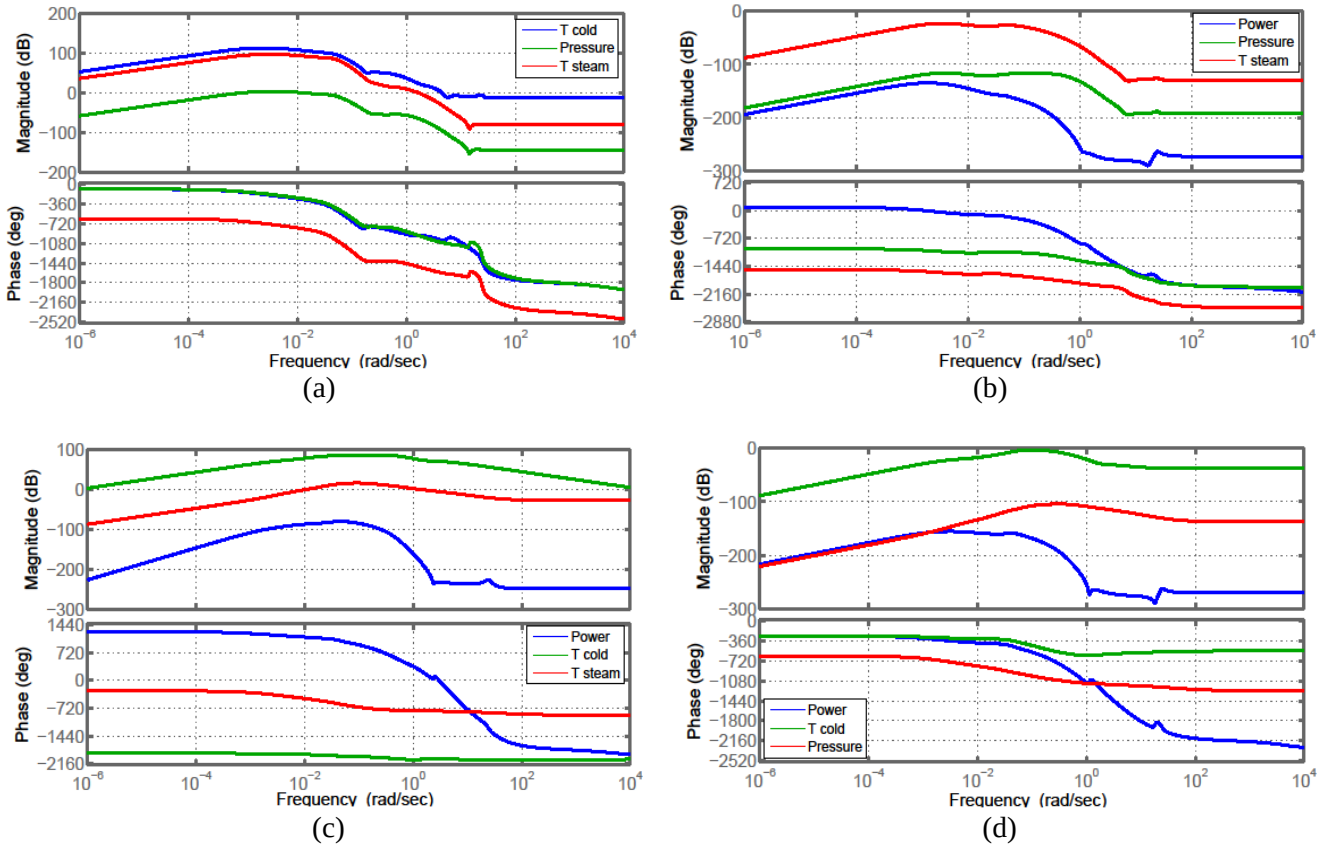

Figure 4.13. Representation of the several transfer functions which allow evaluating the interactions between the control loops, (a) A(s) transfer functions representing the impact of *T_cold_leg* ^{ref}, *Pressure*^{ref} and *T_steam*^{ref} on the output Power, (b) A(s) transfer functions representing the impact of *Th_Power*^{ref}, *Pressure*^{ref} and *T_steam*^{ref} on the output *T_cold_leg*, (c) A(s) transfer functions representing the impact of *Th_Power*^{ref}, *T_cold_leg*^{ref}, *T_steam*^{ref} on the output Pressure, (d) A(s) transfer functions representing the impact of *Th_Power*^{ref}, *T_cold_leg* ^{ref}, *Pressure*^{ref} on the output *T_steam*.

The transfer function $A(s)$ represents the influence of $y_1{}^{ref}$ on y_2, whether the influence performed by u_2 on y_1 is not allowed for. Indeed, the disturbance produced by the first loop on the second one is caused in part by the control variable u_1 and in part by the interference due to the second loop, and the latter exercises through the first loop an interference on the variable of interest y_2. Nevertheless, this additional noise is secondary since its effect is filtered twice by the transfer functions of the first and second loop, before producing an effect on y_2. Therefore, the approximation of neglecting this contribution can be adopted for our purposes and $A(s)$ represents the transfer function between $y_1{}^{ref}$ on y_2.

After having ordered the transfer functions so that the functions *h_CR/Th_power*, *G_water/T_cold_leg*, *G_att/T_steam* and *kv/Pressure* were diagonal, non-diagonal transfer functions *kv/ T_cold_leg* and G_{att}/ *T_cold_leg*, have been considered. This verification has been

performed for the loop *G_att/T_steam* and for the loop *kv/Pressure*, in order to evaluate the impact of the two disturbances on the controlled variable y_2. Once obtained the function $A(s)$ for both the control loops, the maximum values assumed by these functions have been evaluated in order to provide an upper bound of the maximum interference produced on the controlled variable

$$y_2(s) = A(s) \cdot {y_1}^{ref}(s) \Rightarrow \|y_2(j\omega)\| < \|A(j\omega)\| \cdot \left\|{y_1}^{ref}(j\omega)\right\| \tag{4.16}$$

On the basis of this inequality, the maximum value assumed by the module of the transfer function $A(s)$ in the considered frequency range and, once the value of the variation imposed to the set-point, it is possible to obtain the desired upper bound (Table 4.6).

Table 4.6. Upper bound of the disturbances performed by the different control loops on each other.

INPUT VARIATION	CONTROLLED VARIABLES			
	δTh_Power [MW]	δT_cold_leg [°C]	$\delta Pressure$ [bar]	δT_steam [°C]
1MW on $Power^{ref}$	-	0.1827	$1.111 \cdot 10^{-3}$	0.0172
1 °C on $T\_cold\_leg^{ref}$	0.4803	-	0.2259	0.6679
1 bar on $Pressure^{ref}$	0.1603	0.1528	-	0.6157
1 °C on T_steam^{ref}	0.07609	0.0715	$6.912 \cdot 10^{-5}$	-

In order to assess the analytically derived bounds, a simplified model, based on the calculated transfer functions, has been implemented in SIMULINK® (Figure 4.14). The transients have been performed imposing to the system the step-wise inputs shown in the first column of Table 4.6. In particular, as far as the lead temperature evolution is concerned, it is possible to see that the maximum elongations during the transient are coherent with the foreseen upper bound (Figure 4.15).

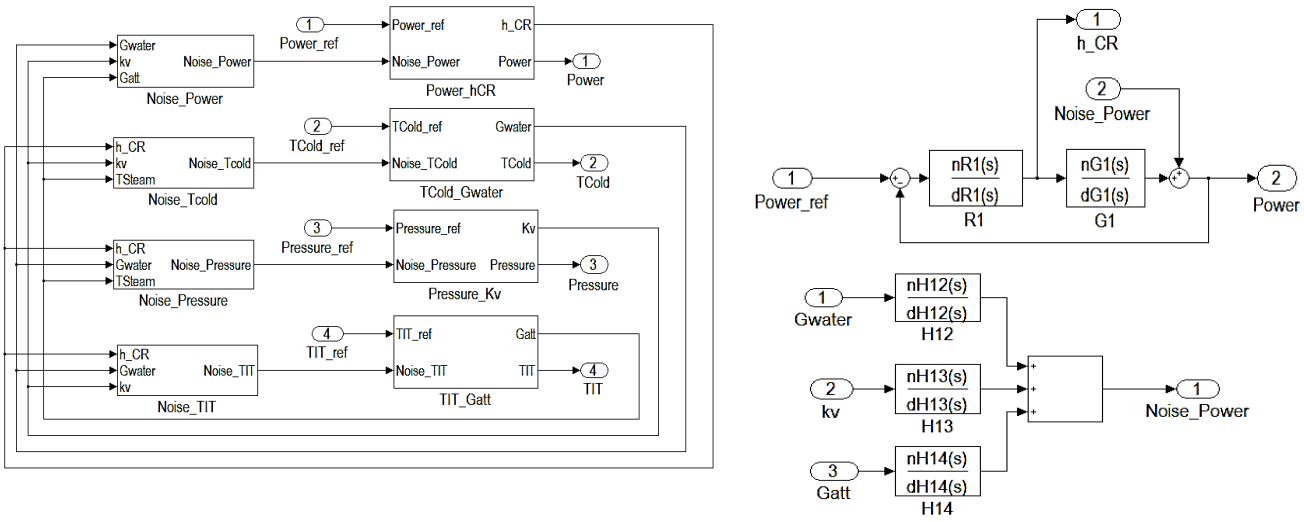

Figure 4.14. Block scheme employed to evaluate the mutual influences of the different control loops on each other.

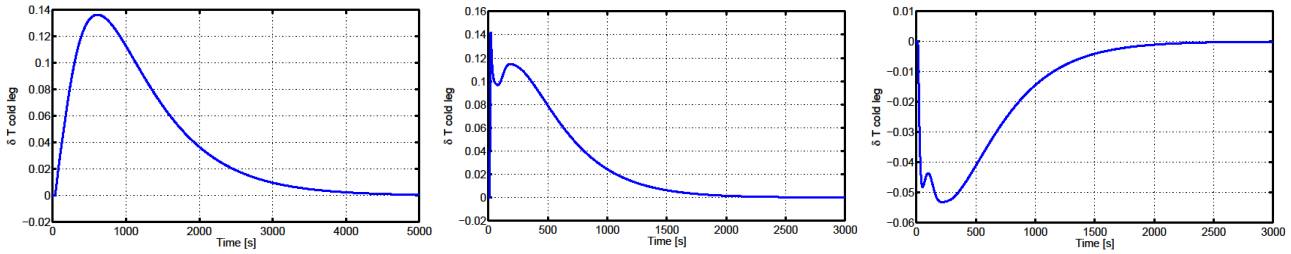

(a) (b) (c)

Figure 4.15. Effects on the *T_cold_leg* due to the different control actions performed by changing the set-point of the other controlled variables, (a) *T_cold_leg* behaviour during a transient produced by a 1 MW variation imposed on Th_Power^{ref}, (b) *T_cold_leg* behaviour during a transient produced by a 1bar variation imposed on $Pressure^{ref}$, (c) *T_cold_leg* behaviour during a transient produced by a 1 °C variation imposed on T_steam^{ref}.

4.4. Rate limiter definition on CRs extraction

In the finalization of the control scheme, after having selected the most effective pairings between the input and output variables and assessed the level of decoupling of the control loops, the actuators design has been carried out. In control systems, limiters are usually set on the rate of variation of the performed control actions, so as to avoid jeopardizing the integrity of the components. This aspect assumes a dramatic relevance in NPPs as far as the externally imposed reactivity control loop is concerned (Bernard, 1999). During any power transient, prompt criticality condition must be avoided, otherwise the multiplying system turns out to be critical without the contribution of delayed neutrons, and the power increase can no longer be controlled by handling the control rods. Since the reactivity cannot be directly measured, most operational procedures do not refer to it. Instead, a dedicated constraint is specified on the value assumed by the *reactor period*, which is defined as

$$\tau^* = \frac{n(t)}{dn/dt} \tag{4.17}$$

The reactor period must be large enough to allow performing control actions on the system. If its value drops below a certain threshold, the power level increases so fast that the actuators does not have the physical time to try to govern the challenging transient. This aspect must be taken into account in the design of the dedicated controller by imposing an upper limit to the maximum extraction speed of the CRs. Based on the outcomes of the linear stability analysis of the ALFRED reactor, the Bode diagram of the transfer function between the reactivity inserted by extracting CRs and the reactivity due to the different thermal feedbacks has been derived. In Figure 4.16, the bundle of Bode diagrams of this transfer function evaluated at different power levels (from 30% to nominal power level) is represented. In particular, Bode diagrams for the module can be approximated by employing first order transfer functions (Åstrom and Hagglund, 1995), as follows:

$$G(s) = \frac{\rho_{temp}}{\rho_{rods}} = -\frac{1}{1 + s\tau_{temp}} \qquad \tau_{temp} = \frac{1}{\omega_{temp}} \tag{4.18}$$

where τ_{temp} is the reciprocal of the characteristic angular frequency at which the Bode diagram undergoes a change of slope.

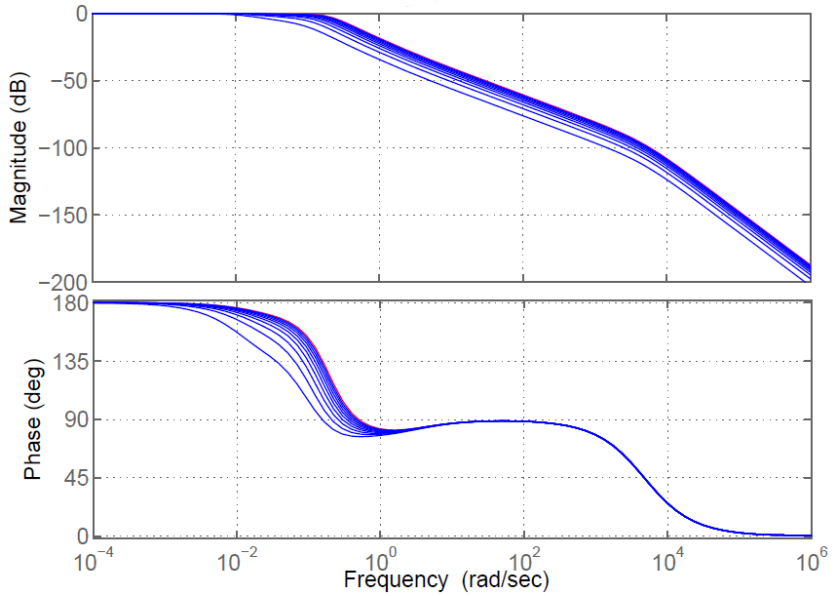

Figure 4.16. Bode plots for the transfer functions between externally-induced reactivity and system reactivity feedback at different power levels.

As far as the reactivity insertion is concerned, it has been modelled as it would take place in a continuous way as a ramp. The slope of this ramp has been parameterized, imposing that the time necessary to the CRs to insert a reactivity equal to one dollar, τ_{rise} , allows the reactivity feedbacks to restore criticality conditions.

$$\frac{d\rho_{rods}}{dt} = \frac{\beta}{\tau_{rise}} \quad \Rightarrow \quad \rho_{rods}(s) = \frac{\beta}{s^2\tau_{rise}} \tag{4.19}$$

where ρ_{rods} is the positive reactivity induced in the system by extracting CRs and $\rho_{rods}(s)$ represents the corresponding Laplace transform. At this point, it is necessary to find out an expression that allows associating the state variable ρ_{rods} to the CRs extraction speed. The curve of integral reactivity shows a sinusoidal dependence of the CRs position such as

$$\rho_{rods}(x) = A_{CR} \cdot sen(B_{CR}x_{CR} + C_{CR}) + D_{CR} \tag{4.20}$$

The positive reactivity insertion rate can be expressed as function of the CRs extraction speed, v_{ext}, as follows:

$$\frac{d\rho_{rods}}{dt} = \frac{d}{dt}\left[\left(\frac{d\rho_{rods}}{dx}\right) \cdot dx\right] = \left(\frac{d\rho_{rods}}{dx}\right) \cdot v_{ext} \tag{4.21}$$

Inserting Eq.(4.20) in Eq. (4.21), it is obtained

$$\frac{d\rho_{rods}}{dt} = \frac{\beta}{\tau_{rise}} = \left(\frac{d\rho_{rods}}{dx}\right) \cdot v_{ext} \;\Rightarrow\; v_{ext}(x) = \left(\frac{\beta}{\tau_{rise}}\right) \cdot \left(\frac{1}{d\rho_{rods}/dx}\right) \tag{4.22}$$

The response of reactivity determined by the thermal feedbacks consequent to a reactivity insertion after a control rods ramp is given by the expression

$$\rho_{temp}(s) = G(s) \cdot \rho_{rods}(s) = -\frac{1}{1 + s\tau_{temp}} \cdot \frac{\beta}{s^2 \tau_{rise}} \tag{4.23}$$

Decomposing this expression by means of the Heaviside method (Ogata, 2009), it is obtained

$$\rho_{temp}(s) = -\frac{\beta\, {\tau_{temp}}^2/\tau_{rise}}{\left(1 + s\tau_{temp}\right)} + \frac{\tau_{temp}}{\tau_{rise}}\frac{\beta}{s} - \frac{\beta}{\tau_{rise}}\frac{1}{s^2} \tag{4.24}$$

Calculating the inverse transform of Eq. (4.24), the system reactivity given by the thermal feedbacks is obtained

$$\rho_{temp}(t) = \left[\beta \frac{\tau_{temp}}{\tau_{rise}}\left(1 - e^{-t/\tau_{temp}}\right) sca(t) - \frac{\beta}{\tau_{rise}} ram(t)\right] \tag{4.25}$$

If the positive reactivity introduced into the system by handling CRs is added to Eq. (4.25), the overall system reactivity during the power transient can be finally achieved

$$\rho(t) = \rho_{rods}(t) + \rho_{temp}(t) = \beta \frac{\tau_{temp}}{\tau_{rise}}\left(1 - e^{-t/\tau_{temp}}\right) sca(t) \tag{4.26}$$

The maximum value assumed by this function is equal to

$$\rho(t)_{max} = \beta \frac{\tau_{temp}}{\tau_{rise}} \tag{4.27}$$

In order to avoid prompt criticality conditions, the system reactivity must not exceed the value of one dollar during operational transients. Consequently, a constraint can be set by imposing that the maximum values assumed by the reactivity is less than a certain fraction of the dollar, represented by a suitable coefficient.

$$0 < K_{safety} < 1 \;\Rightarrow \rho(t)_{max} < K_{safety} \cdot \beta \tag{4.28}$$

Substituting in this expression the definition of the maximum value of the CRs extraction speed obtained in Eq. (4.27) and using the Eq. (4.23), it is obtained

$$\beta \frac{\tau_{temp}}{\tau_{rise}} < K_{safety} \cdot \beta \;\Rightarrow\; v_{ext}(x) \leq \frac{K_{safety} \cdot \beta}{\frac{d\rho_{rods}}{dx}(x) \cdot \tau_{temp}} \tag{4.29}$$

Thanks to the results obtained by performing the linear stability analysis of the ALFRED reactor, it has been possible to derive an upper saturation limit for the CRs extraction speed, which has been implemented in the control scheme. It can be noted that v_{ext} is

- proportional to $1/\tau_{temp}$, i.e., the faster the dynamics of reactivity feedback is, the higher extraction speed of CRs can be adopted and therefore faster power transients can be achieved.
- proportional to β, i.e., the higher the fraction of delayed neutrons is, the easier controlling the transients of the system is.
- inversely proportional to $d\rho_{rods}/dx$, i.e., the higher value of the CRs is, the lower the speed of extraction must be.

Table 4.7. Parameters used to evaluate the maximum CRs extraction speed.

Parameter	Value
K_{safety}	0.4
β	334.6 pcm
τ_{temp}	10s
$\frac{d\rho_{rods}}{dx}$	132.81 pcm·cm^{-1}
v_{ext}	0.126 cm·s^{-1}

4.5. Controlled system simulation

In order to assess the performance of the developed control scheme, several operational transients have been simulated. In this work, two of them have been selected to be presented. The former consists in a 10 % reduction of the reactor power from nominal load conditions, while the latter consists in a 10 % increase of the reactor power starting from 60% load conditions. For each transient, the dynamic behaviour of the controlled variables (i.e., thermal power produced within the core, SG pressure, lead temperature in the cold leg, steam temperature at the turbine inlet) have been reported. In Figure 4.17- Figure 4.18, the red lines represent the set-points of the controlled variables, while the blue ones are their effective trajectories.

4.5.1. 10 % power level reduction starting from nominal conditions

Firstly, the control system effectiveness has been tested around the nominal working point, simulating a step-wise load reduction of 30 MW_{th}. As far as the thermal power control loop is

concerned, the most relevant figure of merit is constituted by the settling time, which is defined as "the time required for the response curve to reach and stay within a 2% of the final value" (Ogata, 2009). In the simulated operational transient, its value is about 700 s and the definitive equilibrium condition is reached in 1000 s, as shown in Figure 4.17a.

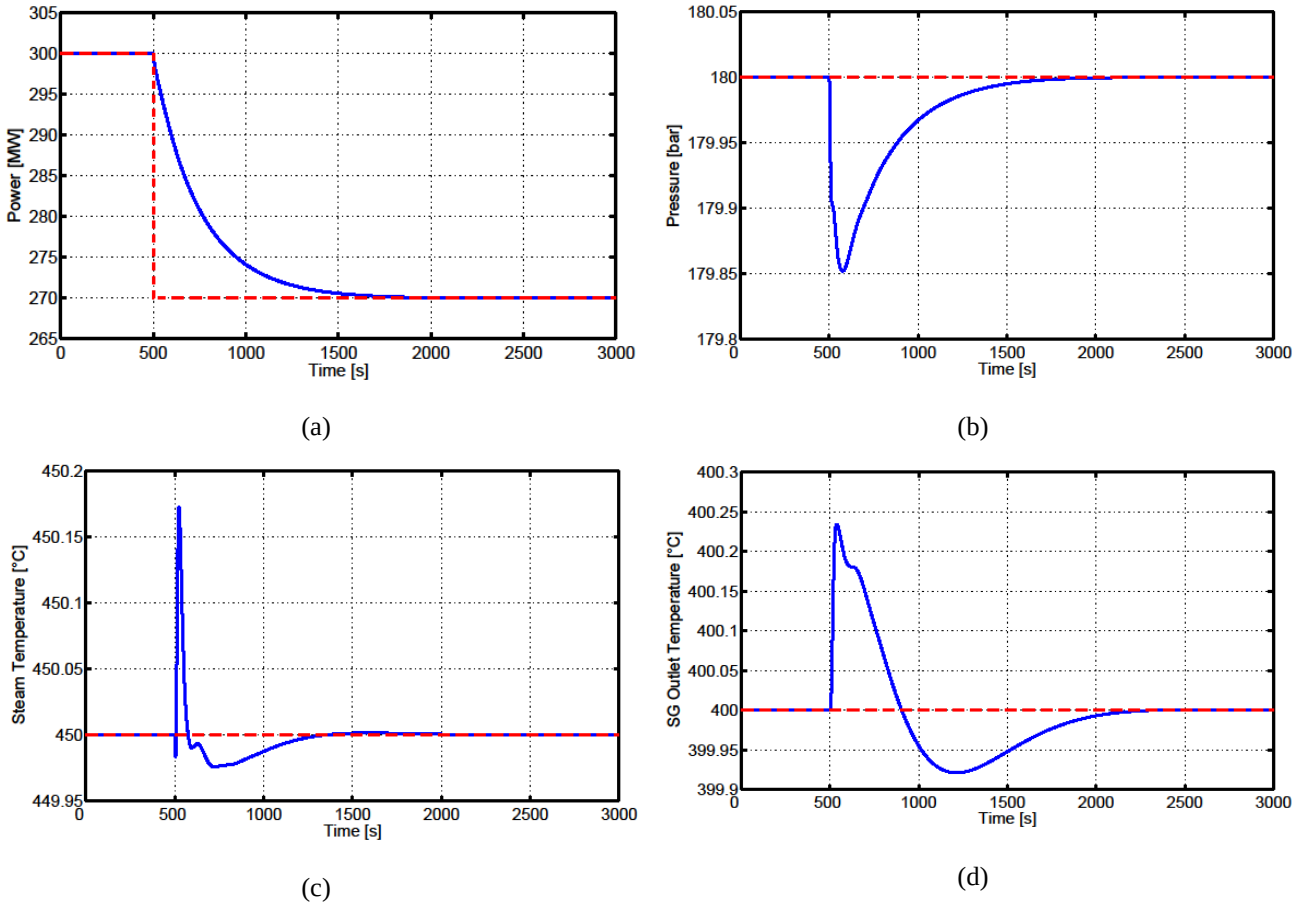

Figure 4.17. Controlled responses of the output variables after a 10% power level reduction starting from nominal conditions, (a) Reactor power evolution, (b) SG pressure evolution, (c) Steam temperature evolution, (d) Lead temperature in the cold leg evolution.

The relevant slowness of the dynamic response is partially due to the choice of reducing the control system performance in order to ensure control system robustness, but it is mainly a inherent feature of LFRs. As observed in the free dynamics simulations (Chapter 3), its characteristic large thermal inertia due to the pool and the transport phenomena along hot and cold collectors inevitably influences the controlled system response. On the other hand, as far as the other control loops are concerned, the SG pressure reaches a maximum elongation of 0.15 bar, while the steam temperature at the turbine inlet never deviates by more than 0.2 °C from its nominal value (Figure 4.17b-c). Finally, the evolution of the lead temperature at the SG outlet (Figure 4.17d) confirms the effectiveness of the proposed control scheme, since the value of the controlled variable never deviates for more than 0.25 °C from the set-point.

4.5.2. 10 % power level increase starting from 60% load conditions

Secondly, a demanding operational transient has been simulated in order to test the performance of the proposed control scheme in quite different conditions from the nominal ones as well. After having achieved 60% load conditions, the system has been stabilized, and then a 10% power increase has been simulated. As it can be seen in Figure 4.18a, the control loop dedicated to govern the thermal power produced in the reactor core shows satisfying performance even at 60% load factor, since the power transient can be considered exhausted within 1000s. It is then relevant to consider the lead temperature in cold leg control loop (Figure 4.18b). Even after a 40% load transient, the adopted control scheme manages preventing the temperature of the lead to deviate by more than 1°C from the reference value.

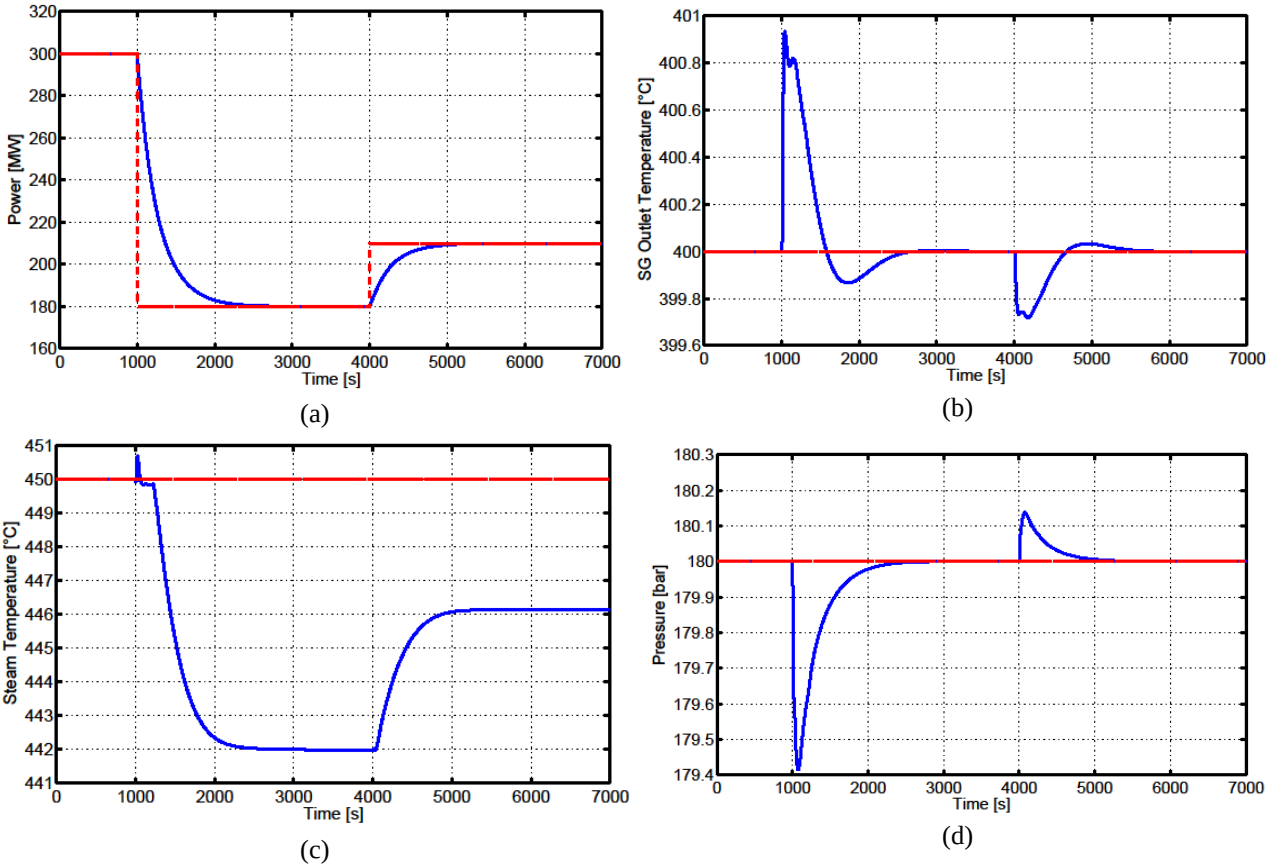

Figure 4.18. Controlled responses of the output variables after a 10% power level reduction starting from 60% load conditions, (a) Reactor power evolution, (b) SG pressure evolution, (c) Steam temperature evolution, (d) Lead temperature in the cold leg evolution.

The most challenging aspect concerns the steam temperature at the turbine inlet, (Figure 4.18c). Indeed, the lead temperature control in the cold leg is performed by operating on the feedwater mass flow rate in the secondary circuit. Therefore, it is not possible to adjust this control variable to meet the BoP demands. In nominal conditions, a minimum flow of water is introduced into the superheated steam mass flow, but during very demanding transients at reduced load conditions the steam temperature cannot be regulated any more. Therefore, the under certain load conditions, it is

not possible to keep the steam temperature close to its set-point. Finally, SG pressure control loop (Figure 4.18d) has demonstrated very satisfactory performance, even after a step change in the power and then after a rather abrupt variation of the water mass flow rate. Indeed, the pressure never deviates for more than 0.5 bar of the set-point, thus avoiding relevant mechanical stress to the SG.

4.6. Concluding remarks

In this Chapter, the development of the control system operating in full power mode, based on the well-proven approach of PI feedback regulators, has been described. For the tuning of the controllers, it has been necessary to adopt a low-order linear model. Afterwards, the nonlinear model has been linearized around full power conditions, its validity in representing system transients has been verified, and finally the order reduction has been performed. After having described the definitive version of the control system and defined the pairings imposed by the technological constraints of the reactor, the procedures used for the parameter tuning of regulators designed to control *Power*, *T_cold_leg*, *T_steam* and *Pressure* have been reported. According to the outcomes provided by the RGA matrix, it has been possible to adopt a decentralized control scheme given that control loops can be regarded independent of each other, except for the *G_water* / *T_cold_leg* loop, in which the influences of other inputs cannot be neglected. In this perspective, the analysis of mutual interactions among loops has been carried out, taking into account also the filtering performed by the PI controllers, whose tuning has allowed to limit the impact of the mutual influences. Since the control system has been designed by adopting the transfer functions derived by the linearized model, its performance will be satisfactory as long as operating in the neighbourhood of equilibrium conditions. The calibration of the characteristic controller parameters has been realized in order to ensure a suitable phase margin to the loop function. In this way, the robustness, the efficiency, and the asymptotic stability on the basis of Bode criterion of the control loop have been ensured, even though the system would operate at lower load factors (i.e., in operating conditions quite different from the rated one). Finally, the effectiveness of each control action and associated control strategy has been evaluated. In particular, two demanding transients for the plant have been analysed and a system response to a 30 MW_{th} increase in the reactor power, starting from 60 % load conditions, has been simulated in order to assess the robustness of the developed control scheme. The obtained results are really encouraging, and indicate the effectiveness of the proposed linear control system, whose controllers parameters have been tuned so as to provide a good compromise among performance, robustness and safety margins, also in conditions very different from the nominal ones.

5. Logic and modulating control for the reactor start-up and coordination with the full power mode

Outline

Once developed the control strategy for the full power mode of the ALFRED reactor, the reactor start-up procedure has been studied, laying the basis for the preliminary version of the control system architecture. As far as the differences will make it possible, it has been considered appropriate to begin from the experience gained in the operation of LWRs. The term reactor start-up refers to the operational sequence whereby all the operating system (i.e., core, primary circuit, pressurizer, SGs, turbines) are brought from cold shutdown to full power conditions. Even though the attainment of the criticality is a major part of this process, the coordination of pressure and temperature for plant heat-up and the initial steam production are fundamental to the plant safety as well. Therefore, it has been tried to redefine the paradigm of the start-up of a conventional reactor in order to adapt it to the constraints and the needs of a LFR. In common practice, the reactor start-up procedure is described by defining the initial conditions of each component of the plant and focusing a sequence of control actions to be carried out. However, such a schematic approach does not allow figuring out quantitatively the problem and, most of all, does not provide information on the control system layout. Hence, the reactor start-up procedure has been represented by adopting a synchronized Petri net (a modelling tool which has several applications in industrial field and in safety risk assessment). It is a useful formalism for the modelling and the analysis of Discrete Event Systems, which allows identifying the events coming from the plant that enable the switches among the modulating controllers. The most important advantage of representing the system desired evolution by adopting such a logic-mathematic formalism is the possibility of getting hints for the development of a control scheme that ensure the system the defined controlled evolution. Indeed, by adopting the Petri net modelling approach, the architecture of the supervisory control system has been built as well, so as to coordinate the switching of the considered operational modes. In this way, a two levels control system architecture has been developed, namely: the "master system" coordinates the plant operation by sending suitable signals to the "slave system", in which modulating regulators have been implemented.

The main results have been published in:

- Ponciroli, R., Lorenzi, S., Cammi, A., Luzzi, L., 2013. *Petri net approach for a Lead-cooled Fast Reactor start-up design*. Proceedings of the International Conference on Fast Reactors and related Fuel Cycles: Safe Technologies and Sustainable Scenarios (FR 13), Paris, France, March 4-7, 2013.

Introduction

Once developed the control strategy for the full power mode of the ALFRED reactor (Chapter 4), the issue concerning the reactor start-up procedure has been studied, laying the basis for the preliminary version of the control system architecture. The expression reactor start-up refers to the procedure whereby all the system components (i.e., core, primary circuit, SGs, turbines, etc.) are brought from cold shutdown to full power conditions, close to the load-frequency control. Even though the attainment of the criticality is a major part of this process, the coordination of pressure and temperature during the plant heat-up and the initial steam production are fundamental to plant safety as well. In the definition of a viable start-up procedure, it has been considered reasonable to begin from the experience gained in the procedure currently adopted in the operation of LWRs, as far as the differences between these two reactor concepts may allow it. In this perspective, it has been tried to adapt the paradigm of the conventional reactor start-up to the constraints and the needs of a Gen-IV reactor such as the LFR. In common practice, the reactor start-up procedure is modelled by defining the initial conditions of the several components of the plant and outlining the set of operations necessary to bring the system to the full power mode. However, such a schematic approach does not provide accurate information about the control system layout, and the regulators ensuring the desired behaviour to the plant.

In this work, a formalization of the candidate procedure for ALFRED reactor start-up has been carried out by adopting a modelling tool not particularly diffused in the nuclear field, such as Petri net (Petri, 1962; Peterson, 1981), which instead has several applications in other industrial applications. By means of this approach, it is possible to:

- Identify the different steps to be taken and establish the necessary system conditions so that the control actions can be carried out;
- Verify the possibility to perform two or more operations in parallel in the system, in order to make more efficient the start-up sequence;
- Represent the controlled evolution of the system in order to obtain hints for the development of the related control system.

Once the configuration of the controllers to be used in each operational mode has been finalized, it is possible to develop the supervisory control system architecture in order to coordinate the transition from start-up to full power mode. Indeed, by employing the Petri nets formalism to describe the system controlled evolution, the configuration of the control system ensuring the NPP to follow the envisaged sequence is derived accordingly.

5.1. Definition of the ALFRED reactor start-up mode

5.1.1. System issues and reactor start-up candidate procedure

In the development of the reactor start-up procedure, the sequence of operations to be taken and their synchronization are fundamentally determined by the fulfilment of the system technological constraints. As it has been mentioned in Section 4.2, the most challenging issue for LFRs regards the lead temperature in the cold leg. Besides the lower limit fixed by the melting point (327 °C), the lead temperature has to be set in a narrow range. Indeed, the vessel temperature should not exceed 420 °C (negligible creep threshold), whereas the minimum temperature is fixed at 380 °C because of the embrittlement of the structural materials enhanced by the fast neutron irradiation.

In this perspective, the coupling between the primary and the secondary circuit during the start-up and the role played by the latter in this phase is a troublesome aspect. For LFRs, this aspect turns out to be more challenging than in other reactor concepts because, during the pressurization and the heat-up of the BoP, the constraints regarding the lead temperature have to be rigorously respected. Therefore, in-vessel heaters may be useful, preventing at the same time dangerous boosts of positive reactivity to the reactor core. Nevertheless, such an aggressive environment may jeopardize the operation of in-core devices. An alternative may be constituted by the use of an auxiliary system which feeds the SG with a reduced overheated steam mass flow rate, preventing lead from freezing at the interface. This solution has been adopted in this work. Since the pool temperature in cold shutdown mode is close to 380 °C, the water inlet temperature has been fixed at the same temperature when the auxiliary system is used. After the attainment of the criticality and the achievement of a scheduled level of power, the feedwater inlet temperature is gradually reduced to 335 °C as long as the nominal conditions are reached. Henceforth, the feedwater inlet conditions are not modified any more, the auxiliary system is switched off and the secondary circuit begins operating in full power mode. The proposed solution for the auxiliary system operation has the advantage of using water flow rates, temperatures and pressures which are close to the nominal ones.

As far as the power rise is concerned, the procedure is similar to the one adopted in acknowledged reactor concepts. In particular, it has been envisaged that a suitable neutron source is inserted within the core both to initiate the chain reaction and to monitor the neutron flux which may be so low to not be detectable. Indeed, even small movements of the CRs may determine large reactivity insertion, causing the power to reach unacceptable levels which compromise the integrity of the reactor before the safety systems manage to intervene.

In this work, the very first reactor start-up has been studied. As far as the dynamic simulations are concerned, the initial conditions are such that the primary circuit is filled with the molten lead at

cold shutdown temperature, whereas the BoP is pressurized to the nominal value and the feedwater inlet temperature is equal to 380 °C. On the other hand, the previous stages of the reactor start-up require the filling of the vessel with the molten lead and the verification of the operating conditions of the several devices in the primary circuit. Afterwards, it is necessary to heat-up and pressurizing the BoP avoiding the overcooling. Nevertheless, these operations have not been fully characterized because it is quite premature to deepen such a complex aspect of the start-up sequence at this stage of the system conceptual design.

5.1.2. System evolution during start-up

As a first step in the development of a suitable start-up procedure, it is necessary to define the system *desired behaviour*, i.e., the sequence of states and operations to be performed on the system during the power rise until the achievement of nominal conditions. The state of the overall system is given by the sum of the partial states describing the conditions of the individual constituents. Thus, the main components of the plant involved in the start-up sequence and the respective modes in which they have to operate during the reactor start-up have been outlined (Table 5.1).

Table 5.1. Plant components and respective operational conditions

Component	***Operational Conditions***
A. Core Power Level	(0) off (1) subcritical (2) critical [0 ÷ 0.1 MW_{th}] (3) critical [0.1 MW_{th} ÷ 60 MW_{th}] (4) critical [60 MW_{th} ÷ 300 MW_{th}]
B. Core Composition	(0) composed entirely of dummy elements (1) replacement of dummy elements with fuel assemblies (2) core composition at Begin of Life (BoL)
C. Primary Pumps	(0) off (1) increasing speed of rotation (2) steady-state conditions
D. Secondary Pumps	(0) off (1) increasing water mass flow rate [0 ÷ 20%] (2) minimum mass flow rate (20%) (3) mass flow rate regulated by the dedicated controller
E. By-pass Valve	(0) open (1) SG pressure control (2) closing ramp (3) closed
F. Turbine Admission Valve	(0) close (1) SG pressure control

G. Feedwater inlet temperature	(0) room temperature (1) heating up to 380 °C (2) temperature kept close to 380 °C (3) cooling to 335 °C (4) steady-state conditions (335 °C)
H. Attemperator	(0) no mass flow rate (1) Turbine inlet temperature control

At this point, in order to define a procedure which ensures a good compromise between system cost and safety, an ordered sequence of actions to be carried out has been defined. In Table 5.2, the state trajectory of the system has been reported. It is defined as a tuple of natural numbers which represent partial states of the involved components.

Table 5.2. Descriptions of the state evolution during the start-up procedure.

State	Components state	State Description
M0	*[0, 0, 0, 2, 1, 0, 2, 0]*	The primary loop filled with lead is kept at 380 °C. Primary pumps are switched off. The BoP is pressurized at 180 bar, the feedwater inlet temperature is equal to 380 °C and a reduced water mass flow rate is circulating (~20%). These conditions are necessary to avoid local lead solidification.
M1	*[0, 1, 0, 2, 1, 0, 2, 0]*	At the beginning, the core is constituted entirely by dummy elements in order to test the primary circuit devices in the filled vessel configuration. The core is gradually loaded with FAs. First of all, the neutron source is inserted in order to monitor the neutron flux. Afterwards, most of the dummy elements are replaced with the fuel assemblies in order to achieve the BoL configuration. Hereinafter, the neutron source is inserted in a dummy element in order to monitor the neutron flux.
M2	*[0, 2, 1, 2, 1, 0, 2, 0]*	Once obtained the BoL configuration, the pumps are brought to nominal operational condition.
M3	*[1, 2, 2, 2, 1, 0, 2, 0]*	The SRs are extracted in order to get closer to criticality conditions.
M4	*[2, 2, 2, 2, 1, 0, 2, 0]*	The CRs are extracted in order to achieve the criticality. Afterwards, a power ramp is given. In this phase, the power is comprised between 0 and 0.1 MW_{th}.
M5	*[3, 2, 2, 2, 1, 0, 3, 0]*	When the core power level reaches 0.1 MW_{th}, the feedwater inlet temperature is reduced to gradually reach the rated value (335 °C).
M6	*[3, 2, 2, 2, 1, 0, 4, 0]*	Once the feedwater inlet temperature reaches 335 °C, it is no longer modified and a suitable controller to keep it constant is envisaged. The power continues rising to 60 MW_{th}.
M7	*[4, 2, 2, 3, 2, 1, 4, 0]*	Once the thermal power produced in the core reaches 60 MW_{th}, the water mass flow rate in the secondary circuit is governed by means of a feedforward-feedback controller. Indeed, the feedforward is necessary to gradually increase the mass flow rate in a programmed way until the nominal conditions are reached, whereas the feedback loop is used to govern the lead temperature in the cold leg. Up to this moment the SG pressure has been controlled by using the bypass valve. At this point, since the steam quality at the SG outlet is good enough to be admitted in the turbine, the bypass valve is gradually closed according to a user-defined ramp, whereas the turbine admission valve begins to be opened allowing steam flowing into the turbine. Henceforth, the SG pressure is

		governed by using a PI controller operating on the turbine inlet valve.
M8	*[4, 2, 2, 3, 3, 1, 4, 1]*	Once the bypass valve is completely closed, the steam mass flow rate entirely flows in the turbine, and the feedwater mass flow rate is updated according to the adopted control scheme. CRs are progressively extracted up to reach rated power level. At this point, a dedicated attemperator adjusts the steam temperature at the turbine inlet.

5.1.3. Discrete Event System representation of the reactor start-up

In the perspective of developing the ALFRED reactor control system, it is necessary to provide an adequate formalization of the sequence of the several control actions to be performed during start-up phase. In this way, once having rigorously defined the system desired behaviour, it is quite easy designing and developing the start-up mode for the control system. To this aim, the proposed overall procedure can be studied as a Discrete Event System (DES), so that the state of the system is characterized by variables assuming symbolic values rather than numerical, which change correspondently to the occurrence of certain *events*.

In spite of the apparent simplicity (i.e., state variables assume only discrete values and the time variable is not explicitly modelled), the study of DES is made complicated by some issues involving the dimensions of the studied system, its representation and finally the definition of the control problem. In particular:

- *Dimensions*. A considerable number of states, and consequently the transitions among them, has to be managed even in case of very elementary systems. In order to properly describe industrial processes with DES models, it is necessary to adopt formal tools and follow a rigorous approach.
- *Representation*. At the state-of-the-art, there is no convergence on the standards of representation and manipulation of DES because of the wide field of applications and needs. Moreover, if compared with time dependent systems, DES constitute an abstraction of physical systems which does not necessarily derive from first principles of mass, energy and momentum conservation. For the same plant very different models, according to modeling, controlling and simulating requirements can be derived.
- *Definition of the control problem*. Unlike time-dependent control systems, in the control of DES it is not possible to define set-points and neither parameters that allow quantifying the desired behaviour of the closed-loop system (e.g., cut-off frequency, phase margin or gain margin). Actually, the desired behaviour is usually specified in terms of DES and represents a specified sequence of discrete states through which the scheduled final state can be reached.

As far as the dynamics evolution of DES is concerned, the state variables summarize the past evolution of the system just to allow the description of the future evolution. In this way, its dynamics can be represented by plotting the movement of the state even if this description does not facilitate the understanding of the internal structure of the system characterized by a given dynamics. It is necessary to provide a mathematical description of a DES in terms of more detailed models, in order to be able to analyse and understand the behaviour. Models with a transition structure corresponding to discrete event systems are called *discrete event models*. DES in which only the order of events that occur is relevant (i.e., the time at which an event occurs is not meaningful) are called *logical models*, which are commonly used to solve problems of sequencing. The most common are those characterized by a procedural nature which are based on the description of how the system evolves (i.e., starting from an initial state and an event input, the next state is obtained). For control purposes, these models are easier to use because they allow the description of the evolution of a DES step by step. In addition, the other major family of models, i.e., the declarative ones, besides requiring a greater abstraction effort to the designer, needs very complex algorithms for the examination of the set of rules and constraints that describe the behaviour of a discrete event system.

5.2. Modelling tool options for reactor start-up description

In the formalization of the reactor start-up, the proposed procedure has been treated as a sequence of states, whose transitions are enabled by the occurrence of certain events. Two different modelling tools have been considered to represent the desired behaviour, i.e., the Finite State Machine and the Petri nets. In the following paragraphs, the formalism of these approaches will be described, and advantages and drawbacks will be focused in the perspective of developing the ALFRED reactor control system in the start-up mode.

5.2.1. Finite State Machine

A Finite State Machine (FSM) is a quadruple $(U,\ X,\ f(\cdot,\cdot),\ x_0)$ where:

- $U = \{u_1,\ u_2,\ u_3, \dots\}$ is the set of events;
- $X = \{x_1,\ x_2,\ x_3, \dots\}$ is the finite set of states;
- $f(\cdot,\cdot)\colon X \times U \to X$ is the transition function, which for each pair *(state, event)* determines the next state of the FSM;
- x_0 is the initial state of the system.

The state of a FSM evolves as follows. Starting from the state x_i, the occurrence of an event u_k changes the current state according to the transition function. Clearly, it is necessary that the event

u_k is acceptable by the state of the FSM x_i, i.e., the pair (x_i, u_k) belongs to the domain of f. The so defined FSMs are called *deterministic* since, given a current state and an incoming event, there is always only one state in which the system moves. In this definition of an FSM there is no discrimination between input and output variables. Nevertheless, the actions of a controller could be represented by a FSM in which some events are considered as input (i.e., the system remains in the state x_i until the occurrence of the event u_k) and other ones regarded as output (i.e., when the system arrives in the state x_i the event u_k is performed).

5.2.2. Petri Nets

Petri nets constitute a useful formalism for the modelling and the analysis of the DES dynamic behaviour and control, with particular attention to the description of causal relationships between events. In particular, Petri nets allow to compactly represent general concepts such as synchronization between processes, the asynchronous succession of events, concurrent operations, conflicts and resource sharing. Petri nets have been proposed as a tool for formal modelling useful both to eliminate any source of ambiguity in the representation and to perform analyses and verification on the system behaviour. In addition, they are equipped with an intuitive graphical representation, which makes them easy to use, besides representing a significant extension of the concept of FSM. In this sense, in the Petri nets the state and the transitions can be considered as a distributed system. The overall state of the net can be interpreted as being composed of multiple states related to partial and independent subnets. Similarly, a transition is limited to affect only a part of the overall state. For this reason, it is possible to represent two events that can occur independently of each other by means of two net transitions which can shoot in a "competitor" way. Conversely, in the FSMs, being the state considered as a whole, the possible state transitions are mutually exclusive to each other.

A *net* is a triple $N = (P, T, F)$, where P is the set of *places*, T is the set of *transitions*, and F is the set of flow relations.

- $P \cap T = \emptyset$, the set of places and of transitions are disjoint;
- $P \cup T \neq \emptyset$, the net must have at least a place or a transition;
- $F \subseteq P \times T \cup T \times P$: F is the set of ordered couples of places and transitions and of transitions and places allowed.

A net can be graphically represented using a bipartite graph, in which there are two distinct kinds of node connected by oriented arcs indicating the existing flow relations, namely the *places* and the *transitions*.

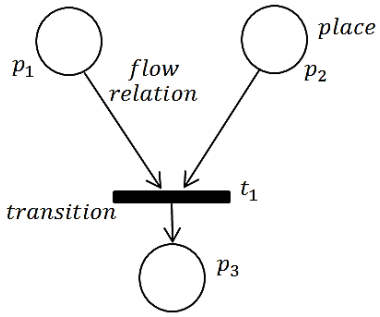

Figure 5.1. Graphical representation of net elements.

Places contain information about the state of the net, whereas transitions are associated with events that change the state. The elements of the flow relations represent the characteristic structural links, which rule the system evolution. The flow relation is characterized by defining for each element of the net the connected ones, indicating the direction of the transition. These concepts can be formalized by defining the *Pre* and *Post functions*, as follows:

- Given $X = P \cup T$, the *preset* of an element $\alpha \in X$ is the set of elements connected upstream to α, defined as

$$Pre(\alpha) = {\bullet}\alpha = \{\delta \in X | (\delta, \alpha) \in F\} \tag{5.1}$$

- The *postset* of an element $\alpha \in X$ is the set of elements connected downstream to α, defined as

$$Post(\alpha) = \alpha{\bullet} = \{\delta \in X | (\alpha, \delta) \in F\} \tag{5.2}$$

The provided definitions refer to the topological aspects of a net which are necessary to represent the structural links among its elements. Starting from these "static" definitions, several "dynamic" models have been proposed which allow describing the dynamic evolution of the net. In a Petri net, the basic idea is that places play the role of the system state variables and integer numerical values (represented by *tokens*) can be associated to them. A *Petri net* is a 5-tuple $PT = (P, T, F, W, M_0)$ where P, T and F are necessary to define a net and W and M are the following functions:

- $W: F \to N_0$ is the *weight function*, which associates to each element of the flow relation a positive integer.
- $M_0: P \to N$ is the *initial marking* of the net, which associates to each place a positive integer.

The initial marking defines the set of partial states which describe the system initial conditions. The net evolution will be associated to the change in the place marking, following dedicate rules (*rules of net evolution*). In the graphical representation, the weight function W is indicated by a label on the corresponding arc. The function marking M is represented by black dots that stands for the tokens within the place.

Similarly to all DES representations, the dynamic behaviour of a Petri net is determined by the occurrence of one or more events. An event is modelled by representing the possibility of occurrence (*transition enabling*) and the effect on the system (*firing rules*). The marking of the net describes the overall state of the system and indicates whether the transitions are enabled or not. The fire of a transition changes the state of the system determining a change in the current marking.

- A transition t is said *trigger enabled* when the system state is represented by the marking M if and only if all the upstream places (i.e., the preset of transition t) have at least a number of tokens equal to the weight of the arc which is connected to t.

$$\forall p \in \bullet t \rightarrow M(p) \geq W(p,t) \tag{5.3}$$

- Given the marking M, the firing of a transition t enabled in M produces a new marking M' such that

$$\begin{aligned} \forall p \in \bullet t - t\bullet \quad & M'(p) = M(p) - W(p,t) \\ \forall p \in t\bullet - \bullet t \quad & M'(p) = M(p) + W(t,p) \\ \forall p \in t\bullet \cap \bullet t \quad & M'(p) = M(p) - W(p,t) + W(t,p) \\ elsewhere \quad & M'(p) = M(p) \end{aligned} \tag{5.4}$$

The conditions on the left indicate the places that are just upstream of the transition, the places that are just downstream, the places that are both upstream and downstream, and the places that do not belong to either the preset or the postset of t. Regarding the relationships on the right, the fire of the transition t causes the removal of a number of tokens equals to the weight of the arcs connected from every place upstream and the adding to each place downstream. The marking of all places that are neither upstream nor downstream remains unchanged. The firing rules define the change in the number of tokens in the Petri net, whose total number is not necessarily preserved. The firing of a transition represents a local event in the net. Indeed, the places that do not have arcs coming from or going to the considered transition do not affect the enabling or are influenced by its firing. Therefore, the firing of any transition of the net has only local effects and cannot influence components of the net that are not directly connected.

5.2.3. Reasons for choosing Petri Nets for the start-up description

Because of the sequentiality of the actions to be performed, FSMs may be suitable for the modelling of the start-up sequence. Indeed, certain operations during this phase can be performed only when particular conditions have been established. For instance, it is not possible to reduce the feedwater inlet temperature or increasing the water mass flow rate at the secondary side before the thermal power produced in the core reaches a certain value because of the above-mentioned

technological constraints. FSMs are well-suited to model the DES on a conceptual level, but they are particularly difficult to develop and modify, especially whether there are operations to be performed in parallel as commonly take place in almost all the DES adopted in industrial automation. Moreover each transition is limited to have exactly one input and one output. This restriction greatly restricts the possibilities of this representation since it is necessary to use very complex models to overcome the problem of not being able to simultaneously perform two operations. It is worthwhile to remind that FSMs can be considered as a particular type of Petri net, in which

$$\forall t_j \in T, \qquad \left|\bullet t_j\right| = 1, \qquad \left|t_j \bullet\right| = 1 \tag{5.5}$$

The impossibility to run parallel operations determines an inefficient use of available resources and then an additional modelling effort to develop a configuration which optimizes the process is required. Moreover, the FSMs grow in size very quickly even in simple cases. This problem becomes critical if unexpected components have to be added in the plant configuration. In this case, the overall number of states for the studied system would greatly increase since it is given by the combination of all possible states.

In order to overcome these limitations, it has been decided to use the Petri nets approach to model the start-up sequence. This high-potential tool allows representing even complex situations, with a simple and intuitive formalism that enables interfacing the controller model to the plant model from a logical and implementing perspective. The most classic use of Petri nets is the representation of the desired behaviour of DES. Indeed, Petri nets are not properly used to define the constraints on the model of the system that must be controlled. In this sense, they are mainly used to design the model that represents the *overall* desired behaviour. They are characterized by all the modelling features oriented to the DES description:

- *Parallelism*, since it is possible to model the performing of two simultaneous activities;
- *Competition* in case of sharing resources;
- *Synchronization* since a certain transition is enabled by the occurrence of suitable operating conditions.

In addition, the widespread use of Petri nets is due to the fact that it is relatively easy to derive the model of the controller from the desired behaviour representation, as it will be showed in the next Section.

5.3. Logic control design for the start-up procedure with Petri nets

The control system is usually designed by adopting the techniques of ICT (Information and Communication Technology), according to a multi-step procedure. In this work, the *Preliminary Design* (IEEE Std 610.12-1990) of the ALFRED reactor control system has been performed. In this stage, the architecture, components and interfaces are preliminarily defined. According to the prescribed procedure, first of all, the system operational requirements have been evaluated. Both the expected system behaviour and the forbidden ones, which could compromise its integrity, have to be specified. Generally, the functionalities of the control system are subdivided into simpler functions, obtaining in this way a hierarchy of features to be implemented with dedicated components. The set of decision-making responsibilities are divided into different levels. Each level has its own objective and its own function and it is associated with a certain level in the control system hierarchy.

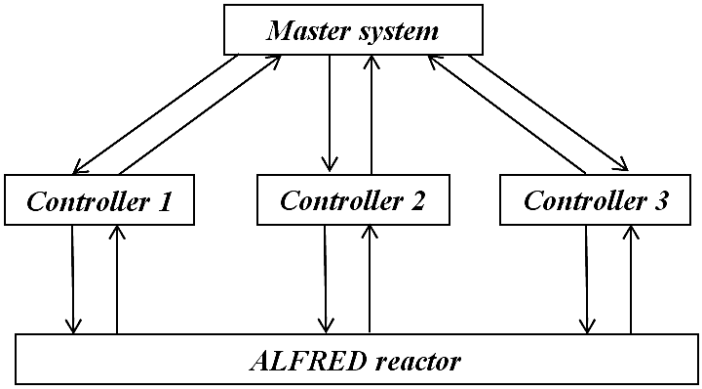

Figure 5.2. Layout of the control system architecture.

All the activities of subordinate levels (*slave*) are prescribed by the immediate supervisory level (*master*). At the top of the hierarchical pyramid, there is only one centre of control which is responsible for all the decisions. Distributed throughout the plant, dedicated regulators execute the commands received from the host computer, which receives information by appropriate sensors and uses them to formulate global decision. In particular, the lower levels of the control system mostly perform *modulating control*. These devices, in digital or analogic technology, instantaneously force the controlled variables following the corresponding set-points. On the other hand, higher levels perform *logic control* functions, which are concerned with devices ensuring that sequences of activities are carried out according to the occurrence of certain events (e.g., the conclusion of an activity, the occurrence of a failure, the interaction with the user…). Therefore, while the logic control schedules the control actions to be performed, their implementation is up to the modulating control.

The specifications of a supervisory control system are made up of sequences of actions, described generally by adopting a natural language. In the perspective of developing the ALFRED reactor control system, it is necessary to provide a suitable formalization of the sequence of the several control actions to be carried out. Once focused the specification for the desired behaviour of the overall plant, the aim is to define a DES connected to the plant to be controlled constituting a "closed loop" which behaves as much as possible the desired way. Therefore, after having focused the main steps to be taken, a formal model is realized aimed at describing the system desired behaviour. In this way, it is possible to develop the model of the controller by implementing few conceptual changes. The desired behaviour model contains the sequence of the desired events coming from the plant, mainly represented by the plant measures, $m(t)$, which constitute the inputs of the controller. When these events occur, the appropriate logic conditions are verified allowing the transitions to fire. At the same time, the control actions, $u(t)$, allow updating the state of the system. In this way, the control system is built starting from the given specifications.

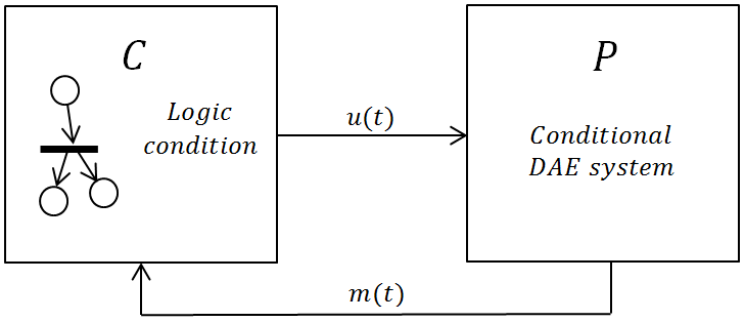

Figure 5.3. System closed loop configuration.

In this work, the logical-mathematical formalism of Petri nets has been employed both to represent the desired behaviour of the plant during the phase of start-up and to coordinate the several operations to be performed during this operational mode. According to what has been stated in the model developed to describe the start-up of the ALFRED reactor, Petri nets have been employed to represent the controller, whereas the plant has been described by using a conditional system of DAEs. In particular, the control system have been modelled by adopting a *synchronized Petri net*, i.e., an extended version of a Petri net to which a new element, namely the *event*, is added. An event is modelled by representing the possibility of occurrence (*transition enabling*) and its effects on the system evolution, described by dedicated rules (*firing rules*), as shown in Figure 5.4. In particular, the latter define the variation in the number of tokens, whose total number is not necessarily fixed. Whether an external event, e_i, is associated to a transition t_i, the latter fires *only* if it is enabled when the corresponding external event occurs. Therefore, an additional logical

condition must be verified to permit the transition firing. Such a condition is typically expressed as a function of the controller input variables (i.e., measures coming from the plant).

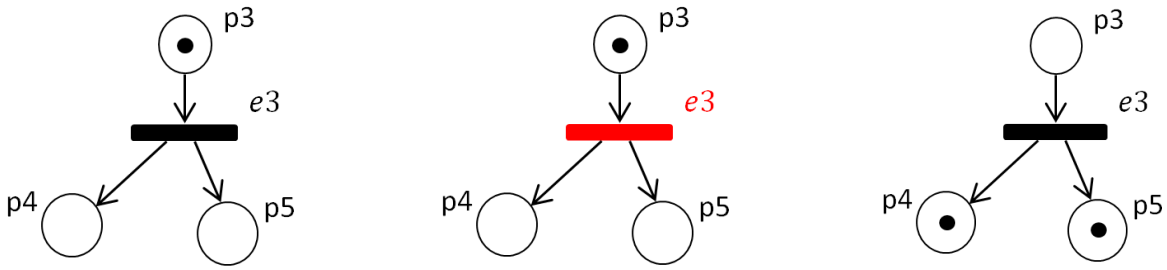

Figure 5.4. Example of the evolution of the ALFRED synchronized Petri Net.

The outputs of the controller (i.e., the control variables) are associated to the places of the Petri nets. In this way, the meaning of the controller output is related to an action which has a time duration. The performed influence of a control variable associated with a place is represented by its marking. According to this representation, when particular scheduled system conditions take place, the enabled transitions in the controller Petri net may fire. In this way, the place associated to a particular control action is marked by one or more tokens. In that instant, the considered control action starts being performed on the system. This influence is carried out as long as there is at least one token in the corresponding place. An example is shown in Figure 5.5, in which the activity A_1 begins at the instant t_1 since the place p_1 is marked and it ends when there are no more tokens in p_1.

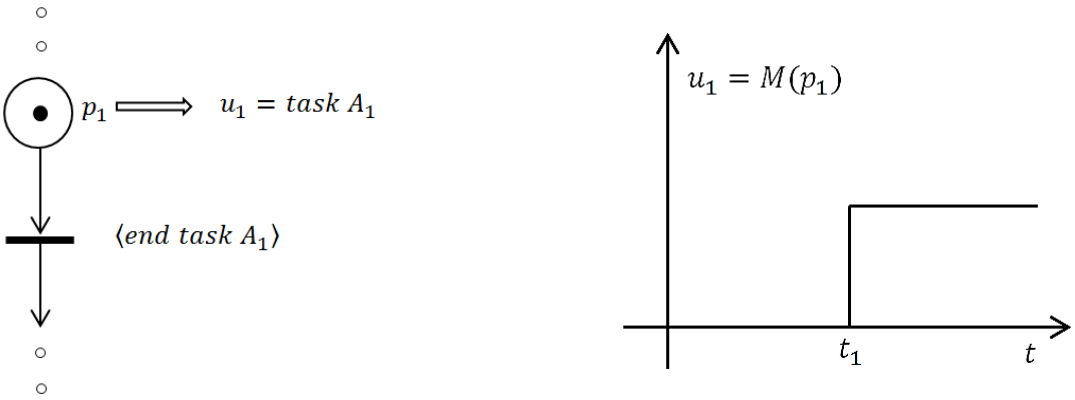

Figure 5.5. Examples of outputs associated to places.

Table 5.3. Description of the events of the Petri Net represented in Figure 5.6.

#	Event Description
e0	The beginning of the start-up procedure is decided by the user
e1	The source is inserted
e2	The BoL configuration is achieved
e3	The lead mass flow rate reaches its nominal value
e4	The SRs are totally extracted
e5	The thermal power level is 0.1 MW_{th}
e6	The thermal power reaches the 20% of the nominal value
e7	The feedwater temperature reaches 335 °C
e8	Rated thermal power level is achieved

Table 5.4. Description of the places of the Petri Net represented in Figure 5.6.

#	Place Description
p0	Primary loop filled with lead, fake core configuration, secondary system pressurized
p1	The source is being inserted
p2	The core is loaded with FAs in order to reach the BoL configuration
p3	The lead mass flow rate increases
p4	The lead mass flow rate is kept at the nominal value
p5	The SRs are being extracted
p6	The power build-up is regulated by the CRs modulating controller
p7	The feedwater temperature is kept constant at 380 °C
p8	The thermal power level is 0.1 MW_{th}
p9	The thermal power rise continues
p10	The feedwater temperature is being decreased
p11	The feedwater temperature is kept at the nominal value
p12	The thermal power is kept constant at 20% of the nominal value
p13	The pressure is kept constant with the bypass valve PI controller
p14	The feedwater flow rate is kept constant at 20% of the nominal value
p15	The thermal power rise continues
p16	The thermal power is kept constant at nominal value
p17	The pressure is kept constant operating on the turbine admission valve
p18	The feedwater mass flow rate is adjusted through a feedforward-feedback scheme

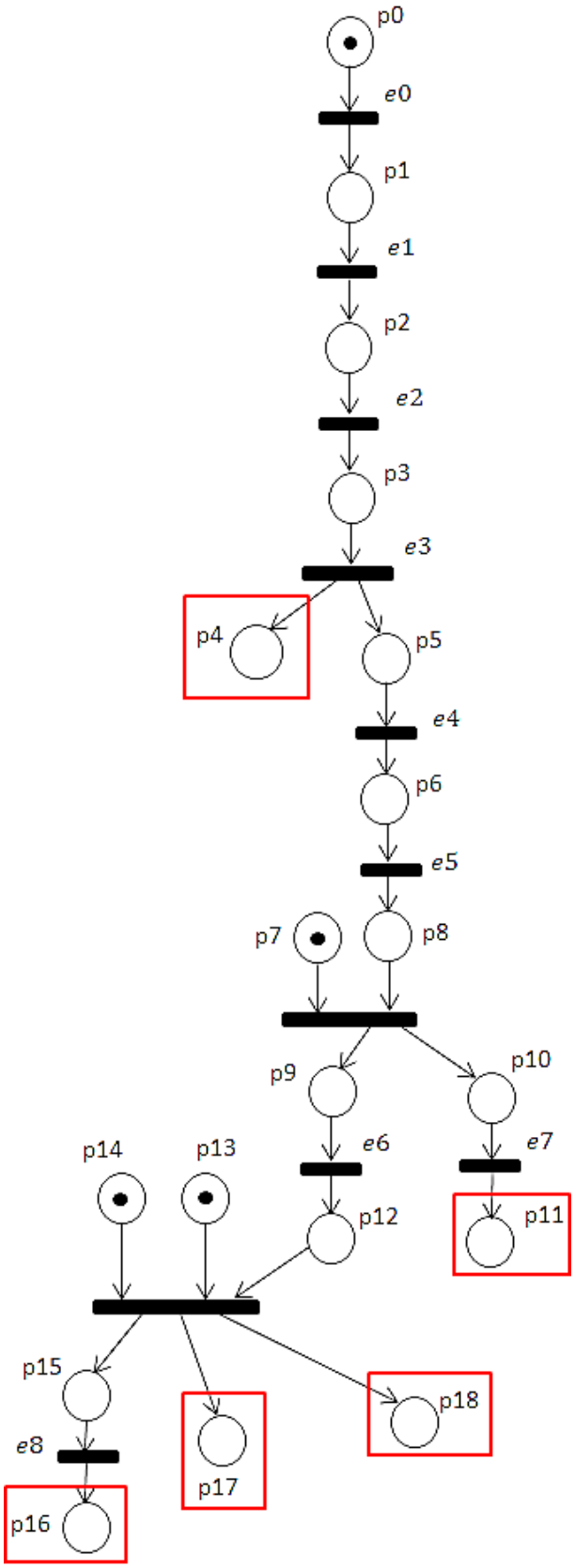

Figure 5.6. Desired behaviour model of the ALFRED reactor during the start-up procedure. The squared red places refer to the full power mode conditions.

5.4. Logic control system implementation and coordination with full power mode

Once the system desired behaviour during the reactor start-up has been modelled by means of a synchronized Petri net, the next step is the definition of the control scheme ensuring such a controlled evolution. The formalization of the desired behaviour allows focusing both the processes which take place in parallel, and the constraints to be satisfied so as to determine the scheduling of the control actions. The control system design directly derives from the definition of the NPP desired behaviour. The Petri nets formalism has been adopted both to regulate and synchronize the control actions and to coordinate the transition from the start-up to the full power mode. As far as the modulating controllers are concerned, the FSMs concept has been adopted due to the simplicity and the conceptual affinity with the Petri Nets, adapting the same formalism used in the desired behaviour modelling in a simpler configuration. Therefore, even though the FSM approach is not suitable for the modelling of the overall system desired behaviour due to the impossibility of operating parallel processes and to the inefficient use of the available resources, such a tool turns out to be suitable for modelling the operation of the single regulators. Indeed, the modulating controllers are enabled or disabled according to the plant conditions. These particular conditions are characterized by the values assumed by certain *switching variables* (e.g., thermal power, lead mass flow rate, SRs position…), which rule the scheduling of the control actions to be performed. The state of the controllers can be described by means of boolean variables, i.e., the master control system sends appropriate ON/OFF signals to the slave controllers, according to the measures carried out on the plant.

Petri nets approach has not been used only to simulate the procedure of the reactor start-up, but also to operate the transition between start-up and full power modes as well. In particular, during the power build-up, when a power level equal to the 40% of the rated one has been achieved, the start-up mode is considered finished and the full power mode operation can begin. Once such a threshold is reached, the controllers which have operated in the start-up mode are disabled and those within the block representing the full power mode operation are enabled. As far as the implementation of the proposed logic control architecture is concerned, the Stateflow modelling tool has been employed. Stateflow is a graphical design and development tool for the supervisory and logic control used in conjunction with Simulink (Figure 5.7-Figure 5.8). It provides clear, concise descriptions of complex system behaviour using FSM theory, flow diagram notations, and state-transition diagrams.

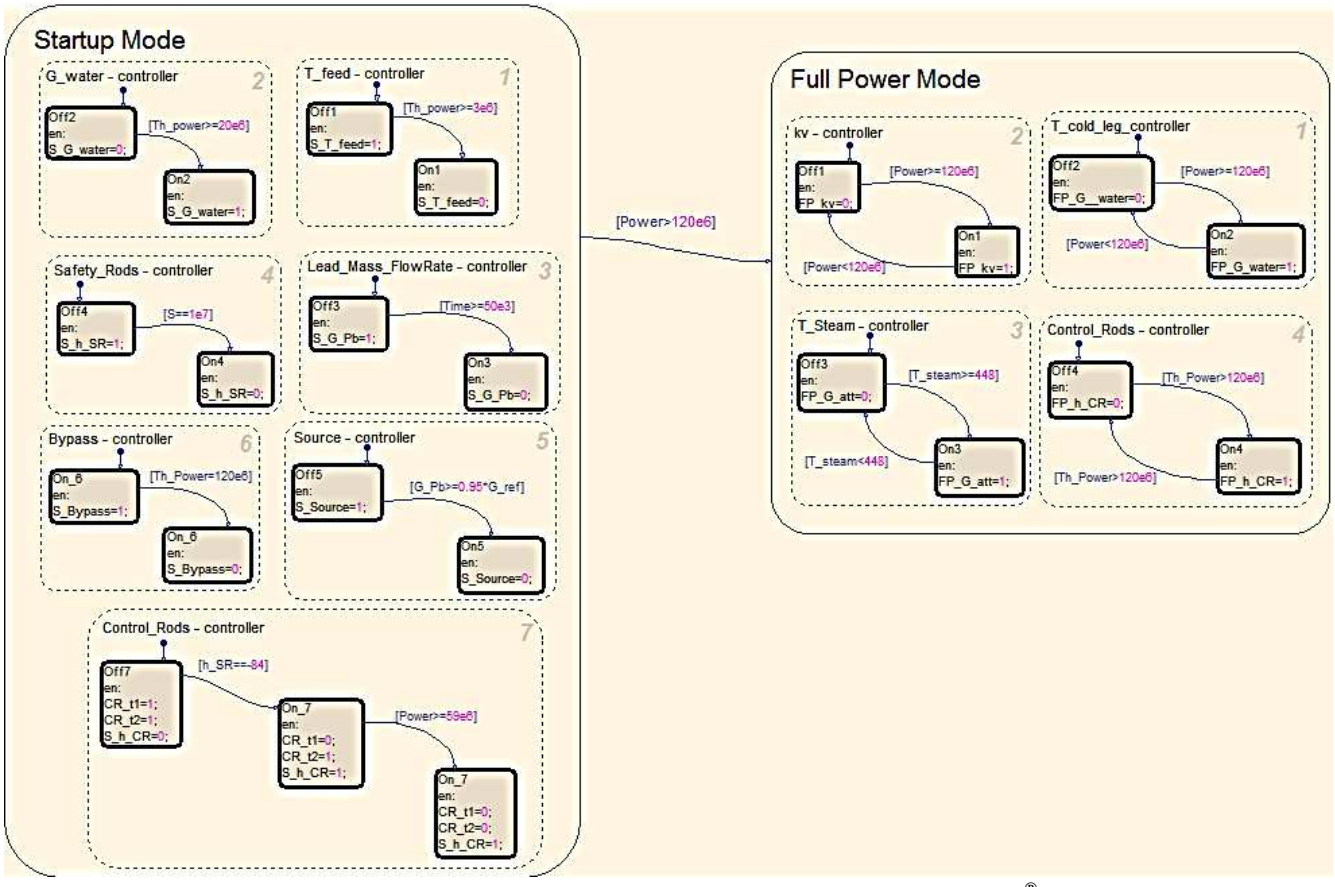

Figure 5.7. Detailed view of the master level of the ALFRED control system (Stateflow® modelling environment).

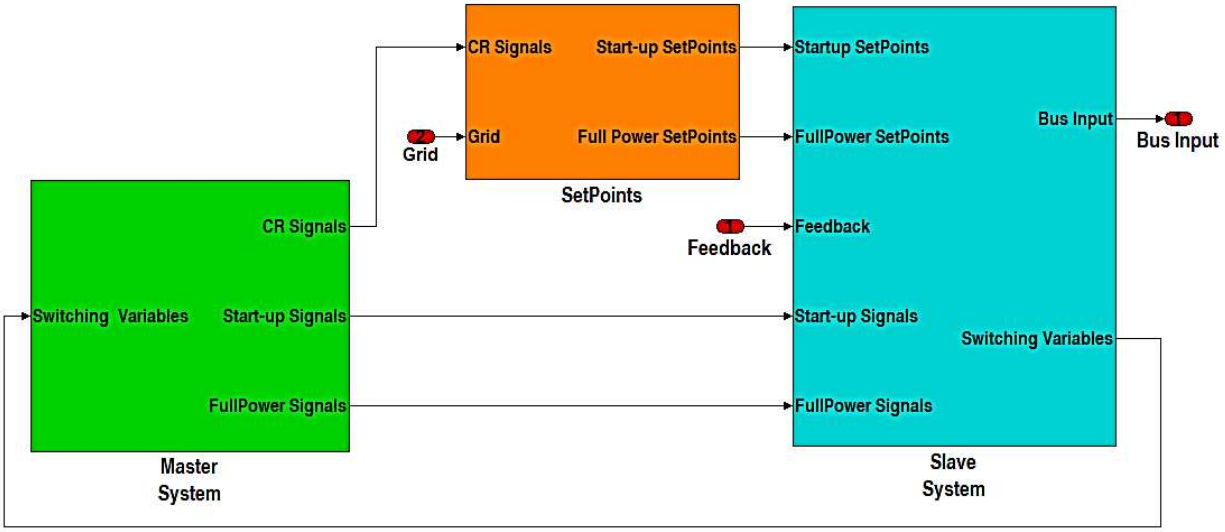

Figure 5.8. Preliminary Control system Architecture of the ALFRED reactor (Simulink® environment).

Once the supervisory control system has been developed, the modulating controllers have been implemented. The regulators characterizing the slave control system can be adapted both during the start-up mode and the full power model, as shown in Figure 5.10. In particular, the blue blocks represents the controllers which are enabled only in the start-up phase, the green ones operate only at full power mode, while the orange ones are used in both the modes.

As shown in Figure 5.8 and Figure 5.10, in the developed control system architecture, dedicated system buses containing signals from both the master control system and the object-oriented model have been implemented. The former (indicated as *Start-up Signals* and *Full Power Signals*) represent the signals that enable the corresponding controllers, according to the transitions governed by the supervisory control system. Otherwise, the *Feedback* bus drives the instantaneous values of the variables of interest, which allow deriving the value of the control actions to be taken. In this sense, they represent the measures to be carried out on the plant, $m(t)$, as previously shown in Figure 5.3. In addition, the buses containing the reference values for the controlled variables both in start-up and full power mode are indicated (*Start-up Setpoints* and *Full Power Setpoints*).

As far as the implemented controllers are concerned, open-loop regulators have been used as well. In particular, the handling of the SRs, the lead mass flow rate, the feedwater inlet temperature and the neutron source are operated through appropriate ramps that allow passing from the cold shutdown conditions to the corresponding rated values. On the other hand, PI regulators and combined feedforward-feedback regulators are employed to operate the other control variables. In Figure 5.9, a detailed view of the modulating controller devoted to the thermal power control has been reported. In order to implement the transitions between the regulators in the feedback scheme, the error between the set-point and the measure of the controlled variable is weighted by the signals sent by the master control system. If the value is equal to one, the suitable estimated control action will be carried out, whereas if it is equal to zero the PI controller does not perform any influence on the system. In this way, when the system is operated is start-up mode, only the control action of the enabled controller (i.e., PID 1) is performed on the system. When the suitable conditions are achieved, the transition in the master control system switches, the weight on PID 1 turns to zero and the weight on PID 2 turns to one. Accordingly, the start-up mode feedback regulator stops operating the CRs, replaced by the full power mode feedback regulator.

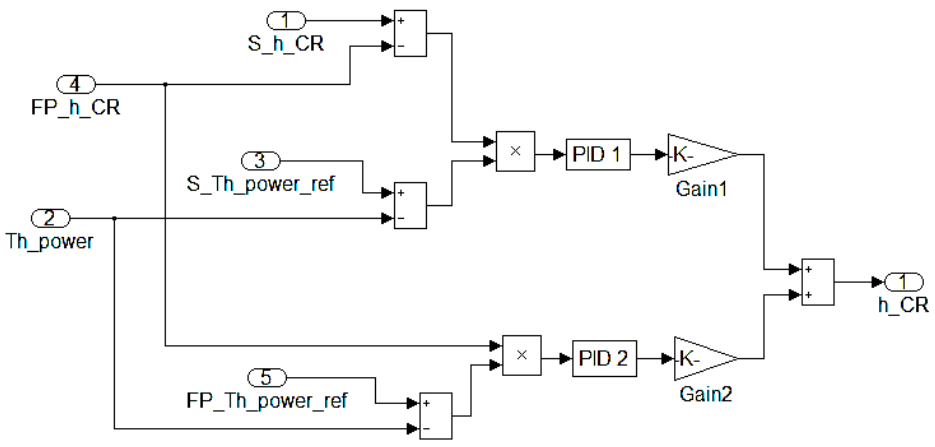

Figure 5.9. Detailed view of the modulating controller devoted to the thermal power control.

Table 5.5. Parameters of the PI controllers for both start-up mode and full power mode.

Control loop		**Start-up mode**		**Full power mode**	
Controlled variable	*Control variable*	K_p	K_i	K_p	K_i
T_cold_leg [°C]	G_water [kg s^{-1}]	$-9\cdot10^{-1}$	$-4\cdot10^{-4}$	$-6\cdot10^{-1}$	$-5\cdot10^{-4}$
Th_power [W]	h_CR [cm]	$-4\cdot10^{-11}$	$-2\cdot10^{-13}$	$-4\cdot10^{-11}$	$-1\cdot10^{-13}$
Pressure [Pa]	kv [-]	-	-	$-3\cdot10^{-7}$	$-1\cdot10^{-8}$
Pressure [Pa]	Bypass [-]	$-7\cdot10^{-7}$	$-9\cdot10^{-8}$	$-3\cdot10^{-6}$	$-9\cdot10^{-8}$
T_steam [°C]	G_att [kg s^{-1}]	-	-	$-1\cdot10^{-1}$	$-5\cdot10^{-2}$

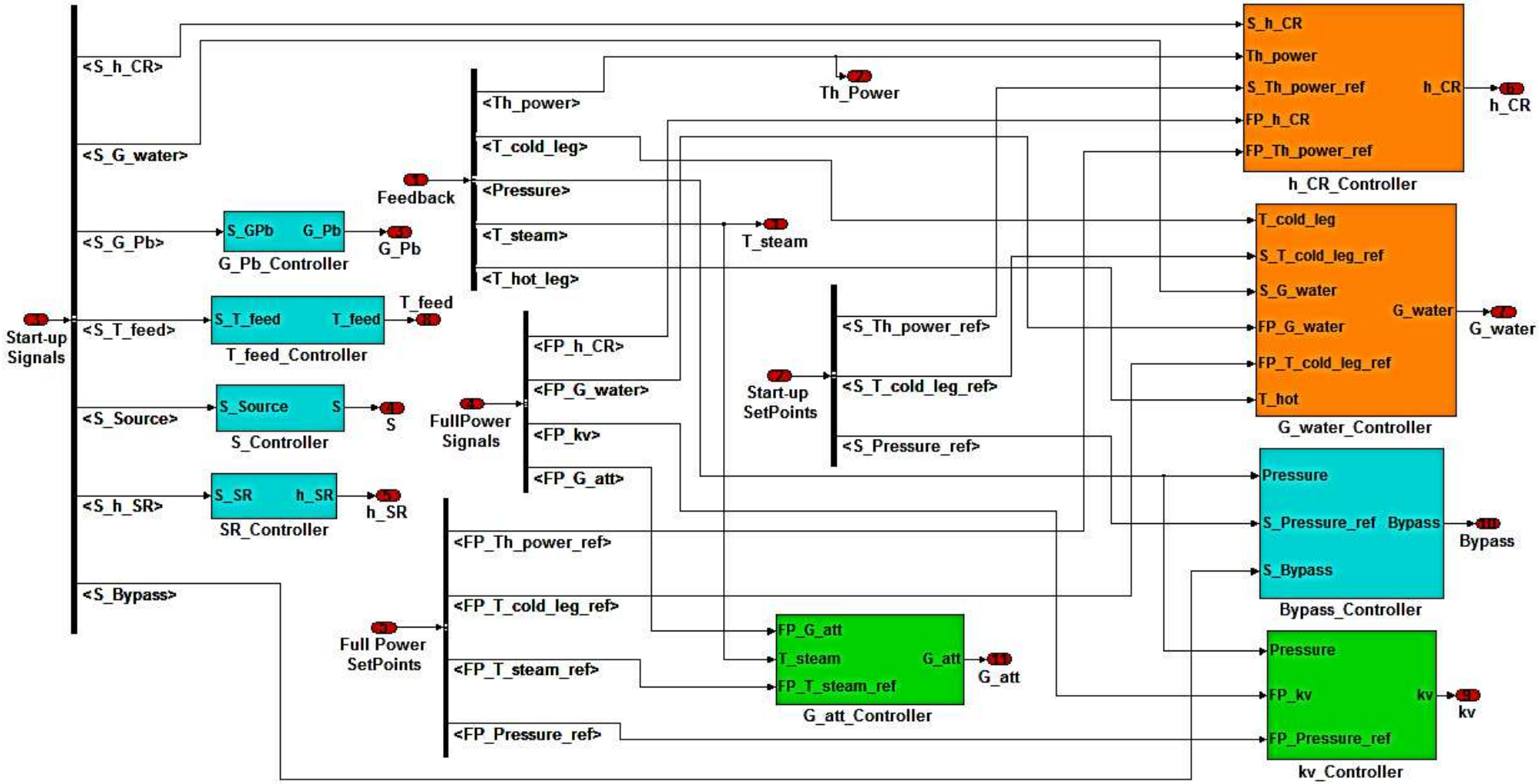

Figure 5.10. Detailed view of the slave control system of the ALFRED reactor.

5.5. Simulation results

In order to demonstrate the feasibility of the proposed procedure and verify that all the constraints are satisfied during the attainment of the rated power conditions, the proposed procedure for the ALFRED reactor start-up has been implemented and simulated in MATLAB® Simulink environment. In particular, the system response has been reproduced by employing the overall plant object-oriented model (Chapter 3). Indeed, as it has been mentioned in Section 4.2.4, Dymola enables models to be compiled as C-Mex S-functions for use in Simulink. This option turns out to be very useful whether the physical system is meant to be controlled by means of an advanced control architecture, designed in Simulink. Therefore, once having added input and output signals to the top-level of the Dymola model, it is possible to switch to Simulink and open the Dymola Block S-function, thanks to which the physical model is interfaced with the control system model.

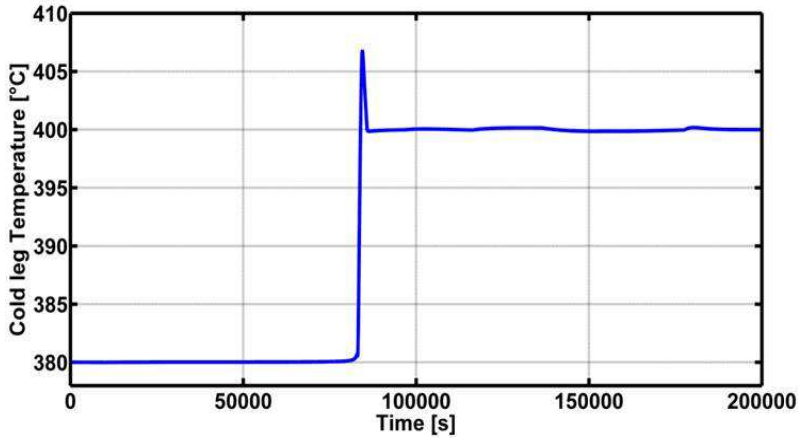

Figure 5.11. Cold pool lead temperature evolution.

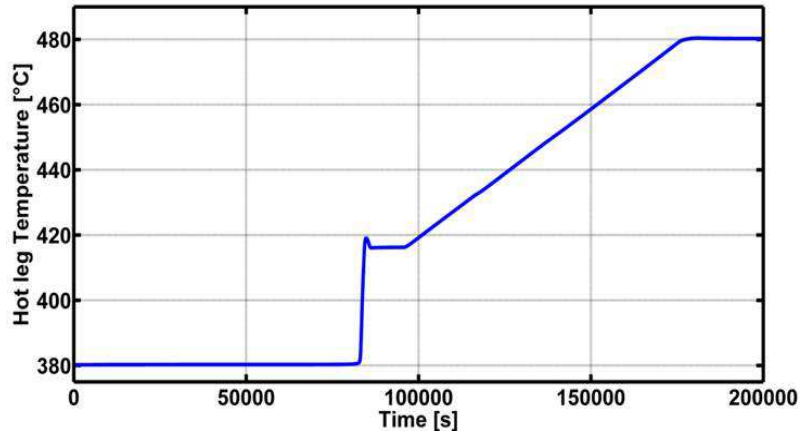

Figure 5.12. Lead temperature evolution at the core outlet.

The overall designed procedure takes almost 42 hours. This time duration is indicative and it can be optimized reducing some “dead time” and establishing the maximum rate for the controlled variables. During the start-up sequence, the lead temperature in the pool (Figure 5.11) is envisaged not to exceed 405 °C respecting the conservative limit of 410 °C imposed by corrosion problem on

the vessel steel (AISI316L). As far as the lead temperature at the core outlet is regarded, the temperature does not exceed the nominal value of 480 °C (Figure 5.12).

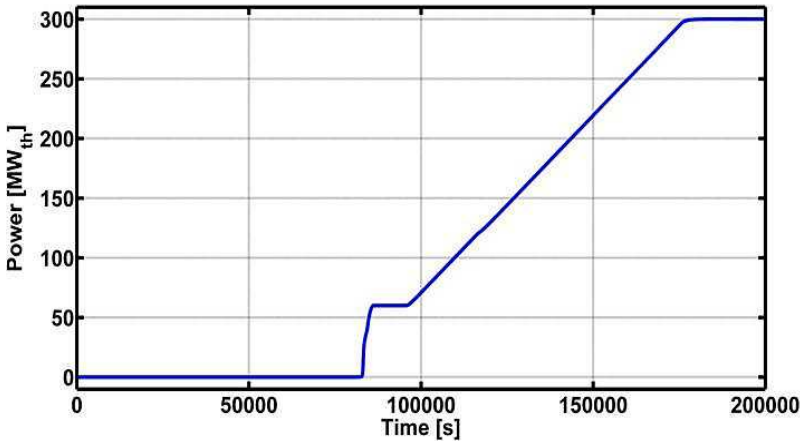

Figure 5.13. Reactor thermal power evolution.

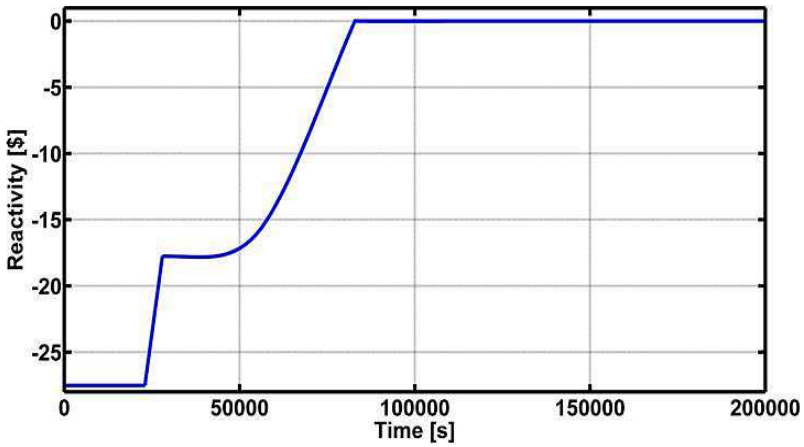

Figure 5.14. System reactivity evolution.

During a cold start-up, the CRs extraction induces a thermal power increase in the core, and therefore a lead temperature rise in the in the hot pool and cold pool, which induces a temperature rise in the BoP temperature field. In this perspective, two different set-point ramps with different slopes have been set in order to allow a gradual heat-up of structural materials (Figure 5.13). In the first phase, the temperatures are not likely to constitute a problem and the only limit is given by the controllability of the reactor, which have been carefully evaluated because of the absence of thermal reactivity feedbacks. After having achieved the 20% of the rated power, a “plateau” in the set-point has been provided so as to keep the condition of the primary circuit constant during the switch between auxiliary and normal mode of the BoP. This level has been chosen since it has been considered sufficient to produce steam which can be admitted in the turbine, and the system heat-up begins causing concerns to the structural materials.

As far as the second phase is concerned, with respect to the vessel, the part in contact with the lead rises almost instantly in temperature, whereas the structures above the free level would heat much more slowly through exchange due to the convective motion of gases and radiation. Therefore, the limited speed of power build-up is due to the necessity of meeting a bearable thermal gradient in the vessel suspension system in order to avoid affecting the integrity of sensitive components (Guidez, 2013).

As far as the first stages are concerned, especially at zero power conditions, it is important to include appropriate rate limiters on the modulating controllers regulating the control rods handling, avoiding that system reactivity could reach too high values. In this sense, during the start-up, the elongation of reactivity, starting from a subcritical level, does not exceed the peak value of 0.2$ (Figure 5.14).

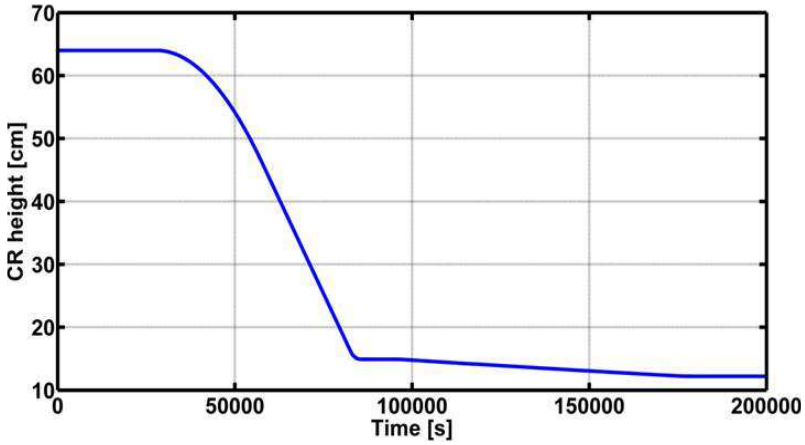

Figure 5.15. CRs position evolution.

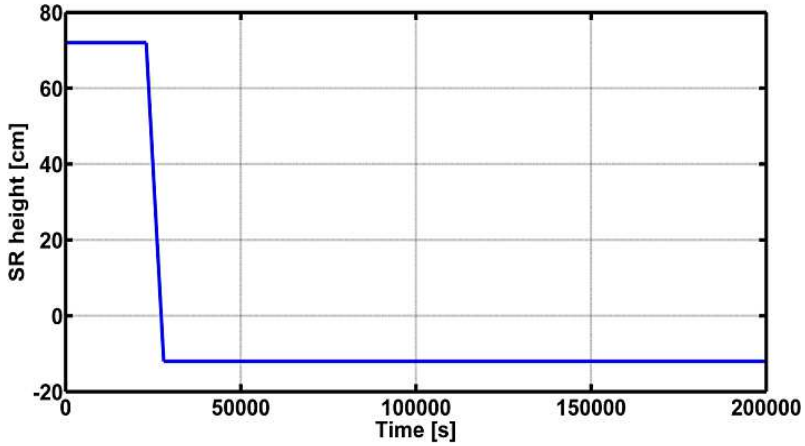

Figure 5.16. SRs position evolution.

Observing the evolution of the secondary circuit quantities of interest, it can be stated that the steam temperature at the turbine inlet (Figure 5.17) cannot be properly controlled until the reactor power reach 250 MW_{th}. This is due to the fact that the feedwater mass flow rate (Figure 5.18) has

already been adopted to govern the lead temperature in the cold pool and it cannot be used to govern other output variables, such as the steam temperature. This aspect has to be taken into account for the BoP operation since the steam temperature is 30 °C/40 °C lower than its nominal value when the steam starts flowing into the turbine. The solution could be found in a proper control of the extractions or using only the HP turbine stages. Finally the pressure (Figure 5.19) shows a very good evolution during the entire procedure since variations are minimal, limiting mechanic stress on secondary circuit components. This is obtained thanks to the tuning of the parameters of the devoted controllers (i.e., the turbine admission valve and the bypass valve) which allow limiting the overshooting during the power build-up.

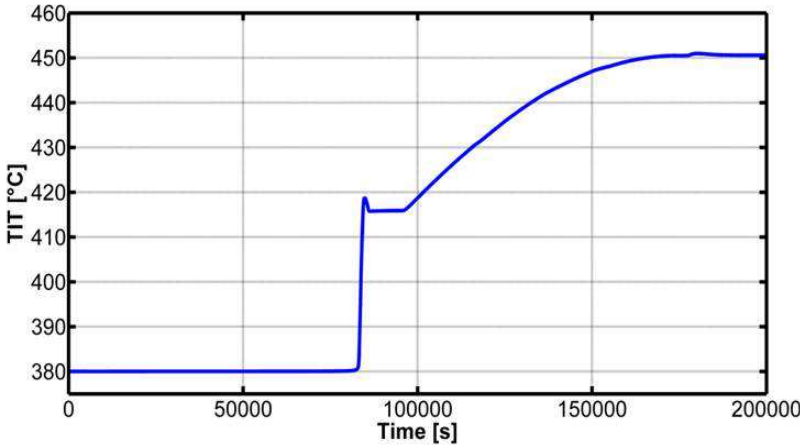

Figure 5.17. Steam temperature evolution.

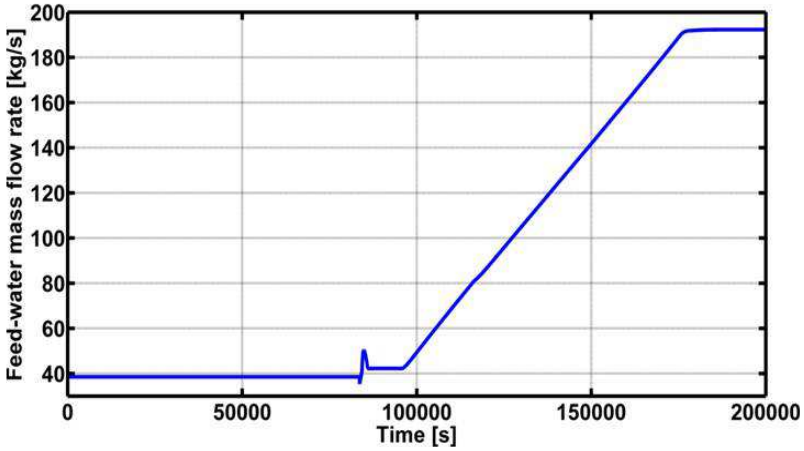

Figure 5.18. Feedwater mass flow rate evolution.

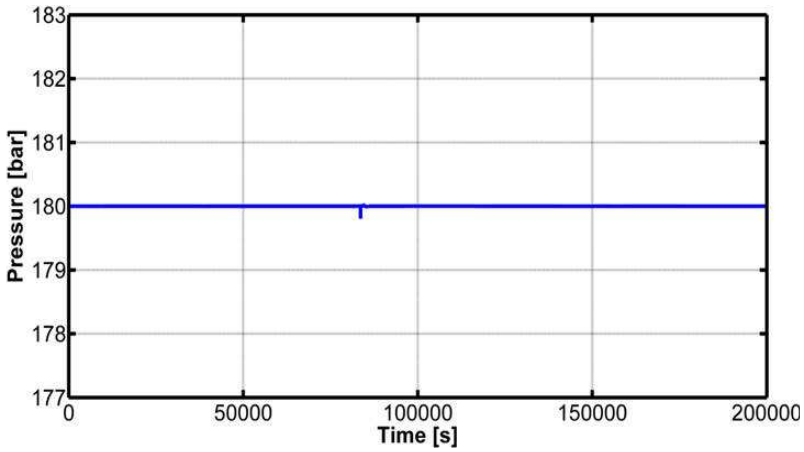

Figure 5.19. SG pressure evolution.

5.6. Concluding remarks

In this Chapter, the development of a preliminary version of the control system architecture of the ALFRED reactor has been presented. In particular, a procedure to achieve the reactor start-up has been proposed and implemented, and the transition from the start-up to the full power mode has been simulated by adopting the object-oriented model. In the first part, the issues that characterize this challenging operational mode have been described and a feasible start-up procedure to bring the reactor to full power conditions (fulfilling the system technological constraints) has been proposed.

In common practice, the operational sequence to bring a NPP from cold shutdown conditions to rated power is not suitably formalized with a quantitative description. Indeed, in order to comply with the severe constraints that characterize the ALFRED reactor, it is necessary to properly coordinate the different control actions to be taken. The Petri Nets modelling approach has been adopted to describe the desired behaviour of the overall plant and to coordinate the several control actions to be performed. This tool has permitted to define exhaustively and unambiguously the operational sequence so as the system evolution can proceed in the desired way. By adopting the Petri net formalism, the architecture of the supervisory system has been built as well, so as to coordinate the switching of the considered operational modes. The outcomes of the simulation of the reactor start-up have shown that the proposed control system architecture allows achieving the power build-up in compliance with the above-mentioned constraints.

After having tested the potentialities of this approach, future development may consist in coordinating the alternation of the different operational modes (i.e., start-up, full power, shutdown...). In this way, by representing the overall control system architecture through synchronized Petri net, it is possible to represent the transitions among the operational modes of a NPP by adopting the same effective and functional formalism.

6. Connection of the ALFRED reactor to the electrical grid

Outline

One of the most pressing issues in the study of the power generation and distribution is the characterization of the grid behaviour, whether a relevant fraction of the connected power plants are based on Renewable Energy Sources (RES). Indeed, because of the discontinuous power supply and the reduced presence of energy accumulators, power imbalance may take place on the grid. The power plants ensuring high reliability performance should be ready to feed the loads when the RES are not available. Since the ALFRED reactor has been designed to be a demonstrator of LFRs technology, the adoption of such a reactor concept within the grid has been studied. In virtue of the system large thermal inertia, the classical "reactor-following-turbine" approach used in the PWRs cannot be adopted. For this reason, an alternative solution has been proposed, in which the set-point for the thermal power is kept constant at the rated value, while the set-point for the mechanical power available to the alternator is adjusted according to the instantaneous grid power imbalance. In this way, thanks to the coordinated use of the bypass valve and the turbine admission valve, it is possible to meet the grid demands, by running the SG at constant pressure. In order to assess the performance of the developed control scheme, as a case study, a frequency profile of the synchronous Continental European grid with a resolution of second has been provided. The controlled response of the NPP to this profile has shown that such a scheme allows prompt variations of the produced mechanical power, complying with the requirements of the primary frequency regulation.

Introduction

Being the ALFRED reactor designed to be a demonstrator of LFR technology, the adoption of such a reactor concept within the electrical grid has been preliminarily studied. In particular, one of the most pressing issues in the study of the power generation and distribution is the characterization of the grid behaviour, whether a relevant fraction of the connected power plants is based on Renewable Energy Sources (RES). Indeed, because of the discontinuous power supply and the reduced presence of energy accumulators, power imbalance may take place on the grid. The power plants ensuring high reliability performance should be ready to feed the loads when the RES are not available. Therefore, the ALFRED reactor will need to respond to not only to the predictable time demands of a conventional customer base, but also to changes in demand arising from variability in production by RES that depend on the weather.

Generally, NPPs do not provide primary governing response and automatic generation control in reaction to frequency deviations. Most of them are also limited in providing voltage support. It is often stipulated that frequency control participation could accelerate the NPP wear and tear. In addition, operating NPPs at their maximum load significantly improves their overall efficiency. However, the presence of a relevant fraction of RES-based power plants makes necessary to define different control strategies so as to contribute dynamically to the equilibrium between the power generation and the load requests. Consequently, even if the NPP operational flexibility costs (maintenance and possible lifetime reduction), it gives elasticity to the power system management and allows damping the unpredictable power supply variations due to the weather conditions. In this perspective, firstly, the procedure currently employed in PWRs, namely the “reactor follows”, has been considered to be adapted to the LFR technology. However, given that the time constants ruling the primary circuit dynamics do not allow such an approach, it has been necessary to decouple the operation of the primary circuit and the BoP. In this way, it is possible to meet the grid demands according to the time constants of the conventional part of the NPP, which are compatible with the requirements of the primary frequency regulation.

6.1. Frequency regulation and UCTE requirements

6.1.1. Primary frequency regulation

The aim of the *primary frequency regulation* is to restore the power balance in order to stabilize the frequency on the grid. All the power plants connected to the grid having an effective power greater than 10 MW perform the primary frequency regulation, increasing or decreasing the active power generated accordingly in a proportional way. Thanks to this kind of regulation, it is possible to limit the frequency deviation, which is affected by the total inertia of the system and by the

effectiveness of the primary frequency regulation itself. Compared to the other control actions on the frequency, the primary one presents shorter times of action, i.e., a few tens of seconds. The primary regulation of a power plant control system is characterized by:

- *Droop*, σ_i: it represents the gain of the primary frequency regulator and it links power variations to frequency variations. In particular, at equal frequency reduction, the lower is the droop, the greater will be the active power increase.

$$\sigma_i = -100 \frac{\frac{\Delta f}{f_0}}{\frac{\Delta P}{P_n}} \tag{6.1}$$

  In particular, the regulators characterized with lower droop mostly contribute to the primary frequency regulation. The form of the adopted controller is

$$R(s) = \left[\frac{1}{\sigma_i}(1 + s\tau_i)\right]\left(\frac{1}{1 + sT_a}\right) \tag{6.2}$$

  In this expression, the dynamics of the actuator is taken into account by the second term through a first order expression, while the first one defines the kind of the used controller. Generally, the integral control action is performed by the secondary control, while a proportional and a derivative ones are sufficient to stabilize the system to a new steady state condition.

Table 6.1. Theoretical speed droop for different kinds of power plants (Sterpu, 2009).

Nuclear	from 4% to 5.7%
Hydro	from 4 to 12%
Fossil	4%

- *Insensitivity region*. In order to avoid excessive stresses to the controlled system, a dead band is introduced, so that the frequency variations, below a certain threshold, are not taken into consideration. In addition to the dead band, which is manually set on the controller, there is also an involuntary insensitivity region, due to the constructional imperfections of the regulator.

In Figure 6.1, a typical frequency evolution following a power imbalance is shown. It is worthy to notice that the final steady state frequency value is different from the nominal one after the primary regulation. The other relevant parameter to be considered during the transient is the maximum frequency variation. The primary frequency regulation must ensure that the latter remains limited within appropriate boundaries. In case of non-compliance of these limits, other burdensome

measures are necessary, such as the disconnection of some loads or the disconnection of the power plants.

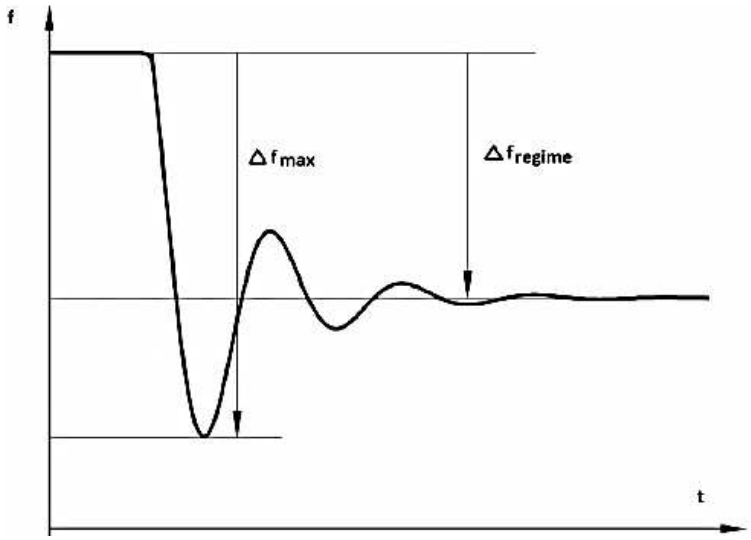

Figure 6.1. Typical trend of frequency during primary frequency regulation.

6.1.2. Secondary frequency regulation

Following the primary frequency regulation, the secondary frequency regulation is performed. Its control action takes several minutes, instead of tens of second as in the case of the primary control. The main functions of the secondary regulation are

- Resetting the value of the frequency to the nominal one. In this way, it is also possible to disengage the primary regulation, thus allowing the primary reserve to be restored and to handle any incoming disturbances.
- Restoring the equilibrium among the different control zones at level of power exchange is, in accordance with the contractual values. The secondary frequency regulation is ensured by a system of automatic control and centralized power generated.

It is important to note that, while the primary frequency regulation takes place everywhere in a distributed way, the control action of secondary frequency regulation must be undertaken only by the control zone within which the imbalance of power occurs and it is in charge of only some power plants. However, the benefits deriving from the disengage of the primary regulation reserve is extended to the whole grid, since the frequency value is approximately the same in all its nodes. The secondary controller is based on a Proportional-Integral action, according to the following equation

$$\Delta P = -K_p e_i(t) - \frac{1}{T_i}\int e_i(t)dt \tag{6.3}$$

The integral control action is necessary to restoring the rated value of the frequency and to achieve the scheduled values for the exchanged power on the interconnection lines. As far as the constant of proportionality is concerned, it is not appropriate to choose a value excessively large in order to avoid instability problems on the grid.

6.1.3. UCTE requirements

After having outlined the fundamental aspects of primary and secondary frequency regulation, the performance required to the regulators performing such control actions are presented. In particular, the requirements of the Union for the Coordination of Transport of Electricity (UCTE), i.e., the organization responsible for the coordination of operations and development of the electricity transmission grid in continental Europe, have been reported. Whether there would be a deficit of generation up to 3000 MW, primary frequency regulation must ensure that the minimum value of frequency, registered during the transient, is greater than 49 Hz. However, in order to get a good margin, it is preferred to set this threshold to 49.2 Hz. This means that, during the transient, the frequency deviation must be kept below 800 mHz. Similarly, the highest permissible frequency, after the loss of a load less than or equal to the so-called *Reference Incident*, is 50.8 Hz. For the primary control, the insensitivity range has to be as low as possible and should not exceed ±10 mHz. As far as the constraints concerning the times constants are regarded, the UCTE establishes that the system must be stabilized to a new steady state conditions thanks to the control action performed by the primary frequency regulation within 30 s.

Furthermore, the UCTE sets characteristic times for the return of the frequency and exchanged power to their nominal values, due to the secondary regulation as well. Whether an important group of production would be lost, the secondary frequency regulation must intervene at the latest 30 s after the occurrence of the disturbance and complete its control action within 15 minutes. The UCTE suggests to adopt a time constant for the controller performing the secondary regulation between 50 and 200 s.

6.1.4. Operational range for the ALFRED reactor

In this Chapter, the possibility of performing primary frequency regulation by means of the ALFRED reactor has been investigated. In virtue of the perspective of having a relevant fraction of RES-based generating units connected to the grid, the innovative NPP must ensure a minimum manoeuvrability. Because of the discontinuous power supply and the reduced presence of energy accumulators, power imbalance may take place on the grid. In this perspective, the power plants which ensure high reliability performance should be ready to feed the loads when the RES are not available. The primary frequency regulation has the most severe time requirements. Therefore, its

characterization turns out to be more relevant in order to assess the feasibility of employing the ALFRED reactor within the grid. Each Transmission System Operator (TSO) is entitled to define a minimum primary control range for generating units in terms of the nominal active power (P_{eff}), i.e., the maximum power that the generating unit can continuously provide. In particular, the operational range of a generating unit can vary between the so-defined P_{min} and P_{max}

$$P_{min} = P_{mt} + 1.5\%\, P_{eff} \tag{6.4}$$

$$P_{max} = P_{th} - 1.5\%\, P_{eff} \tag{6.5}$$

where P_{mt} is the minimum power level that the plant can operate at and P_{th} is the highest power that the generating units can achieve in certain operational conditions (ENTSOE, 2013). For the ALFRED, given that the maximum achievable thermal efficiency of the entire NPP is equal to 44.75% (Empresarios Agrupados, 2012), the value of P_{th} has been easily derived. As far as the definition of the primary reserve is concerned, the P_{eff} has been set equal to P_{th}, obtaining

$$P_{th} = P_{eff} = 134.25\ MW_{el} \tag{6.6}$$

On the other hand, the minimum power level has been set equal to the lower threshold of the full power mode (40%), i.e., the power level at which the start-up mode can be considered finished. Therefore, the operational range for the ALFRED reactor has been set as:

$$[54.81\ MW_{el}\ ;\ 132.27\ MW_{el}] \tag{6.7}$$

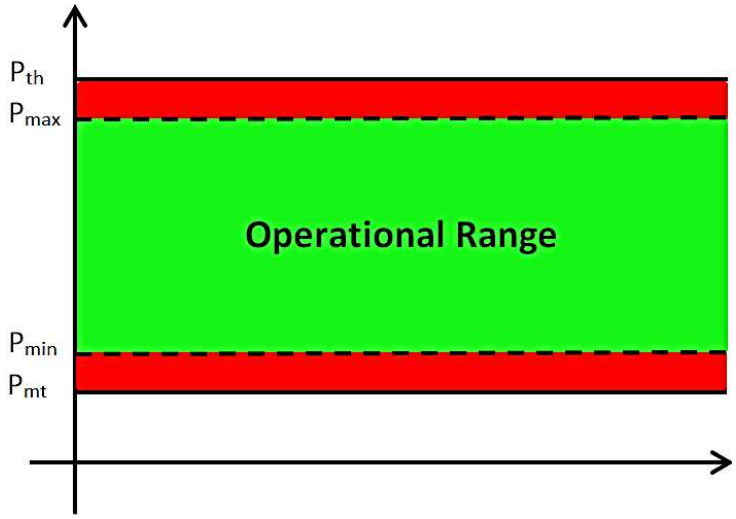

Figure 6.2. Primary control range for a generating unit, according to the UCTE requirements.

6.2. Primary frequency regulation performed by the ALFRED reactor

6.2.1. Main features of the adopted model

As far as the load-frequency regulation is concerned, generally, the mechanical power produced is adjusted according to an opening signal sent to a regulating device (e.g., turbine valves, nozzle). In particular, in the definition of the control scheme employed to perform the primary frequency regulation, it is necessary to adopt the grid pulsation as a controlled variable, operating on the value of the produced electric power. If the synchronous generator is connected to a grid with a much higher installed power, it can be assumed that the frequency is imposed by the grid. Therefore, the nominal value (ω_0) is the fixed set-point closed to which the controlled variable has to be maintained close. In Figure 6.3, the primary frequency regulation control scheme has been represented. Once identified the different control loops, the blocks labelled by $R_i(s)$ represent the adopted controllers, the blocks labelled by $G_{pi}(s)$ represent the generating units which perform the frequency regulation. In particular, if the electrical dynamics are neglected, it can be assumed as first approximation that the synchronous generating units rotate at the same speed as they constitute a unique rotor having an effective moment of inertia, indicated with J.

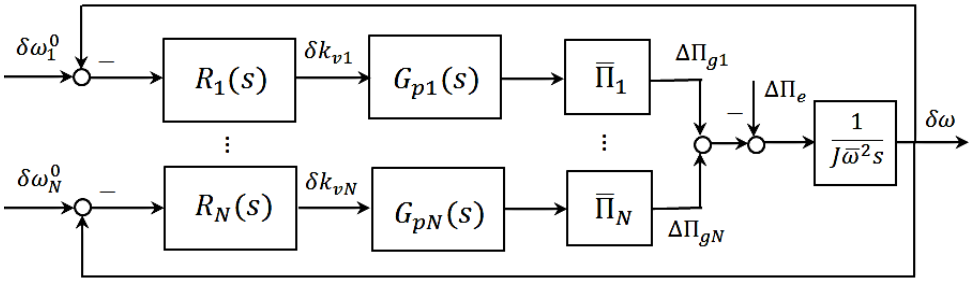

Figure 6.3. Primary frequency regulation control scheme.

As far as the modelling of the turbine is concerned, the turbo-alternator is keyed on the motor shaft of the turbine, providing a not negligible contribution to the inertia of the whole process. In the developed model, in order to correctly describe the dynamics of the turbine/turbo-alternator system, the time constants of the turbine have been suitably chosen. To this aim, the following values which indicate the fraction of the enthalpy disposed by HP stages and the time constants characteristic of the HP and LP stages have been employed (Kundur, 1994).

$$\begin{aligned} HP_{fraction} &= 0.3 \\ \tau_{HP} &= 0.3\ s \\ \tau_{LP} &= 5.2\ s \end{aligned} \tag{6.8}$$

In the control scheme implementation, a classical Proportional regulator, whose K_p parameter has been tuned so as to achieve the desired value for the generating unit droop (4%), has been adopted.

$$\sigma_i = -\frac{\frac{\Delta f}{f_0}}{\frac{\Delta P}{P_n}} = -\frac{d\omega[pu]}{dP[pu]} = -\frac{d\omega}{dk_v}\cdot\frac{dk_v}{dP} = K_p\cdot\frac{dk_v}{dP} \;\Rightarrow\; K_p = \frac{\sigma_i}{\left(\frac{dk_v}{dP}\right)} \tag{6.9}$$

Finally, the presence of the actuator of the turbine valve has been accounted for. For small variations, the actuator response can be approximated through a first-order transfer function with a characteristic time constant equal to T_a = 0.2 ÷ 0.4 s

$$\delta A_u = \delta A_{u,0}\frac{1}{1+sT_a} \tag{6.10}$$

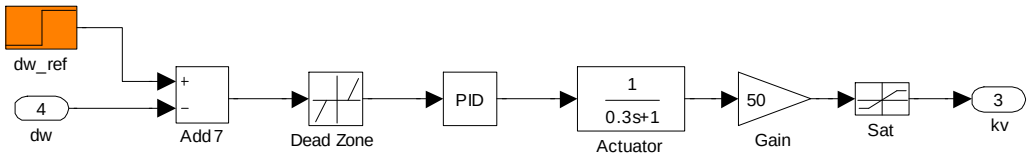

Figure 6.4. Control scheme implemented to perform the primary frequency regulation.

6.2.2. Constant pressure SG operation

As far as the load-frequency control purposes are concerned, it is necessary to point out the SG operational mode since in general the criteria for the control of steam pressure are often related to the effects of load changes on the consumption of plant life. Two possible control strategies can be immediately envisaged. The first one is the *constant pressure mode*, in which the pressure is kept closed to its nominal value and the power variation is obtained by acting on the water mass flow rate and the thermal power exchanged. The second one is the *sliding mode control pressure*, in which the control valve of the steam turbine is fully open and the power variation is a consequence of the pressure variation.

According to the former control strategies, the thermal power exchanged and the area of passage at the turbine inlet are respectively employed to regulate the load and to keep fixed the pressure to the nominal value. Furthermore, the correlation representing the choke flow conditions at the turbine inlet has been implemented so as to describe the evolution of the steam mass flow rate. Ultimately, the thermal power exchange at steady state conditions is proportional to the feedwater mass flow rate, which is in turn proportional to the turbine admission valve coefficient.

$$Q_{c,0} = w_0\left(h_{ss}(T_0,p_0) - h_{l,0}\right) \tag{6.11}$$

$$w_{v,0} = k_v p_0 \tag{6.12}$$

Even though the *sliding mode control mode* ensures a lower consumption of the steam turbine and it does not entail the consumption of pumps at reduced loads conditions, the *constant pressure mode* is more suitable for the SG operation. Indeed, this mode is the commonly adopted procedure in the Rankine cycle-based power plants since it establishes the saturation temperature, allows promptly varying the power produced so as to rapidly meet the grid demands, and to avoid mechanical stresses when the load requests change. Therefore, in the perspective of connecting the ALFRED reactor to the grid, it has been decided to regulate the mechanical power provided to the alternators by operating the SG in constant pressure mode. As far as the SG dynamics is concerned, assuming that the pressure is approximately uniform, the equations of mass and energy conservation for the liquid and the metal wall take the form

$$\begin{cases} \dfrac{dM}{dt} = w_l - w_v \\ \dfrac{dE}{dt} = w_l h_l - w_v h_{ss} + Q_{ml} \\ \dfrac{dE_m}{dt} = Q_c - Q_{ml} \end{cases} \tag{6.13}$$

Starting from these equations, it is possible to derive the system total net energy as

$$\frac{d(E + E_m - h_l M)}{dt} = -w_v(h_{ss} - h_l) + Q_c \tag{6.14}$$

The dynamic model can be expressed as function of the system state variables, i.e., the pressure (P) and the outlet steam temperature (T_s). Since in the operational transients the influence of the pressure on the net energy is much more significant than the one of the steam temperature, the storage term is essentially function of the pressure

$$\frac{dE_t}{dt} = \frac{d}{dt}E_t(P, T_s) = \frac{\partial E_t}{\partial P}\frac{dP}{dt} + \frac{\partial E_t}{\partial T_s}\frac{dT_s}{dt} \cong \frac{\partial E_t}{\partial P}\frac{dP}{dt} \tag{6.15}$$

$$\frac{dE_t}{dt} \cong \frac{\partial E_t}{\partial P}\frac{dP}{dt} = Q_c - \Pi_m \tag{6.16}$$

By considering the term $[h_{ss}(p, T_s) - h_l]$ as a constant, the mechanical power available to the alternator has been derived as

$$\Pi_m = w_v(h_{ss}(p, T_s) - h_l) = k_v p(h_{ss}(p, T_s) - h_l) \tag{6.17}$$

In order to maintain a constant pressure, it is necessary to regulate the valve opening.

$$\mu_v = \frac{\partial \Pi_m}{\partial k_v} = p_0(h_{ss} - h_l) \tag{6.18}$$

Operating the SG according to the *constant pressure mode* allows varying the mechanical power produced. Therefore, in order to achieve a power step equal to $\Delta\Pi_m = \Delta\Pi_{m,0}$, the following coordinated control actions have to be carried out on Q_c and k_v

$$\Delta Q_c = \Delta\Pi_{m,0} \qquad \Delta k_v = \frac{1}{\mu_v}\Delta\Pi_{m,0} \tag{6.19}$$

The final steady-state values for the variables of interest are given by

$$\Delta P = 0 \qquad \Delta\Pi_m = \Delta\Pi_{m,0} \tag{6.20}$$

According to the proposed control strategy, the employed control variables and their task in the SG operation have been defined as follows:

- The opening of the turbine admission valve is used to maintain the pressure close to its nominal value.
- The thermal power supplied to the SG is necessary to regulate the mechanical power produced.
- The feedwater mass flow rate (equal to the steam mass flow rate) must be instantly adjusted to the value of the thermal power produced. By adopting an appropriate feed-forward scheme, it is possible to maintain a constant specific enthalpy $[h_{ss}(p,T) - h_l]$.

6.2.3. Operation of the ALFRED Balance of Plant

In currently operated PWRs, the mechanical power regulation is performed according to the *reactor follows* mode. When the grid frequency drops, in order to increase the mechanical power, the thermal power produced in the reactor is adjusted to the required value together with the feedwater mass flow rate. Ultimately, such a procedure is favoured by the negative thermal reactivity feedback coefficients, which provide the necessary reactivity to drive the NPP towards the power level conditions requested by the load demands.

However, the simulations of the system controlled response during operational transients (Chapter 4) have shown that a similar scheme cannot be adapted to the ALFRED reactor. Indeed, because of the transport phenomena in the collectors, the thermal inertia due to the cold pool, the reduced speed of the coolant in the primary circuit, the governing dynamics of the reactor are particularly slow. The characteristic settling times that could be obtained in the operational power transients are of the order of 1500 s. For these reasons, adjusting the power level to the sudden changes in the grid frequency by relying on the reactor follows approach is not feasible. Consequently, a different approach which exploits the bypass valve has been proposed.

In Chapter 5, the bypass valve has turned out to assumes a key role in the start-up procedure. In particular, when the power level is too low and the steam conditions are not suitable for the turbine admission, the entire water mass flow that circulates in the SG is directly vented into the condenser, without passing through the turbine. As the power level increases, the bypass valve is progressively closed, since the steam conditions are such as to enable the turbine admission. Therefore, when the reactor is operating in full power mode conditions, the bypass valve is kept completely closed. Such a configuration has been adjusted so as to allow the ALFRED reactor performing the load-frequency regulation in accordance with the UCTE time requirements.

The *constant pressure* operation of the SG of the studied NPP is more complicated with respect to the procedure described in Section 6.2.1. Indeed, the coordinated control actions performed on the feedwater mass flow rate, the thermal power and the turbine admission valve are not sufficient. This is due to the tight coupling between the primary circuit and the BoP. As described in Chapter 4, because of the severe technological constraints characterizing the ALFRED reactor, the lead temperature at the SG outlet has been designed to be controlled by adjusting the feedwater mass flow rate. Such a pairing represents a serious issue for the operation of the BoP.

Given that the SG operating points are fixed (i.e., the feedwater temperature variation at the SG inlet are effectively damped and the steam conditions at the turbine inlet are meant to be kept constant), the mechanical power is proportional to the produced steam mass flow rate, which is equal to the feedwater mass flow rate. The latter, besides the feedforward control action, is determined by a dedicated PI controller which governs the cold leg temperature. Therefore, the value of the water mass flow is no longer the one necessary to meet the grid demands. For this reason, it is necessary to have an additional degree of freedom in order to produce the electrical power in accordance with the load demands, govern the cold leg temperature and, at the same time, operate the SG at constant pressure.

As mentioned before, a possible solution may be represented by operating the bypass valve. According to this scheme, the turbine admission valve regulates the mechanical power starting from the frequency variation, whereas the bypass valve governs the SG pressure by adjusting the mass flow vented into the condenser. In this way, it is possible to develop a control strategy in which the reactor dynamics is uncoupled from the evolution of the secondary circuit. According to this procedure, the reactor core is constantly operated at rated power level and the heat produced in the primary circuit is effectively disposed to the BoP. In so doing, in every moment the maximum steam mass flow rate is produced so as to determine the maximum mechanical power to the alternator. In order to meet the load demands, a fraction of the steam flow will be directly disposed to the condenser, without passing through the turbine. In this way, the load-frequency control will

be performed, in accordance with the time constants of the SG and not according to the ones of the primary loop. These coordinated control actions do not affect the primary circuit, since the lead temperature in the cold leg is effectively controlled through the previously developed control scheme.

In summary, two possible control strategies for the ALFRED reactor have been identified:

- *Reactor Follows*: the reactor thermal power follows the variations of the load demands by handling of the control rods.
- *Uncoupled Reactor*: once reached the nominal thermal power, the reactor core operates always at this conditions independently of the load requests. The correct value of mechanical power is achieved by adjusting the bypass valve and on the turbine admission valve.

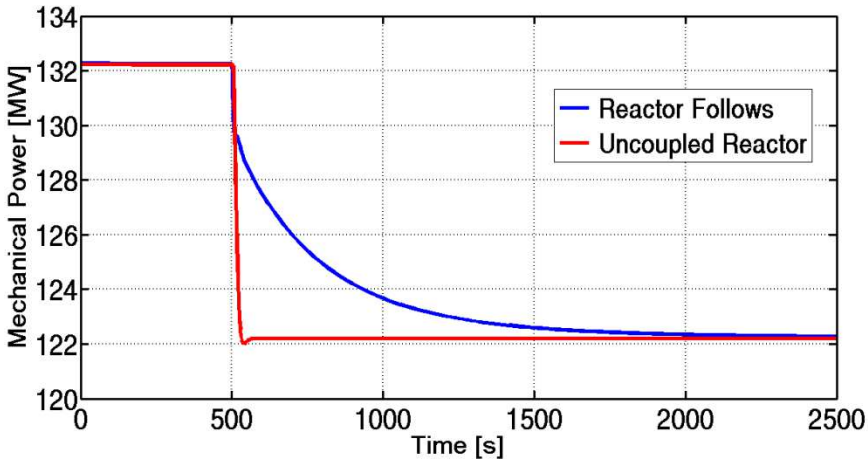

(a)

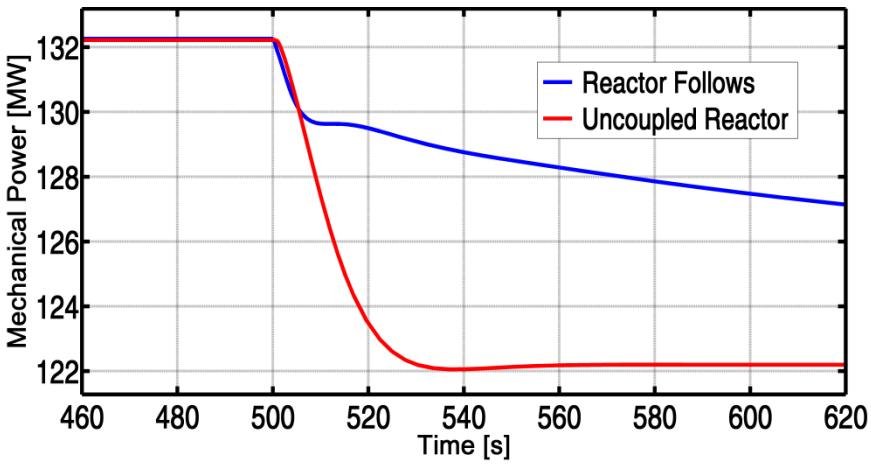

(b)

Figure 6.5. (a) Mechanical power controlled evolution, simulated by adopting both the "Reactor Follows" and the "Uncoupled Reactor" schemes, (b) Detailed view of the simulated transient, showing the different time constants involved.

In Figure 6.5, the outcomes of the simulation of the same operational transient performed on the ALFRED reactor by adopting the two proposed control schemes are shown. In particular, a 10MW

step on the mechanical power has been simulated. The red track represents the system response whether the classic approach adopted in PWRs is followed. The large settling time is due to the involved dynamics of the primary circuit. Indeed, besides the thermal capacity of the secondary circuit, in order to provide the requested mechanical power, it is necessary to bring the reactor core to the suitable load factor. This process is heavily affected by the thermal fields whose evolution has shown to be particularly slow if compared to one of PWRs. Conversely, the blue track represents the system response whether the reactor core is working at rated conditions and the coordinated control of mechanical power and pressure is achieved by adjusting, respectively, the bypass valve and the turbine admission valve. Such a control scheme turns out to be more effective (the desired power level is reached in less than 30s), complying with the time requirements of the primary frequency regulation.

In this Section, the primary frequency regulation over a limited time interval accounting for limited power variations in load demands has been studied. Conversely, if the secondary and tertiary frequency regulation process over longer intervals would be studied, significant changes in the power output would be needed, and then it would become necessary to adjust the operating conditions of the primary circuit as well. Indeed, whether the grid is characterized by a non-negligible fraction of RES-based power plants (in particular wind farms), it may happen during the day that the NPP must be operated at reduced loads because of the hourly fluctuations related to the weather conditions.

Therefore, it would be beneficial foreseeing that the thermal power disposed to the BoP would be reduced in order to balance the power injections of the RES-based power plants. Then, according to the forecast requests of the secondary control reserve, a dedicated slowly varying set-point for the regulation of the reactor thermal power would be derived. Conversely, the instantaneous fluctuations related to the load demands would be compensated by means of the described scheme, based on the coordinated use of the bypass valve and the turbine admission valve.

6.3. Simulation results

After having designed an appropriate strategy to control the mechanical power produced and having defined a feedback scheme for load-frequency control, in order to assess the effectiveness and the performance of the proposed scheme, a frequency profile with a resolution of seconds has been provided. In particular, it is a case study referred to the frequency in the synchronous grid of the Continental Europe over a period of 1000 seconds. Indeed, the mains frequency is in all countries, which are directly connected to the synchronous grid, the same (except short-term fluctuations). The test data set is referred to the 8 March 2011, between the 6 p.m. and the 7 p.m. (Measurement of the utility frequency, 2014). Being the ALFRED reactor connected to the

synchronous grid, the installed power is much higher than its own rated mechanical power. Therefore, the ALFRED reactor cannot provide a relevant contribution in restoring the nominal conditions. In this work, the grid has not been modelled and the frequency regulation process has been represented by means of an open loop scheme (Figure 6.4). The aim of this simulation is showing that, thanks to the proposed procedure, it is possible to accurately follow the grid frequency variations, without being conditioned by the primary circuit dynamics. As shown in Figure 6.7 and Figure 6.9, the results of the simulation assess that the proposed control scheme allows adjusting the mechanical power produced, according to the adopted droop, by operating the turbine admission valve. Even though the presented outcomes are very preliminary since the modelling of the BoP is not fully characterized, these simulation may help to evaluate the possibility of employing this reactor concept in a grid.

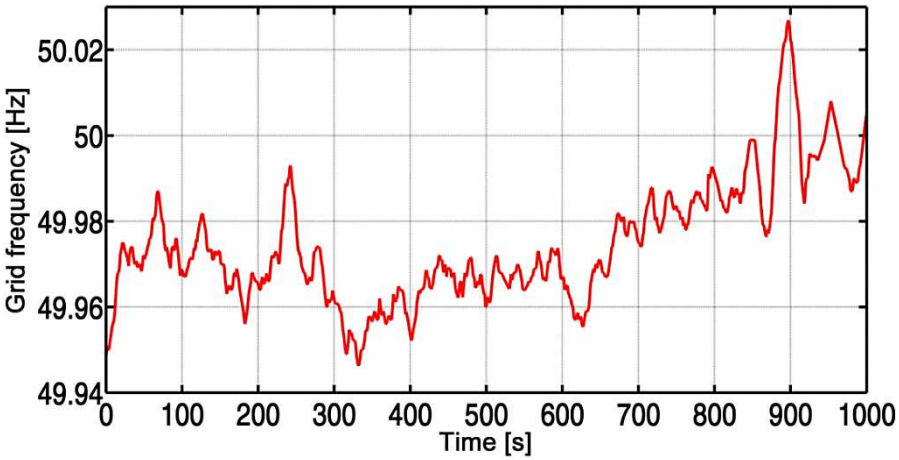

Figure 6.6. Case test frequency profile.

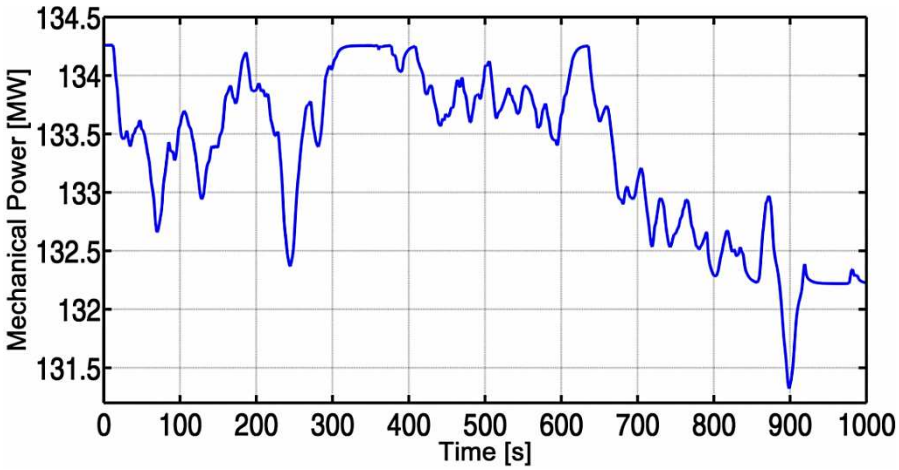

Figure 6.7. Mechanical power response to the provided frequency profile.

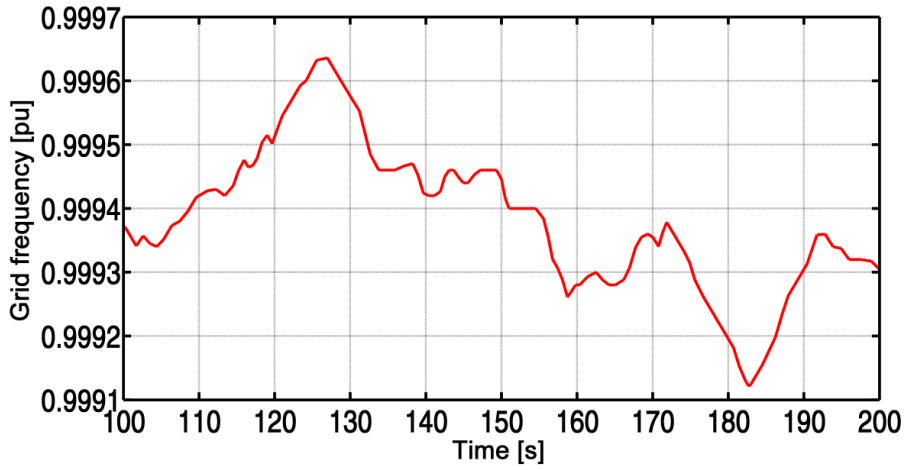

Figure 6.8. Detailed view of the frequency profile.

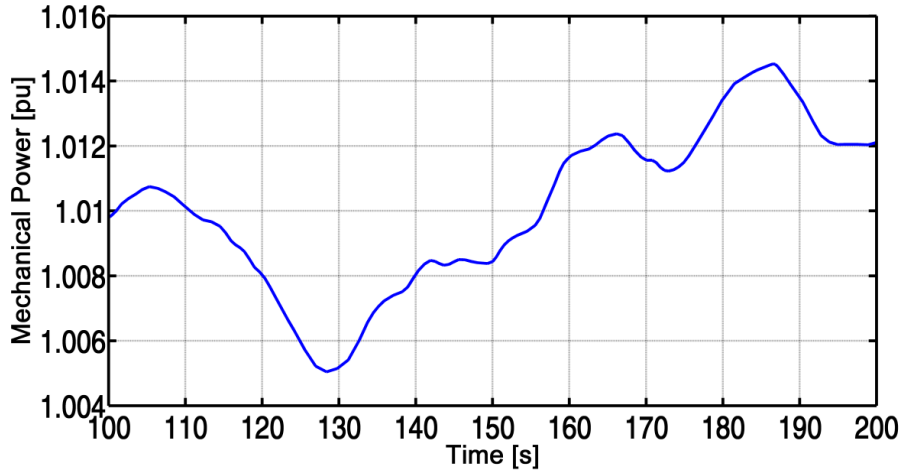

Figure 6.9. Detailed view of the mechanical power response.

Thanks to the developed control scheme, only the pressure variations may influence the primary circuit controlled variables. Indeed, when the reactor is operating at nominal power (300 MW_{th}), in virtue of the feedforward control loop, the value of the feedwater mass flow is very close to the rated one (192 kg/s). In this way, the scheme decouples the operation of the SG by the dynamics of the primary circuit and, at the same time, avoids that the operation of the BoP excessively disturbs the value of the reactor controlled variables. Therefore, the only interference that can affect the value of the reactor power are the pressure fluctuations due to the instantaneous load variations. However, in addition to the effective pressure controller which operate on the bypass valve, these fluctuations are further damped by other feedback regulators, as shown in Section 4.3.2. Indeed, thanks to the adopted tuning of the controllers parameters, the disturbances that can influence the value of the controlled variable are effectively filtered by the implemented PI regulators.The lead temperature in the cold leg (Figure 6.10), which can be affected by the heat transfer conditions, does not perceive the load variation at the secondary circuit (Figure 6.11).

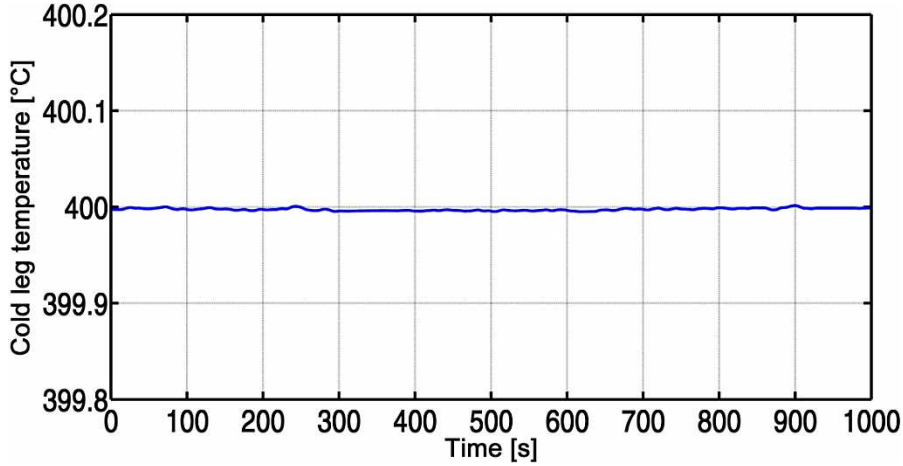

Figure 6.10. Lead temperature evolution in the cold leg.

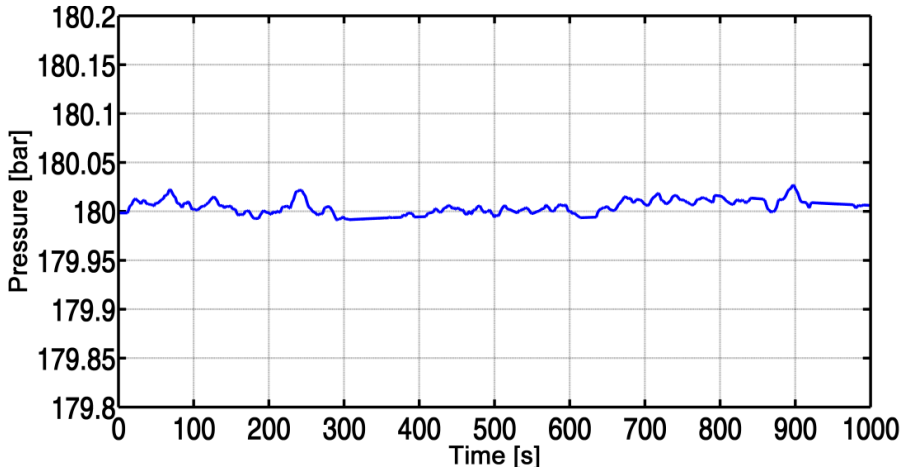

Figure 6.11. Pressure evolution.

6.4. Concluding remarks

In this Chapter, the possibility of performing the load-frequency control using the ALFRED reactor has been assessed. Being ALFRED a demonstrator whose aim is assessing the feasibility of LFR technology, the system performance at providing primary governing response in reaction to frequency deviations by adjusting the mechanical power output has been evaluated. After having outlined the primary regulation features, the requirements in terms of times performance and maximum elongations imposed by the UCTE have been described.

Firstly, it has been tried to adapt to the ALFRED reactor the procedure validated in the PWR operation. However, such an approach has turned out not to be suitable since the simulation of the controlled operational transients has shown that the involved dynamics is too slow to comply with the primary frequency regulation requirements. For this reason, it has been necessary to decouple the operation of the SG from the dynamics of the primary circuit. The proposed control strategy foresees to adjust the mechanical power produced by regulating the bypass valve and the turbine admission valve, operating the SG in constant pressure mode so as to balance the frequency

fluctuations over few seconds, without affecting the primary circuit. The outcomes of the performed simulations have demonstrated the capability of the studied NPP to promptly adapting the electrical power production to the instantaneous variations of the load demands with a resolution of the second. Furthermore, it has been assessed that the adopted tuning for the implemented regulators allows damping any feedback or perturbation on the primary circuit. As a future development of this work, it would be interesting to simulate the behaviour of the ALFRED reactor within a grid, allowing for the presence of wind farms and photovoltaic plants so as to assess the effectiveness of the procedure which foresees the slow varying set-point for the thermal power control.

Conclusions

In this thesis work, the system governing dynamics of LFRs has been studied, and the issues related to the definition of dedicated control strategies have been investigated. As a major outcome of the performed research activities, an integrated methodological approach for the study of dynamics and the assessment of control strategies for LFRs (adopting ALFRED as a reference reactor configuration) has been conceived. At the present time, dedicated analyses regarding the control strategies allowing for the specific constraints of this reactor concept are not available in literature. Therefore, given that for the considered system neither prior experience nor operational data are available, a suitable model-based approach has been developed, and quantitative well-proven investigation tools have been employed.

In this perspective, an extended characterization of the system dynamics has been preliminarily performed. As a first step, the system stability features over the entire power range have been assessed by adopting the root locus method so as to verify that no problems arise in system operation even at reduced load factors. In this perspective, a simulation tool has been built expressly meant for such an early phase of the reactor pre-conceptual design, aimed at evaluating the stability and robustness of the dynamic system. In addition, it has been demonstrated how such a tool may be useful for providing useful guidelines to core designers. In the LFR core design, the reactivity feedback coefficient related to the lead density variations in the active region is particularly important since it is deeply influenced by the core geometry. Thanks to the root locus, it has been possible to estimate the allowable range of variation of this parameter so as to avoid instabilities in the reactor operation. According to the performed sensitivity analysis, the system has turned out to be inherently stable at all power levels, independently of both the fuel burn-up and the value of the coolant density coefficient, which should reach unrealistic high values to make the reactor unstable even allowing for the destabilizing action of the SG on the primary circuit.

For both conceiving and assessing the control strategies, a dedicated control-oriented simulator has been developed by adopting the object-oriented Modelica language. The features of the object-oriented modelling approach have been exploited in order to obtain a very flexible, straightforward, and fast-running simulator aimed at testing the control strategies proposed for ALFRED. The adoption of this tool has revealed very useful since a simplified tool providing the time constants characteristic of the system has been built, but at the same time it has allowed a sufficiently accurate description of the overall plant response (from the NSSS to the interface on the grid). Furthermore, the possibility of easily coupling the model of the system with the model of the control scheme has been a key-advantage in the development and implementation of the proposed model-based approach.

As far as the definition of a suitable control strategy is concerned, there are no assessed studies regarding the specific pairings between input and output variables or how to adapt the strategies conventionally used in LWRs to the characteristics of this innovative reactor concept. Therefore, the indications provided by the simulation of the system dynamic response have been supported by a dedicated quantitative technique, i.e., the RGA method. This quantitative algorithm, widely used for industrial applications, has allowed evaluating the effectiveness of the proposed pairings between input and output variables, starting from the constitutive equations of the physical system.
In this sense, the importance of employing the lead mass flow rate as a control variable so as to improve operational flexibility of the reactor has been assessed, proposing an alternative control scheme. Once finalized the control strategy allowing for the needs of the studied reactor, a suitable control scheme has been implemented by adopting reliable feedback regulators, and then assessed by simulating the controlled system response.

At this point, once having finalized the control system for the plant operation in full power mode, the modelling of the reactor start-up has been undertaken. It is a particularly delicate operational stage (even for a LWR), since it is quite difficult complying with all the technological constraints that characterize the system. Indeed, given that different variables of interest have to be effectively governed, it is essential to coordinate the control actions to be carried out. In this perspective, a modelling tool mainly used in industrial automation, such as synchronized Petri net, has been used. In the common practice, the characterization of the reactor start-up does not provide any hint on the regulators ensuring the desired evolution. Conversely, the provided formalization allows obtaining indications on the key-events that rule the transitions between the controllers involved in the proposed procedure, and the control system configuration has been easily derived. Indeed, thanks to this approach, it has been straightforward to develop the dedicated Finite State Machines that rule the operation of the different regulators. The reactor start-up procedure has been assessed by means of the object-oriented simulator, demonstrating that the several constraints on the controlled variable (i.e., lead temperature in the upper plenum and in the cold leg) and the corresponding rates of variation (i.e., thermal power and reactivity) have been satisfied. By adopting the Petri net formalism, the preliminary version of the architecture of the supervisory control system has been built as well. In particular, a two-level control system architecture has been developed, namely: the “master system” coordinates the plant operation by sending suitable signals to the “slave system”, in which feedback modulating regulators are implemented. Such a scheme constitutes a preliminary attempt of building the control system architecture starting from a Petri net allowing for the characteristic features of the controlled process. As a further development of this work, synchronized Petri nets may be adopted for coordinating the alternation of the different plant

operational modes. In this way, both the coordination of the several control actions to be taken and the plant supervisory control system would be represented by adopting the same effective and functional formalism.

As a last step, the concerns related to the load-frequency regulation through the ALFRED reactor have been studied. Indeed, whether a relevant fraction of the connected power plants are based on RES (Renewable Energy Sources), because of the discontinuous power supply and the reduced presence of energy accumulators, it is fundamental to develop appropriate and highly reliable automated controls, in order to avoid voltage and frequency fluctuations that may result in a worsening of the plant availability. In this sense, an alternative solution has been proposed, in which two different set-points have been defined for the thermal power produced in the core and the mechanical power available to the alternator, according to the corresponding time constants.

The developed approach has the advantage of not being tailored to the ALFRED reactor but it can be extended to other LFR reactor designs or other advanced SMR concepts as well. As shown in the Appendix, the modelling tools adopted in the thesis work have been employed to study the fast-runback operational transient for a Sodium-cooled SMR. Therefore, even though the features of the studied reactor concept are quite different from the ALFRED reactor ones, the proposed investigation procedure has turned out to be effective, demonstrating its validity and versatility. In particular, the potentialities of the Petri nets and the effectiveness of the object-oriented approach have been assessed. In addition, this work has shown the necessity of developing and implementing MIMO control schemes, so as to achieve flexible operation procedures for the Gen-IV NPPs. Such aspects assume a particular importance whether SMRs are considered, given the role played by the operational costs in achieving economic competitiveness. In the fast runback operational transient, the limits of the currently employed SISO controllers have been pointed out. Conversely, the adoption of MPC-based control system would allow achieving faster control transients, maintaining the temperature field close to the nominal one and avoiding the time-consuming operations needed for the reactor start-up. In addition, such a study has shown the importance of a metal-fuelled reactor in the perspective of designing an inherent control scheme, which would allow limiting the contribution of active systems in the reactor operation.

APPENDIX: *Study of innovative control strategies for the Fast-Runback operational transient applied to sodium-cooled SMR*

Outline

In the thesis, several techniques conventionally adopted in industry (e.g., RGA in chemical plants, Petri nets in industrial automation) have been employed to deal with the issues regarding the design of control strategies for an innovative LFR (for which no operational data are available). Such modelling tools have been adopted for studying the fast-runback operational transient of a different Generation IV reactor concept, i.e. the sodium-cooled Small Modular Reactor (SMR). Indeed, over the last years there has been a growing interest in the development of SMRs, whose economic competitiveness mainly relies on plant simplification and reduced operational costs, given the disadvantage with respect to the traditional units in terms of economy of scale. Indeed, plant operation and maintenance costs are driven by plant availability, which can be enhanced by means of innovative control strategies by avoiding unnecessary plant or unit trips. In this perspective, an effective strategy for achieving fast runback of a typical sodium-cooled SMR, which coordinates the operation on the SG and the primary circuit, has been developed and assessed. Once the proposed procedure has been modelled by means of the Petri nets, the feedback modulating regulator based on Model-based Predictive Control (MPC) has been developed. Such a control scheme has been adopted to implement a MIMO control strategy, so as to coordinate different control variables to achieve the power drop. In particular, the thermal power produced in the core and the sodium temperature in the upper plenum have been adjusted by operating the externally imposed reactivity and the primary circuit mass flow rate. In this way, it is possible to reduce the power level as quickly as possible (without scramming the reactor), leading to significant saving in the operational costs of the reactor while also improving the system availability. The proposed procedure has been characterized by simulating the operational transients on both an oxide-fuelled reactor and on a metal-fuelled core, comparing the responses of the two different configurations and the respectively needed control rods contribution.

The main results have been published in:

- Ponciroli, R., Passerini, S., Cammi, A., Luzzi, L., Vilim, R., 2014. Innovative Control Strategy approach for the Fast-Runback operational transient of a Sodium-cooled Small Modular Reactor. International Congress on Advances in Nuclear Power Plants (ICAPP 2014), Charlotte, April 6-9, 2014.

A1. Introduction

In this thesis work, several techniques conventionally adopted in industry (e.g., RGA in chemical plants, Petri nets in industrial automation) have been employed to deal with the issues regarding the definition of control strategies for an innovative LFR for which no operational data are available. The adoption of these tools has allowed to figure out a model-based methodological approach oriented to the characterization of the dynamics and the development of suitable control schemes. In particular, the proposed procedure has been applied to the ALFRED reactor, adopted as case study. However, the adopted techniques are not tied to the studied reactor concept, but they can be employed to investigate other Generation IV reactor concepts as well. Indeed, in this Appendix, such modelling tools have been adopted for studying the fast-runback operational transient of a sodium-cooled Small Modular Reactor (SMR).

Over the last years, there has been a growing interest in the development and deployment of reactors classified as SMRs. The proposed designs for these NPPs generally aim at providing increased benefits in the areas of safety and security, non-proliferation, waste management, as well as to support multiple energy applications and offer flexibility in design, siting and fuel cycle options. In particular, the Department of Energy (DOE) believes that SMRs may play an important role in addressing the energy, economic and climate goals of the U.S. if they can be commercially deployed within the next decade (DOE, 2013).

In virtue of the specific features of SMRs, a new paradigm is required in the design and operation of these NPPs (Holcomb, 2013). To reduce capital costs, it is important to make extensive use of digital technologies and to optimize the I&C architecture. In addition, plant operation and maintenance costs are significantly driven by plant availability, which can be enhanced by means of innovative control strategies by avoiding unnecessary plant or unit trips. Therefore, highly reliable automated control systems that are sufficiently robust to handle an extensive range of plant transients shall be considered, and a control architecture that can respond to events and conditions by adapting the control strategy should be adopted. In the past, NPPs were designed almost exclusively to cover base load demands. This approach, while sound for large units, is not suitable for the SMRs. Indeed, without appropriate and highly reliable automated controls, eventual voltage and frequency fluctuations due to the fractions of RES-based power plants may result in reactor trips and consequently in a worsening of the plant availability (Clayton and Wood, 2010).

In this work, an effective strategy for achieving the fast-runback of a sodium-cooled SMR has been developed and assessed. The runback transient involves the disconnection of the power plant from the grid following a generator trip and the subsequent rapid reduction of the electrical power output. The occurrence of such transients might not be known in advance to the plant operators. In

particular, the runback may be triggered by an event within the NPP and a prompt disconnect from the grid may be needed to bring the system to a safe shutdown condition. In this case, the standard procedure adopted is the immediate disconnection of the power plant from the grid followed by the reactor scram. Later, while in the cold shutdown mode, a series of diagnostic tests are performed in order to assess the impact of the transient, its causes and how to restore the rated operational conditions. On the other hand, it is also possible that the plant must disconnect from the grid as a result of a grid fault. In this case, it would be beneficial for the NPP if the runback could be regarded as an operational transient, since electric power production has been reduced for causes that do not concern the plant conditions. In particular, avoiding a reactor shutdown in favour of a power runback would mean avoiding the related report filing and communication with the regulator as well as all the complex and time-consuming operations needed for a reactor start-up. Such flexibility would therefore lead to significant saving in the operational costs of the reactor while also improving the system availability.

A2. Reference reactor configuration and corresponding object-oriented model

In this work, the fast runback operational transient has been studied in reference to a standard plant in order to establish a baseline for operational performance. The reference design shall reflect the state-of-the-art of conventional fast reactor technology in terms of plant configuration and materials, use of active control systems and standard operation. The considered plant is a pool-type sodium cooled fast reactor, with a Rankine cycle as the BoP power conversion technology. Its design layout is characterized by three forced circulation circuits, i.e. the primary system and an intermediate system, both using sodium coolant, and the BoP for heat removal and electric power production. Primary system pumps take their suction from the pool and deliver the coolant to the reactor. The intermediate system is driven by a pump and heat is delivered to the SG. In order to simulate the overall system response and assess the proposed control strategies for the fast runback, a non-linear one-dimensional model of the reference reactor has been developed adopting the object-oriented approach based on the Modelica language. The developed model has then been simulated in the Dymola environment. In Figure A1, the graphical interface of the object-oriented model is shown. In this work, as far as the neutronics is concerned, reactivity has been defined by referring to the *integral reactivity parameters* (Wade and Fujita, 1988):

$$\rho_{net} = A \cdot (P - 1) + B \cdot (P/W_1 - 1) + C \cdot \delta T_{in} + \rho_{ext} \quad \text{(A1)}$$

In particular, A represents the reactivity variation associated with the fuel temperature increase from the average coolant temperature to the average fuel temperature at nominal conditions. B

represents the reactivity variation associated with the increase in fuel and coolant temperatures from the average coolant temperatures at zero-power conditions to the average coolant temperature. C is the feedback reactivity coefficient associated with the core inlet temperature.

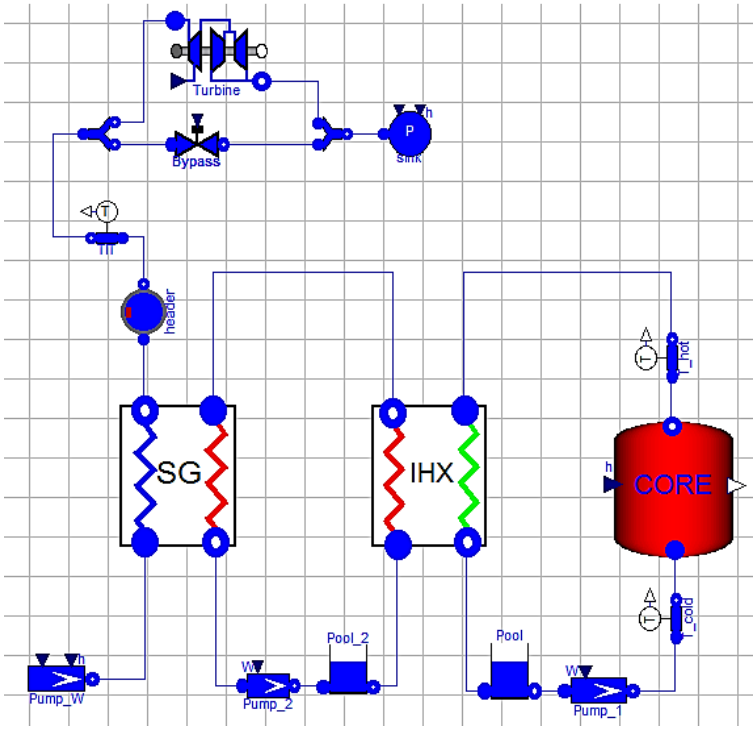

Figure A1. Graphical interface of the object-oriented model of the overall plant.

As far as the choice of fuel is concerned, the fast runback operational transient has been simulated on both an oxide-fuelled and on a metal-fuelled reactor (uranium-plutonium-zirconium, U-Pu-Zr, alloy (Vilim, 2013)), in order to compare the responses of the two configurations. Despite the shorter operational experience compared to oxide fuel, metal fuel has been claimed to behave better than oxide fuel in transients and accidental scenarios. Indeed, inherent design features can improve safety over what can be achieved using active systems alone. Nevertheless, the level of experience gained with oxide fuel is currently unmatched, also considering that a new metal fuel form would have to be tested and licensed before being used as a fuel in a nuclear reactor. Such considerations make oxide fuel the state of the art fuel form for the reference design. In Table A1, the neutronics parameters and thermal features of interest for the two fuel options are resumed. In Table A3 the steady state values for the reference design at rated power have been indicated.

Table A1. Neutronics parameters and thermo-physical properties for the two different fuels (Wade and Fujita, 1988; Wigeland and Cahalan, 2009).

Parameter	Definition	Oxide Fuel	Metal Fuel
β	Fraction of delayed neutron [pcm]	330	330
Λ	Mean time generation [μs]	0.6	0.6
λ	Decay constant of one group precursor [s^{-1}]	0.1	0.1
A	Net reactivity decrement [$]	-1.24	-0.15
B	Power/flow coefficient of reactivity [$]	-0.5	-0.45
C	Inlet temperature coefficient of reactivity [$/K]	-0.0041	-0.0032
k_f	Thermal conductivity [W/mK]	1.55	20
c_f	Specific heat capacity [J/kgK]	290	180
d_f	Density [kg/m^3]	8990	11625

Table A2. SG Main Data for the Reference Reactor Configuration

Steam Outlet Pressure [MPa]	19.3
Feedwater Inlet Temperature [°C]	257
Water/Steam Flow Rate [kg/s]	228
Steam Outlet Temperature [°C]	457
Water/Steam Pressure Drop [MPa]	0.88
Sodium Flow Rate [kg/s]	2228
Sodium Inlet Temperature [°C]	482
Sodium Outlet Temperature [°C]	325
Thermal Power [MWth]	453
Number of Tubes Required	2625
Tube OD [mm]	15.875
Tube Wall Thickness [mm]	2.1082
Tube Pitch [mm]	30.988
Active Length [m]	23.4696

Table A3. Steady state conditions for the reference reactor configuration.

Reactor Nominal Power [MW]	*Primary Loop Flowrate [kg/s]*	*Intermediate Loop Flowrate [kg/s]*	*Secondary Loop Flowrate [kg/s]*	*Rod Reactivity [$]*
900.00	4623	4586	456	0.0
Average Fuel T [°C]	*Average Clad T [°C]*	*Reactor Coolant Tout [°C]*	*Reactor Coolant Tin [°C]*	*IHX Intermediate Coolant outlet T [°C]*
1250	457	508	354	479
IHX Intermediate Coolant inlet T [°C]	*SG Cold Coolant Tout [°C]*	*SG Cold Coolant inlet T [°C]*	*Primary Tank Coolant Mass [kg]*	*Intermediate Tank Coolant Mass [kg]*
324	461	257	379000	37900

A3. Definition of Fast Runback operational procedure

The aim of this investigation is the development and the assessment of a suitable procedure to perform the system fast runback from operating conditions to reduced power output, during grid outages and related idle times. After the grid disconnection, the reactor remains critical at low power levels, while the residual electric power produced (up to about 5% of the nominal value) is disposed of by meeting the demands of the house loads. At last, when it is possible to restart the load-frequency regulation, the power plant is promptly carried back to the nominal conditions.

As far as the BoP operation in fast-runback mode is concerned, the *feedwater leading* control strategy has been adopted (Seong and Kim, 2012). According to this scheme, once the system has been disconnected from the grid, the external power demand first controls the flow rate by adjusting the feedwater control valves. Then, the steam flow rate is changed and the turbine power varies accordingly. These control actions determine a decrease of BoP capability of disposing the thermal power produced in the primary circuit. Therefore, first the temperatures in the intermediate circuit and then in the primary circuit rise, inducing a series of reactivity feedbacks. This strategy minimizes the time lag between the circulation of the coolants of the Nuclear Steam Supply System (NSSS) and the BoP by first controlling the feedwater flow rate through the SG.

During the fast runback mode, the electrical power set-point is set around the 5% of the nominal value in order to power the several systems operating in the plant, namely the house loads. It is good practice not to excessively reduce the steam mass flow rate at the turbine inlet (lower bound is equal to 20%) in order to avoid issues concerning the turbine partialization. To compensate for this mismatch between steam flow rate (20%) and mechanical power (5%), it is advisable to operate only the HP turbine stages. In this way, given that the conditions of the steam admitted to the turbine are kept close to the nominal ones, the value of the electric power generated decreases as well by reducing the specific enthalpy drop across the turbine, achieving the desired electrical power level.

The proposed procedure allows rapidly regulating the BoP conditions to the new set-point for the electrical power generated (time constants of the order of a few seconds). On the other hand, the thermal power generated within the core has to be reduced as promptly as possible, without scramming the reactor and possibly limiting the control rods contribution. In order to avoid reaching design limits set on the coolant temperatures, following the feedwater mass flow rate reduction, it is necessary to adjust the thermal power output to the same level as well. Therefore, it is necessary to introduce negative reactivity to reduce the power level to the 20% of its nominal value. This power drop can be achieved over a few minutes because of the plant thermal capacity, which allows for considerable energy storage.

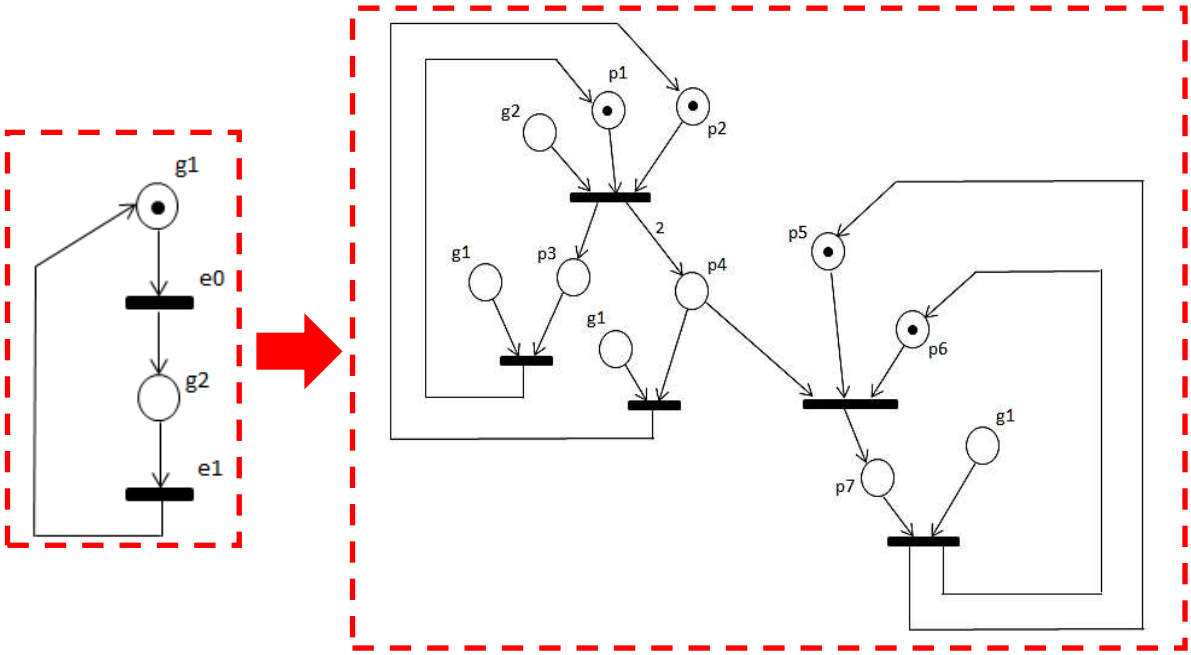

Figure A2. The Petri nets representing the evolution of the grid (on the left) and the overall plant desired behaviour (on the right) during fast runback operational transient.

Table A4. External events regulating the load frequency regulation performed by the power plant.

e0	*Off-line transition* → the plant is disconnected from the grid
e1	*On-line* → the plant is connected to the grid

Table A5. Description of the places constituting the Petri net which represent the status of the grid.

g1	*Load-frequency regulation* → the electrical power produced by the plant is adjusted in order to control the grid frequency.
g2	*Fast-runback operation mode* → after having been disconnected from the grid, the reactor power set-point is promptly reduced and the system starts operating in *fast runback* mode.

Table A6. Description of the places constituting the Petri net which represent the overall plant evolution.

p1	*HP&LP stages operated* → the turbine is run at nominal operative conditions, performing the load-frequency regulation.
p2	W_{fw} *at nominal conditions* → the feedwater mass flow rate is regulated according to the nominal operative conditions.
p3	*HP stages operated* → once the fast runback mode has fired, only the HP turbine stages are operated.
p4	W_{fw} *is kept fixed at 20%* → the feedwater mass flow rate is kept fixed at the 20% of its nominal value.
p5	*Power control loop normal mode operation* → the reactor power is regulated by adopting the normal mode feedback control loop.
p6	W_1 *control loop normal mode operation* → the coolant mass flow rate is regulated by adopting the normal mode feedback control loop.
p7	*Fast runback controller* → the normal mode feedback control loops concerning the control rods and the primary circuit mass flow rate are disabled. Both these two input variables are adopted in a suitable MIMO controller in order to perform an effective regulation of the thermal power in the primary circuit.

A4. Control scheme definition

After the plant has been disconnected from the grid, the objective of the control system operating in the fast runback mode is to reduce as promptly as possible the power level, without scramming the reactor and possibly limiting the control rods contribution. In this perspective, the adoption of feedback SISO control loops based on PID regulators does not yield acceptable performance. The reduction of the feedwater mass flow rate reduces thermal power rejection from the BoP. Because of the intervening presence of the intermediate circuit and its associated heat capacity, the initial temperature increase in the SG does not provide immediate thermal feedback to the primary circuit. Therefore, if we merely change the position of the control rods to reduce thermal power (Figure A3) without changing other control variables in the primary circuit, the net effect is an overall cooling of the plant (Figure A4). Consequently, before the system can be connected to the grid again, the heating up of the structural materials must be carried out and the full power mode attainment will be delayed.

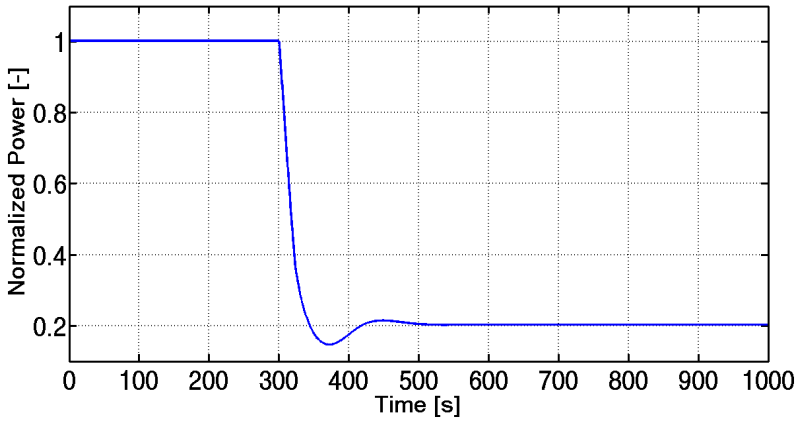

Figure A3. Thermal power evolution in the SISO control scheme configuration.

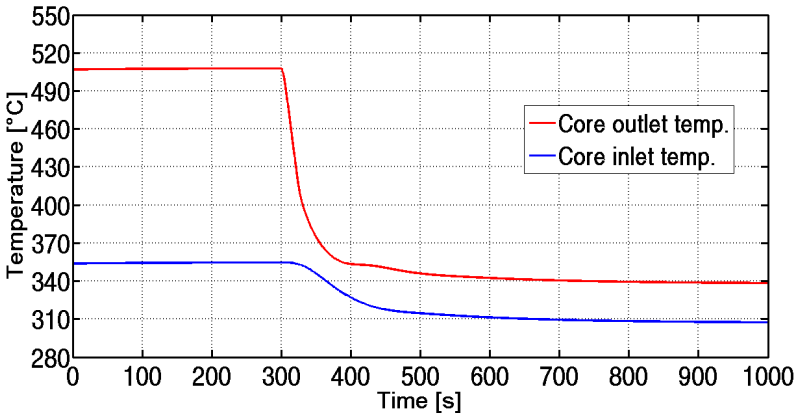

Figure A4. Core outlet and core inlet temperature evolution in the SISO control scheme configuration.

These limitations have been addressed through the use of a MIMO control strategy that provides the capability to employ coordinated control variables to achieve the thermal power drop.

By referring to the quasi-static reactivity balance (A1), in addition to the externally imposed reactivity, the system reactivity can be influenced by operating directly on the coolant mass flow rate in the primary circuit (W_1) or by changing the coolant core inlet temperature (δT_{in}). In this perspective, in the next section, the development of a dedicated MIMO control strategy has been pursued.

A4.1. Operational limits on the control actions to be performed

In the development of a control system, limits on the control actions to be performed need to be set. These thresholds apply both to the point value and to the rate of change of the control variables. In particular, the limits regarding the externally induced reactivity due to control rods motion (ρ_{ext}) and the coolant mass flow rate in the primary circuit (W_1) are hereunder discussed.

Control rods

As it has been indicated in Section 4.4, in nuclear reactors an upper limit is usually set to the rate at which the positive reactivity may be induced. In this sense, in order to avoid prompt criticality, a limit is set to the reactor period, which must be large enough to allow an effective control action on the plant. At the same time, the negative reactivity added to the system must not lead to an excessive local penalization of the neutron flux. In such a case, when the signal from the neutron flux detectors indicates out of range values for the peaking factors, the reactor is scrammed. Therefore, the maximum and minimum rates of variation of the control rods reactivity have been externally set so that the reactor thermal feedbacks manage to restore criticality conditions.

$$\left.\frac{d\rho_{ext}}{dt}\right|_{min} = -25.0\ pcm/s \qquad \left.\frac{d\rho_{ext}}{dt}\right|_{max} = +25.0\ pcm/s \tag{A2}$$

Since the runback consists in a reduction of the power level, it is not necessary to induce any positive reactivity to the system. The minimum value can be estimated through the quasi-static reactivity balance at the desired power level as follows. The system fast runback is initiated by reducing the feedwater mass flow rate which results in a drop of the convective heat transfer coefficient at the interface between the intermediate circuit and the steam generator. Therefore, the thermal power produced in the core leads to the sodium temperatures increase in the intermediate circuit. Consequently, the coolant temperature at the core inlet rises ($\delta T_{in} > 0$). However, in order to be conservative, this negative reactivity contribution has been neglected, while the coolant mass flow rate in the primary circuit has been fixed to its nominal value. Therefore, the externally imposed reactivity must be equal to:

$$\begin{cases} P = 0.2 \\ W_1 = 1.0 \\ \delta T_{in} = 0 \end{cases} \Rightarrow \rho_{ext} = A \cdot (P-1) + B \cdot (P/W_1 - 1) \Rightarrow \rho_{ext} = -545.49\ pcm \quad \text{(A3)}$$

The maximum and the minimum values to the externally imposed reactivity have been estimated as:

$$(\rho_{ext})_{max} = 0\ pcm \qquad (\rho_{ext})_{min} = -545.49\ pcm \quad \text{(A4)}$$

Sodium mass flow rate

Electromagnetic pumps provide the coolant mass flow rate in the primary circuit. Since there are no moving parts, the inertia of these devices is reduced and therefore the variation of the mass flow rate may be achieved in extremely short time. In particular, the inertia is such to ensure a halving time equal to 2.5 seconds. Therefore, the maximum and minimum limits to the rate of change of the mass flow rate are equal to:

$$\left.\frac{dW_1}{dt}\right|_{min} = -0.2\ s^{-1} \qquad \left.\frac{dW_1}{dt}\right|_{max} = +0.2\ s^{-1} \quad \text{(A5)}$$

As far as the maximum and minimum point values are concerned, their evaluation is determined by thermal-hydraulic considerations. In particular, the maximum value has been set equal to the nominal one. On the other hand, it would be worthy that the minimum value assumed by primary circuit mass flow rate leads to a favourable contribution to the reactivity balance. Since B is negative,

$$B \cdot (P/W_1 - 1) < 0 \Rightarrow P > W_1 \quad \text{(A6)}$$

Ideally, the primary circuit mass flow rate shall be reduced more quickly than the power itself. However, it is also necessary to avoid insufficient cooling in the reactor power channel. Therefore, the minimum has been fixed to the 20% of the rated value. Ultimately, the maximum and the minimum value to the primary circuit mass flow rate are set to

$$(W_1)_{min} = 0.2 \qquad (W_1)_{max} = 1 \quad \text{(A7)}$$

A4.2. Theory of Model-based Predictive Control Approach

The main goal of the fast runback control strategy is to bring the system to the desired reduced power level as soon as possible. At the same time, it would be relevant to reduce the control rods contribution, inducing thermal reactivity feedbacks by operating on other control variables. Moreover, whenever the control system is required to perform a significant change on the plant operating point, it is important to set limits on the control actions which can be performed. Consequently, the problem of defining a suitable control strategy to achieve the system fast runback

can be studied as a *constrained optimization problem*. Among the most promising techniques, Model-based Predictive Control (MPC) methodology is an effective mean to deal with large multi-variable constrained control problems. MPC has so far received attention as a powerful tool for the control of industrial process systems, and it has already been applied to NPPs with promising results (Bragg-Sitton and Holloway, 2006; Cammi et al., 2008). The control algorithm seeks to optimize an objective or "cost" function, which is a user-specified mathematical indicator of the desired performance of the feedback regulator. Following a MPC approach, the control actions aim at minimizing a performance criterion over a prediction horizon, whose length is kept constant in time (*receding-horizon algorithm*) (Clarke, 1994). The optimization problem is possibly subject to constraints on the manipulated inputs and outputs, whose future behaviour is estimated according to the model of the plant. In this way, the controller can predict whether or not the proposed control actions will cause future violations of system constraints, while still ensuring that the early control actions do lead to a long term control strategy that minimizes the cost function. The control algorithm of the model predictive controller proposed in this work can be summarized as follows:

a. Past measured outputs and past control inputs are collected up to the present time step k. Future outputs along the prediction horizon (N) can then be estimated using a linearized dynamic model of the plant, initialized with past input and output data.

b. A control sequence $\Delta\hat{u}(k+i),\ i=1,\dots,M$ for the next M time steps is obtained by minimizing the cost function $V(k)$ which takes into account two terms. The first one is the squared tracking error (i.e., the squared difference between the reference output and the estimated output), the second one is represented by the square of the change of control action between two adjacent time steps ($\Delta\hat{u}$), while the third one allows penalizing deviations of control variables from the nominal values. The cost function can be expressed in the following way:

$$V(k)=\sum_{i=1}^{N}\|\hat{y}(k+i|k)-r(k+i)\|^2\cdot Q(i)+\sum_{i=1}^{M}\|\Delta\hat{u}(k+i)\|^2\cdot R(i)+\sum_{i=1}^{M}\|\hat{u}(k+i|k)-u_0\|^2\cdot S(i) \tag{A8}$$

where i is the generic time step, k is the current time step, $Q(i)$ is the weight of the tracking error, $R(i)$ is the weight of the control input rate variations, $S(i)$ is the weight of the control input variations from the nominal conditions, and r is the set-point. Finally, $\hat{y}(k+i|k)$ is the i-th step prediction of the system output, based on measured data up to the k-th step, and on future control variables computed along the prediction horizon.

c. At next time step, only the first value of the control sequence is considered for the plant control, and the other terms of the sequence are discarded. The past measured outputs and control inputs are updated, then the whole procedure is repeated, for the following time step, from (a) to (c). Optimization of the objective function is then repeated at the next sample time, with the horizon shifting forward in time.

A4.3. Development of MPC based controller

To design of a MPC based controller for the NPP control during the fast runback mode it is necessary to adopt a simplified version of the plant model suitable for the control algorithm. The Dymola simulation environment allows linearizing the object-oriented model around the system nominal condition in order to derive the corresponding state-space representation. Therefore, the simulations of the plant responses have been performed adopting the non-linear model, while in the control scheme definition a LTI discrete-time system has been implemented in the MATLAB® MPC control toolbox.

$$\begin{cases} x(k+1) = Ax(k) + Bu(k) \\ y(k) = Cx(k) \end{cases} \tag{A9}$$

In addition to the thermal power (P), the sodium temperature in the hot plenum (T_hot) is considered as a controlled variable as well. The reactor outlet temperature represents the higher fluid temperature in the plant, and is directly related to the achievable thermal efficiency, which ultimately affects the cost of electricity. However, materials and thermodynamic considerations (such as the boiling point of the coolant or the behaviour of structural materials at high temperatures) set an upper limit for such a temperature (550 °C).

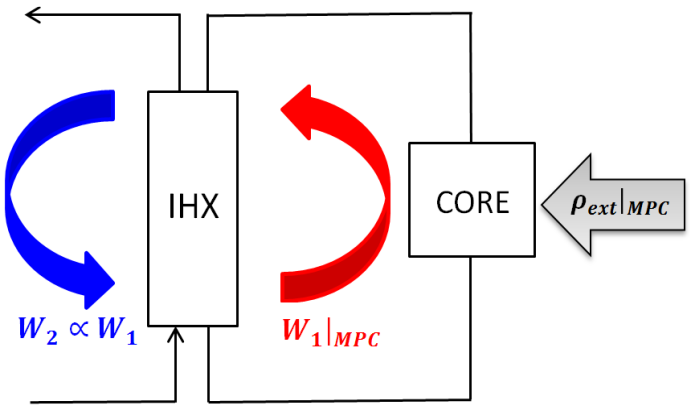

Figure A5. Representation of adopted control strategy.

In the proposed control strategy, as shown in Figure A5, the externally imposed reactivity (ρ_{ext}) and the primary circuit mass flow rate (W_1) are adjusted so as to govern the thermal power and the sodium temperature in the upper plenum. At the same time, the intermediate circuit mass

flow rate (W_2) is changed in proportion to W_1 so as to maintain the same temperature drop across the Intermediate Heat Exchanger (IHX).

$$u = \begin{Bmatrix} \rho_{ext} \\ W_1 \end{Bmatrix} \qquad y = \begin{Bmatrix} P \\ T\_hot \end{Bmatrix} \tag{A10}$$

A quadratic cost function has been considered for the optimization problem (Eq. (A8)) and the adopted constraints are time-invariant and expressed by linear inequalities. The weights has been chosen carefully, as there is no standard methodology to evaluate them. In particular, the values of the matrix Q are the easiest to be evaluated, since they refer to the output variables accuracy in following the corresponding set-points. If these values are set to zero, the output variables are allowed evolving freely. Otherwise, the larger these values, the more their deviations from the set-points are penalized, and the control actions will try to keep the output variables as close as possible to the set-points in attempting to minimize the figure of merit. For this reason, the weight for the coolant temperature in the hot plenum has been set to a reduced value, since achieving an accurate reference value is not so relevant, while excessive thermal stresses to the heat exchanger tube sheets should be avoided. Similarly, increasing the values of the matrix R means increasing the penalty on the control variables variations, and that leads to smoother control actions, while by increasing the values of the matrix S the control scheme attempts to achieve the control goals while keeping the values of the control variables as close as possible to their nominal values.

A4.4. Implementation of the developed MPC controller

The developed MPC controller has to be considered as one of the controllers envisaged to operate in the proposed control strategy for the fast-runback. Indeed, the first control action to be carried out is the mechanical power reduction. Therefore, the turbine admission valve is abruptly closed, allowing minimum steam mass flow rate to the turbine. As soon as the closure of the turbine admission valve begins, the bypass valve controller, which regulates the SG pressure by adjusting the steam mass flow rate to be disposed to the condenser, is switched on. The next step to be taken is the reduction of the feedwater mass flow rate to the desired level (20% of its nominal value in 40 seconds). In order to facilitate the power reduction in the reactor core, the contribution due to the coolant temperature increase at the core inlet ($C \cdot \delta T_{in}$) is initially exploited. It is essential that the feedwater flow rate reduction in the SG occurs before the beginning of the power drop, so that the increasing temperatures from the BoP may reach the primary circuit and give their reactivity feedback contribution. The proposed operational procedure consists in several FSMs implemented in the Simulink environment by adopting the Stateflow toolbox (Figure A6).

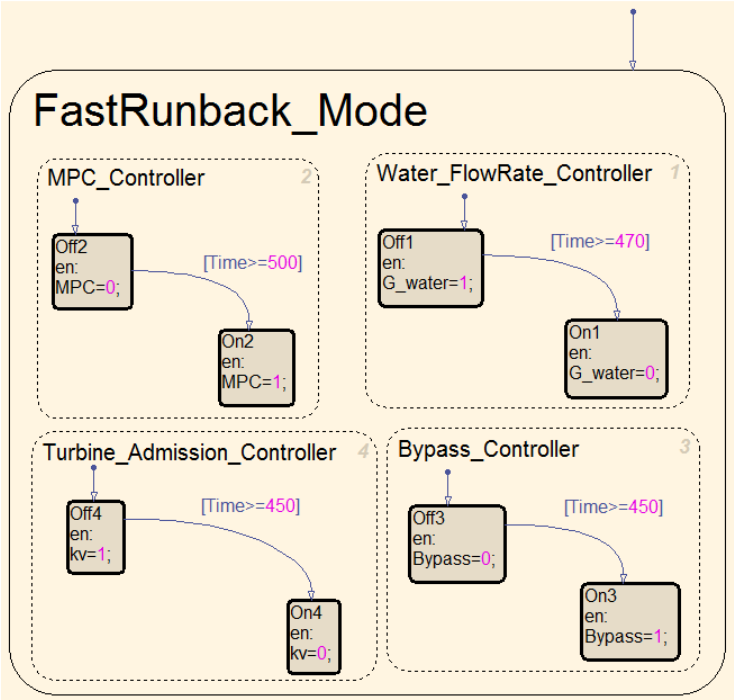

Figure A6. Representation of the implemented Finite-State machines.

A5. Oxide-fuelled reactor simulation results

Once finalized the control strategy and designed the control scheme, the performance of the control strategy and associated controller have been assessed by simulating the system response of developed object-oriented model.

Table A7. Adopted MPC parameters for the oxide-fuelled configuration

Parameter	Value
Time step, T_s	0.1 s
Prediction horizon, N	60 s
Control horizon, M	30 s
Weight of the tracking error, $Q(i)$	[30, 0.2]
Weight of the control input variations, $R(i)$	[0.5, 10]
Weight of the control input absolute values, $S(i)$	[12, 4]

As far as the oxide-fuelled core is concerned, according to the values of the corresponding integral reactivity parameters, the fast runback operational transient may only be achieved by means of relevant control rods contribution. From the plant operation perspective, the larger reactivity contribution to be counterbalanced is given by the $A \cdot (P-1)$ term. Indeed, the value of A represents the reactivity that is vested in the incremental temperature rise inside the fuel. Therefore, when the thermal power level is heavily reduced (Figure A7), the fuel pin incremental temperature collapses, and positive reactivity is introduced. For the oxide fuels, such contribution turns out to be particularly penalizing, being equal to

$$A \cdot (P-1) = -1.24 \cdot (0.2-1) = 0.992\$ \quad \text{(A11)}$$

It is possible to take advantage of thermal feedbacks even if their contribution is modest compared to the positive reactivity insertion due to the power reduction (Figure A8). The reactor coolant inlet temperature tends to increase, resulting in a negative reactivity insertion. Such a temperature rise at the core inlet is important as it contributes to the initial power level drop.

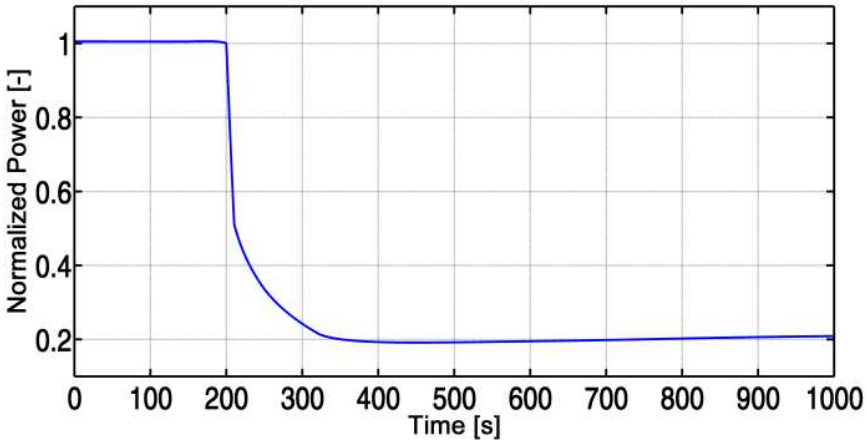

Figure A7. Normalized thermal power vs. time.

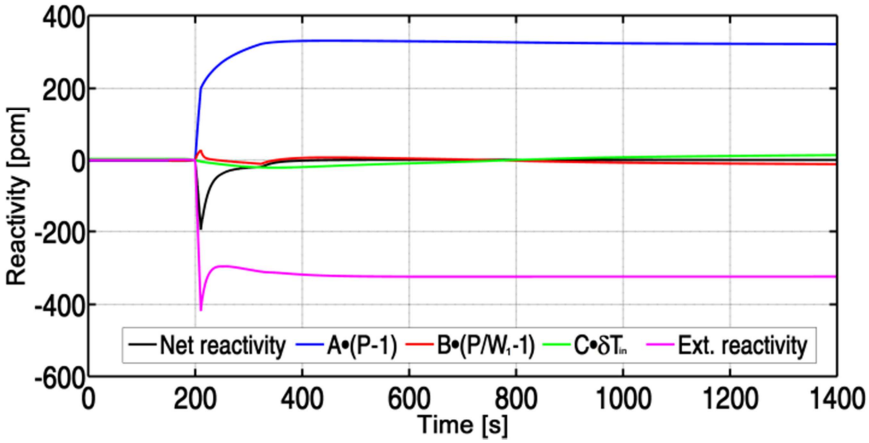

Figure A8. Reactivity contribution vs. time.

As shown in Figure A9, at the end of the transient, the system reaches an equilibrium condition in which the reactor coolant inlet temperature is slightly lower than the nominal one. On the other hand, thanks to the changes of the primary circuit flow rate, the sodium temperature at the core outlet can be effectively governed. Indeed, the conditions in the upper plenum, aside from an initial overshoot, are almost unaltered when the normalized power level of 0.2 is reached.

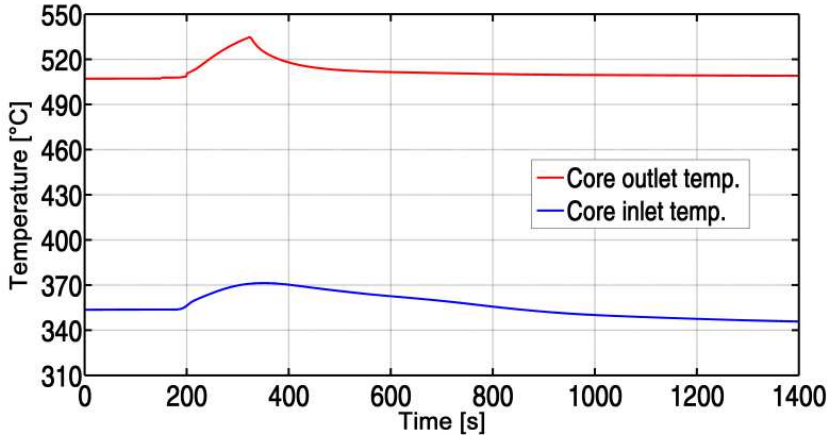

Figure A9. Sodium temperatures in the primary circuit vs. time.

For the negative reactivity insertion due to the $C \cdot \delta T_{in}$ term to become relevant, the primary coolant temperature would have to rise to values incompatible with the reactor safe operation and integrity. Therefore, since the reactor coolant inlet temperature increase does not result in substantial benefit for the control rods operation, the $B \cdot (P/W_1 - 1)$ term has been optimized. In order to get the desired trend of the output variables, the minimum value for the primary circuit mass flow rate has been set equal to 20% and at final steady state conditions the reactivity contribution due to the power over flow ratio vanishes. In addition, by setting the intermediate circuit mass flow rate proportional to the primary one (Figure A10), it would be possible to preserve the nominal temperature variations in the two circuits throughout the transient.

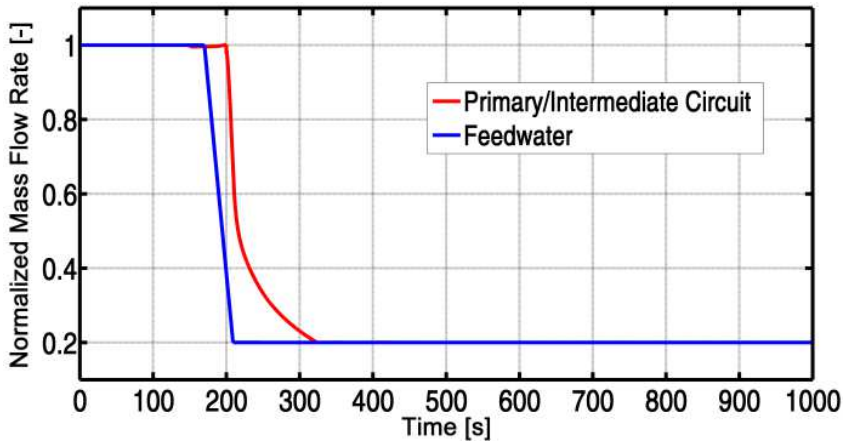

Figure A10. Primary/Intermediate circuit and feedwater mass flow rates vs. time.

In conclusion, in an oxide-fuelled core, because of the constraints on the temperature field and the values of the integral reactivity parameters, the net reactivity decrement contribution can be counterbalanced only by means of active control elements. As far as the other reactivity contributions, it is important to optimize the $B \cdot (P/W_1 - 1)$ term, keeping its value close to zero, thanks to the coordinated control actions of the control rods and the primary circuit mass flow rate. Since the sodium condition at the core inlet cannot provide a relevant contribution to the reactivity

balance, it is judged better to minimize its change to reduce thermal stresses during the transient by minimizing temperature swings across the sensitive components.

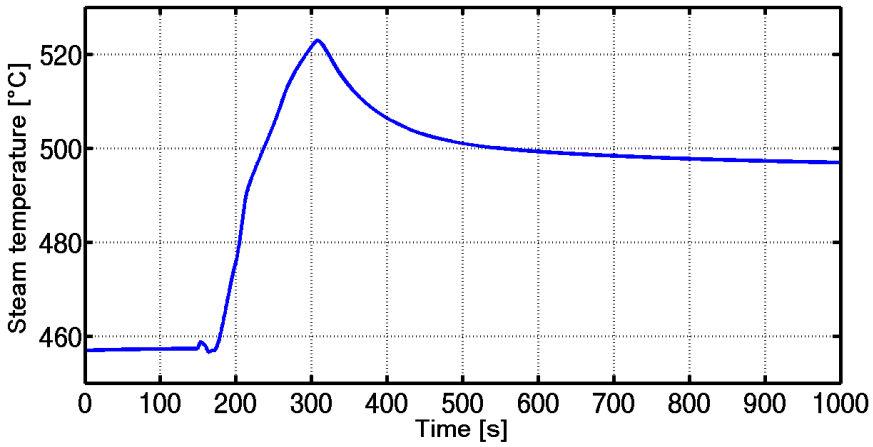

Figure A11. Steam temperature vs time.

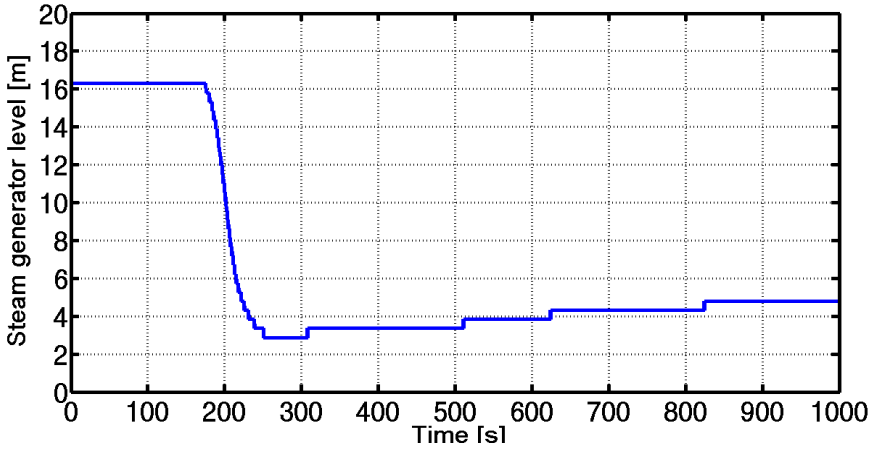

Figure A12. Steam generator level vs time.

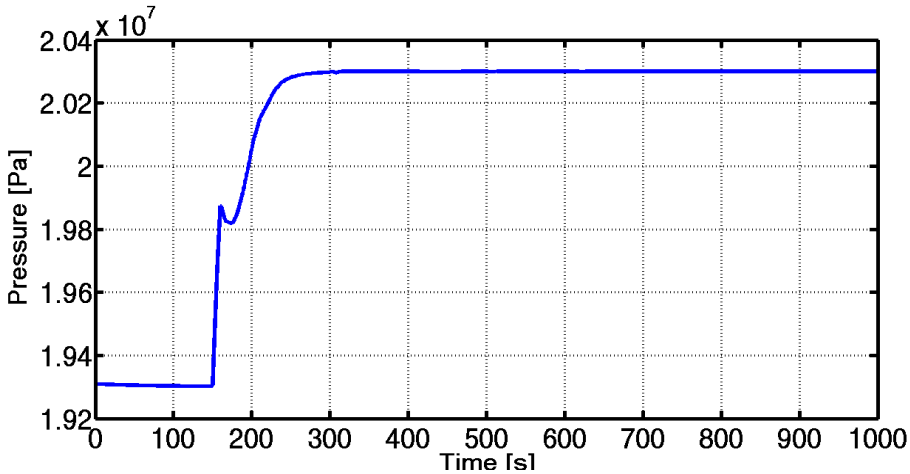

Figure A13. Steam generator pressure vs time.

As far as the BoP quantities of interest are concerned, during the transient, the temperature in the SG increases (Figure A11) and the SG level decreases (Figure A12). In the proposed control strategy, the SG is allowed for an overpressure (Figure A13). Differently from the U-tubes design,

the reference SG concept is characterized by a reduced thermal capacitance, and the adoption of the bypass way is necessary to dispose the excessive thermal power which cannot be admitted to the turbine neither stored in the SG itself. In order to limit the overshoot in the mass flow rate which must be vented to the condenser, the system during this operational transient is operated at a pressure 5% higher than the nominal one. Though the feedwater mass flow rate reduction started simultaneously with the turbine admission valve closure, the peak could not be prevented, because the feedwater pump is characterized by a time constant such that it takes about 40 s to reduce the feedwater mass flow rate to the 20% of its nominal value. In addition, because of the length of the SG, the mass flow rate variation signal takes at least 10 seconds to reach the turbine admission. For these reasons, it could be worthy using pressure relief valves in order to dispose directly into the environment the steam flow that is not required to meet the demands of the house loads, and limit stresses to the condenser.

A6. Metal-fuelled reactor simulation results

As far as the metal-fuelled reactor configuration is concerned, even though the values of B and C are virtually unchanged, there is a dramatic difference in the value of A between oxide and metal core designs. Therefore, in this case, the relative sizes of the feedbacks results in a net cancellation of most of the net reactivity decrement during the power drop, significantly reducing the need for negative reactivity addition through control rods.

Table A8. Adopted MPC parameters, for the metal-fuelled configuration

Parameter	Value
Time step, T_s	0.1 s
Prediction horizon, *N*	60 s
Control horizon, *M*	20 s
Weight of the tracking error, *Q(i)*	[36, 0.4]
Weight of the control input variations, *R(i)*	[0.5, 6]
Weight of the control input absolute values, *S(i)*	[12, 2]

Even though the MPC controller weights are not so different from the ones adopted in the oxide-fuelled configuration, the metal-fuelled design turns out to be particularly flexible in terms of operation, i.e. the system fast runback can be achieved in about one minute (Figure A14). Such favourable behaviour is due to the fact that the positive reactivity to be counterbalanced is quite modest and that since the very beginning the thermal feedbacks provide a relevant contribution to the reactivity balance. Overall, this approach leads to temperatures increase in the primary circuit. In particular, the sodium temperature in the hot leg increases by about 25 °C (Figure A15). Indeed,

since the power drop takes place so promptly, the primary circuit mass flow rate must be reduced even faster to provide a negative reactivity contribution (Figure A16), causing a sudden rise in the sodium temperature at the core outlet (Figure A17).

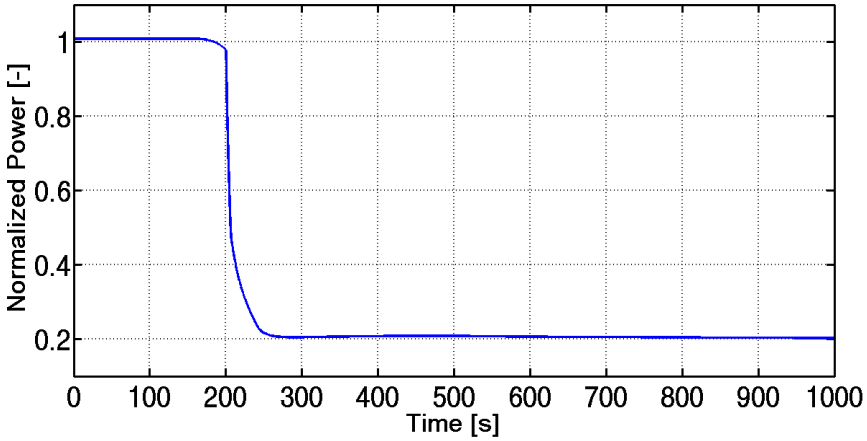

Figure A14. Normalized thermal power vs. time.

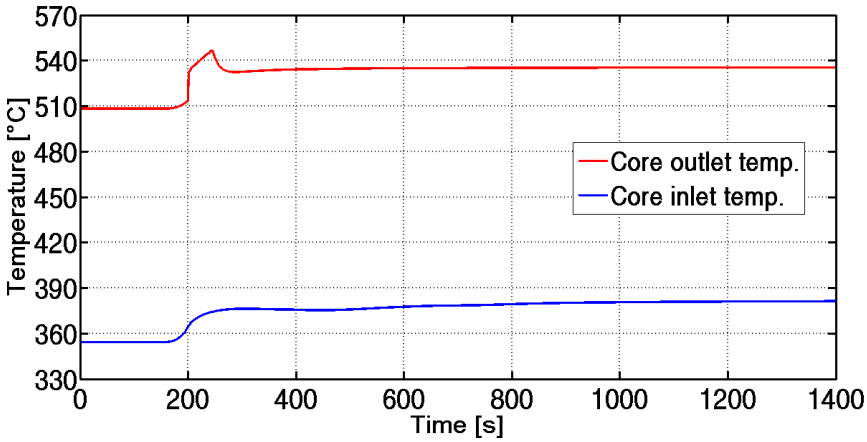

Figure A15. Sodium temperatures in the primary circuit vs. time.

It should be noted that the control strategy has been slightly changed in comparison to the oxide-fuelled configuration, i.e. the feedwater mass flow rate reduction starts earlier than in the previous case in order to result in a more relevant overall temperature rise in the primary circuit. In addition, the feedwater mass flow rate minimum threshold has been set to a lower value than in the previous control scheme.

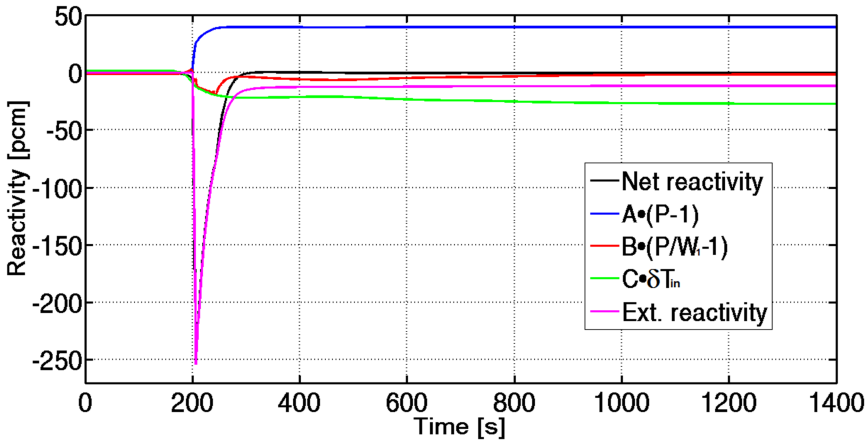

Figure A16. Reactivity contribution vs. time.

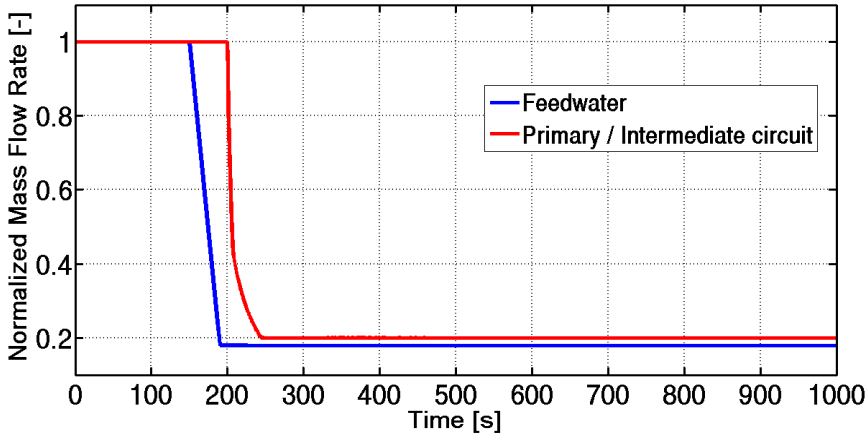

Figure A17. Primary, Intermediate circuit and feedwater normalized mass flow rates vs. time.

Figure A18, Figure A19 and Figure A20 show the quantities of interest for the BoP. As can be seen, the trends are qualitatively similar. The only difference is that, by relying more on temperature effects to achieve also reactivity control in the metal fuel configuration, also the steam temperature at the exit of the steam generator increases compared to the oxide case. In addition, the reduced feedwater mass flow rate contributes to the steam temperature increase and to the reduction of the steam generator level during the transient as well.

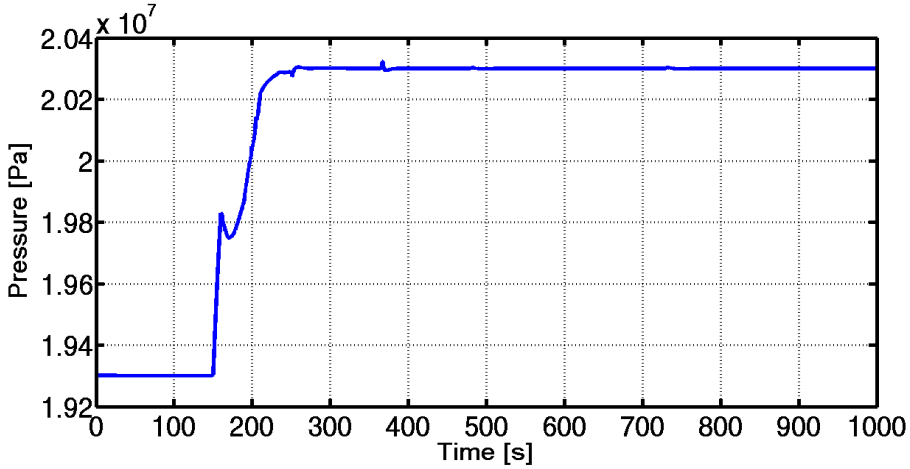

Figure A18. Steam generator pressure vs time.

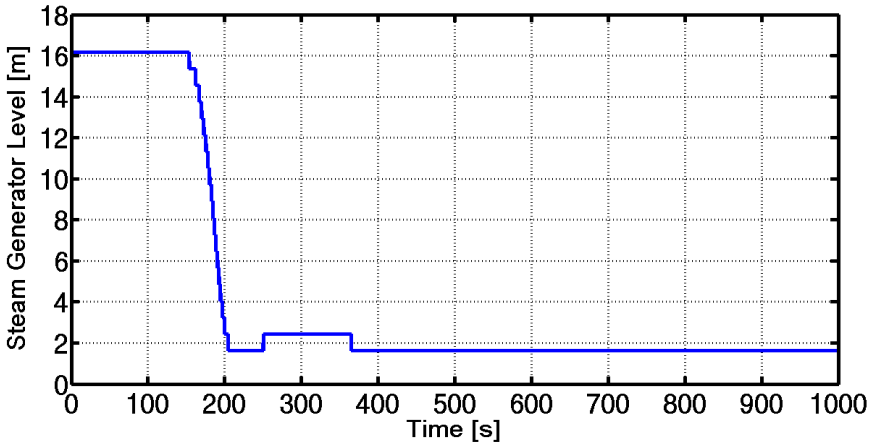

Figure A19. Steam generator level vs time.

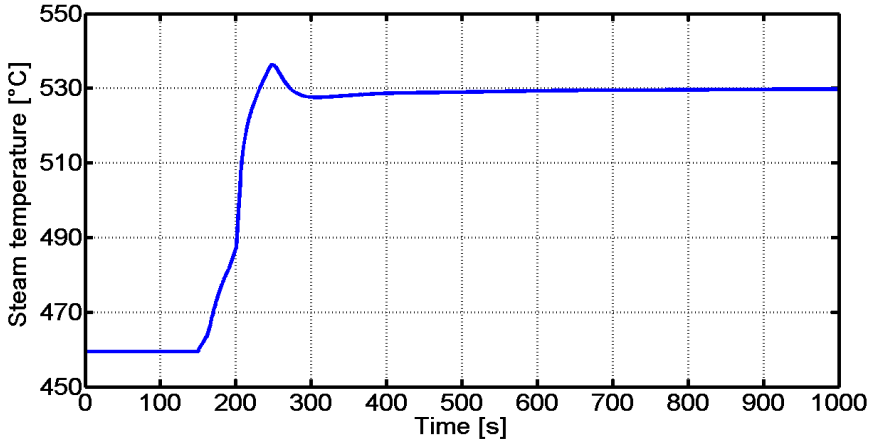

Figure A20. Steam temperature vs time.

Concluding remarks

In this Appendix, the development and the assessment of a suitable strategy to perform the fast runback of a sodium-cooled SMR from operating conditions to reduced power output has been presented. Since this transient involves several components of the plant, the control actions to be taken must be properly coordinated so as to achieve the power drop by exploiting the reactivity feedbacks without exceeding the design limits of the sensitive components. For this reason, in order to perform the power transient while ensuring that the sodium temperature in the upper plenum does not undergo sudden changes, MPC-based controller has been developed in order to optimize the operation of the control rods and primary circuit flow rate. The proposed strategy has been assessed by simulating the plant response by means of an object-oriented model, allowing for the study of the system governing dynamics. In particular, two different reactor configurations have been analysed, i.e., oxide-fuelled core and metal-fuelled core. In the former, because of the constraints on the temperature field and the values of the integral reactivity parameters, the positive reactivity inserted during the power drop can be counterbalanced only by means of a relevant control rods contribution. On the contrary, for the metal fuel case, the reactivity feedbacks assume a higher

relative importance, and a sensibly smaller control rods contribution is needed during the operational transient.

Acronyms

ALFRED	Advanced Lead-cooled Fast Reactor European Demonstrator
ANL	Argonne National Laboratory
BoC	Begin of Cycle
BoL	Begin of Life
BoP	Balance of Plant
CANDU	CANadian Deuterium Uranium
CRs	Control Rods
DAE	Differential and Algebraic Equation
DES	Discrete Event System
DOE	Department of Energy
EA	Empresarios Agrupados
EoC	End of Cycle
FA	Fuel Assembly
FP7	7^{th} Framework Program
FSM	Finite State Machine
HP	High Pressure stages
HV	High Voltage
ICN	Institute de Cercetari Nucleare
ICT	Information and Communication Technology
I&C	Instrumentation and Control
IHX	Intermediate Heat Exchanger
LEADER	Lead-cooled European Advanced DEmostration Reactor
LFR	Lead-cooled Fast Reactor
LP	Low Pressure stages
LTI	Linear Time Invariant
LWR	Light Water Reactor
MIMO	Multi Input Multi Output
MM	Modal Method
MOX	Mixed-Oxide fuel
MPC	Model-based Predictive Controller
MV	Medium Voltage
NPP	Nuclear Power Plant
NRG	Non square Relative Gain array
NSSS	Nuclear Steam Supply System
O&M	Operation and maintenance
ODE	Ordinary Differential Equation
P	Proportional (controller)
PI	Proportional-Integral (controller)
PID	Proportional-Integral-Derivative (controller)
PWR	Pressurized Water Reactor
RES	Renewable Energy Sources
RGA	Relative Gain Array
RS	Row Sum
SFR	Sodium Fast Reactor
SMR	Small Modular Reactor
SG	Steam Generator
SISO	Single Input Single Output
SRs	Safety Rods
UCTE	Union for the Coordination of Transport of Electricity
ULOF	Unprotected Loss of Flow
UTOP	Unprotected Transient of OverPower

Nomenclature

Latin symbol

$\otimes$	Schur product
A	Single channel coolant flow area [m^2]
$\underline{A}$	State matrix
A(s)	Overall transfer function
A_{CR}	Coefficient for CRs calibration [pcm]
A_{SR}	Coefficient for SRs calibration [pcm]
A_v	Flow area [m^2]
A_u	Actuator response
$\underline{B}$	Corresponding matrix
B_{CR}	Coefficient for CRs calibration [m^{-1}]
$\underline{C}$	Corresponding matrix
c	Average specific isobaric heat [J kg^{-1} K^{-1}]
C_{CR}	Coefficient for CRs calibration [-]
C_f	Fanning friction coefficient [-]
c_i	i^{th} precursor density [cm^{-3}]
c_p	Average specific isobaric heat of lead [J kg^{-1} K^{-1}]
$\underline{D}$	Feedthrough matrix
d	Density [kg m^{-3}]
D_{CR}	Coefficient for CRs calibration [pcm]
d_i	Disturbances from i-th control loop
e	Error in PI control loop
e_i	Error between y_i^{ref} and y_i
E	Energy [J]
f	Friction factor [-]
f_0	Nominal frequency [Hz]
F(s)	Complementary sensitivity transfer function
g	Gravitational acceleration [m s^{-2}]
G	Gain
G(s)	Process transfer function
G_{att}	Attemperator mass flow rate [kg s^{-1}]
g_{ji}	Open loop gain between j-th output and i-th input
G_{water}	Feedwater mass flow rate [kg s^{-1}]
h	Specific enthalpy [J kg^{-1}]
H(s)	Cross transfer function
h_{cl}	Cladding-coolant global heat transfer coefficient [W K^{-1}]
h_{CR}	Control rods height [m]
h_{ji}	Closed loop gain of pair j-th output and i-th input
h_{SR}	Safety rods height [m]
j	Complex variable
J	Moment of inertia [kg m^2]
K_d	Derivative regulator parameter
K_i	Integral regulator parameter
K_p	Proportional regulator parameter
K_{safety}	Safety coefficient
K	Pressure coefficient [m^{-2} s^{-2}]
k	Thermal conductivity [W m^{-1} K^{-1}]
K_D	Doppler constant [pcm]
K_{eq}	Equivalent exchange unit [W K^{-1}]
k_{fc}	Fuel-gap-cladding global heat transfer coefficient [W K^{-1}]
k_v	Turbine admission valve coefficient [m s]
L_{SR}	Total length of SRs [m]
L(s)	Loop transfer function

M	Mass [kg]
n	Neutron density [n cm^{-3}]
N_p	Number of polarities [-]
p	Pressure [Pa]
P_{core}	Thermal core power [W]
P_n	Nominal power [W]
q	Reactor thermal power [MW]
q'''	Thermal power density [W m^{-3}]
Q_c	Thermal power exchanged in the SGs [W]
Q_{ml}	Thermal power stored in the SG wall [W]
r	Radial coordinate [m]
$R(s)$	Regulator transfer function
Re	Reynolds number [-]
s	Laplace-transform variable [s^{-1}]
S	Neutron source [cm^{-3} s]
$S(s)$	Sensitivity transfer function
t	Time coordinate [s]
T	Average temperature [°C]
T_a	Actuator time constant [s]
T_{alt}	Alternator start-up time [s]
T_i	Integral time constant [s]
T_L	Laub transformation matrix
u	Input vector
u^*	Controller action
u_i	i^{th} input variable
u_x	Fluid velocity [m s^{-1}]
v_{ext}	CRs extraction speed [m s^{-1}]
w	Mass flow rate [kg s^{-1}]
x	State vector
x_s	Axial coordinate [m]
x_c	Critical ratio [-]
x_{CR}	Axial position of CRs [m]
x_{SR}	Height of SRs at full power [m]
y	output vector
y_i	i^{th} output variable
y_i^{ref}	Set-point of the i-th control loop
z	Elevation [m]

Greek symbol

α_{CR}	Radial cladding expansion coefficient [pcm K^{-1}]
α_{CZ}	Axial cladding expansion coefficient [pcm K^{-1}]
α_D	Doppler reactivity feedback coefficient [pcm K^{-1}]
α_{Dia}	Diagrid expansion coefficient [pcm K^{-1}]
α_{FZ}	Axial fuel expansion feedback coefficient [pcm K^{-1}]
α_H	Control rod reactivity feedback coefficient [pcm m^{-1}]
α_L	Coolant density reactivity feedback coefficient [pcm K^{-1}]
α_{Pad}	Pad expansion coefficient [pcm K^{-1}]
α_R	Radial expansion reactivity feedback coefficient [pcm K^{-1}]
α_{WR}	Radial wrapper expansion coefficient [pcm K^{-1}]
α_{WZ}	Axial wrapper expansion coefficient [pcm K^{-1}]
α_Z	Axial expansion reactivity feedback coefficient [pcm K^{-1}]
β	Total delayed neutron fraction [pcm]
β_i	i^{th} precursor group delayed-neutron fraction [pcm]
Δf	Frequency variation [Hz]
Δh	Enthalpy drop along the SG [J kg^{-1} K^{-1}]
ΔP	Power variation [W]

η	Rankine cycle efficiency [-]
Λ	Invariant neutron average lifetime [s]
Λ_{rg}	Matrix of relative gain
λ	Mean precursor decay constant [s^{-1}]
λ_c	Coefficient of discharge [-]
λ_i	i^{th} precursor decay constant [s^{-1}]
λ_{ji}	Relative gain of pair j-th output and i-th input
μ	Static gain
μ_v	Constant pressure parameter [J m^{-1} s^{-2}]
Π_e	Power absorbed by the loads [W]
Π_{is}	Iso-entropic enthalpy drop [W]
Π_m	Mechanical power [W]
ρ	Reactivity [pcm]
ρ_0	Reactivity margin stored in the core [pcm]
Σ	System desired behaviour
σ_i	Droop [-]
τ	Time constant [s]
τ^*	Reactor period [s]
τ_{CL}	Time delay in cold pool [s]
τ_{HL}	Time delay in hot leg [s]
τ_i	Derivative time constant [s]
τ_{SG}	Time delay in steam generator [s]
φ	Heat flux entering the tube (lateral surface) [W m^{-2}]
φ_m	Phase margin [°]
ω_t	Tube perimeter [m]
ω	Angular frequency [rad s^{-1}]
Ω	Turbo alternator rotational speed [rad s^{-1}]

Superscripts/Subscripts

†	Moore-Penrose pseudo-inverse
0	Steady-state
c	Cladding
CL	Closed Loop
D	Doppler
down	Downstream
eff	Effective
eq	Equivalent
ext	External
f	Fuel
in	Inlet
int	Internal
l	Lead coolant
m	Mechanical
OL	Open Loop
out	Outlet
rods	Control rods
s	Steam
sat	Saturation
sg	Steam generator
ss	Superheated steam
sv	Saturated vapour
t	Total
T	Matrix transposition
temp	Reactivity feedback due to thermal effect
up	Upstream
v	Vapour

References

- Advanced Small Modular Reactors, Office of Nuclear Energy, US Department of Energy (DOE), Energy.gov, November 2013.
- Alemberti, A., Carlsson, J., Malambu, E., Orden, A., Cinotti, L., Struwe, D., Agostini, P., Monti, S., 2010. *From ELSY to LEADER - European LFR Activities*. Transactions of the American Nuclear Society, European Nuclear Conference 2010, Barcelona, Spain, May 30 - June 2, 2010.
- Alemberti, A., Frogheri, M., Mansani, L., 2013. *The Lead fast reactor Demonstrator (ALFRED) and ELFR design.* Proceedings of the International Conference on Fast Reactors and related Fuel Cycles: Safe Technologies and Sustainable Scenarios (FR 13), Paris, France, March 4-7, 2013.
- Artioli, C., Grasso, G., Petrovich, C., 2010. *A new paradigm solution for core design aimed at the sustainability of nuclear energy: The solution of the extended equilibrium state*. In: Annals of Nuclear Energy, **37**, 915-922.
- Åström, K.J., Hägglund, T., 1995. *PID Controllers: Theory, Design and Tuning*. Instrument Society of America, Research Triangle Park, NC, USA.
- Bernard, J.A., 1999. *Light Water Reactor Control Systems*. In: Webster, J.G., Ed., Wiley Encyclopedia of Electrical and Electronics Engineering. New York, NY, USA.
- Bragg-Sitton, S. M., Holloway, J. P., 2006. *Autonomous reactor control using model based predictive control for space propulsion applications*. In: Annals of Nuclear Energy, **33**, 1368-1378.
- Brenan, K.E., Campbell, S.L., Petzold, L.R., 1989. *Numerical solution of initial-value problems in differential algebraic equations.* North-Holland Ed.
- Bristol, E. H., 1966. *On a new measure of interaction of multivariable process control*. IEEE Transactions on Automatic Control, **11**, 133-134.
- Cammi, A., Casella, F., Ricotti, M.E., Schiavo, F., 2005. *Object-Oriented Modelling, Simulation and Control of IRIS Nuclear Power Plant with Modelica*. Proceedings of the 4th International Modelica Conference, Hamburg, Germany, March 7-8, 2005.
- Cammi, A., Casella, F., L. Luzzi, A. Milano, M.E. Ricotti, 2008. *A Model Predictive Control Approach for the Italian LBE-XADS*. In: Journal of Nuclear Materials, **376**, 297-301.
- Cammi, A., Luzzi, L., 2008. Innovative Techniques for the Simulation and Control of Nuclear Power Plants. In: Durelle, V.B., Ed., Nuclear Energy Research Progress. Nova Science Publishers, Inc., Hauppauge, NY.
- Casella, F., Leva, A., 2006. *Modeling of thermo-hydraulic power generation processes using Modelica*. In: Mathematical and Computer Modeling of Dynamical Systems, **12**, 19-33.
- Chang, J.-W., Yu, C.-C., 1990. *The Relative Gain for Non-Square Multivariable Systems*. Chemical Engineering Science, **45**, 1309-1323.
- Cheng, X., Tak, N.-i., 2006. *Investigation on Turbulent Heat Transfer to Lead-Bismuth Eutectic Flows in Circular Tubes for Nuclear Applications*. In: Nuclear Engineering and Design, **236**, 385-393.
- Clarke, D.W., 1994. *Advances in model-based predictive control*. Oxford University Press, New York.
- Clayton, D., Wood, R., 2010. *The role of Instrumentation and Control technology in enabling deployment of Small Modular Reactors.* Seventh American Nuclear Society International Topical Meeting on Nuclear Plant Instrumentation, Control and Human-Machine Interface Technologies, NPIC&HMIT 2010, Las Vegas, Nevada, November 7-11, 2010.
- Damiani, L., Montecucco, M., Pini Prato, A., 2013. *Conceptual design of a bayonet tube steam generator for the ALFRED lead-cooled reactor*. Nuclear Engineering and Design, **265**, 154-163.
- Dolezal, R., Varcop, L., 1970. *Process Dynamics: Automatic Control of Steam Generation Plant*. Elsevier Science.
- Duderstadt, J.J., Hamilton, L.J., 1976. *Nuclear Reactor Analysis*. John Wiley and Sons, New York.

- DYNASIM, 2006. Dymola Version 6.1. Dynasim AB. Lund, Sweden, http://www.dynasim.se.
- Empresarios Agrupados, 2012. Private Communication.
- ENTSOE, 2013. *Network Code for Requirements for Grid Connection Applicable to all Generators.*
- Fritzson, P., 2004. *Principles of Object-Oriented Modeling and Simulation with Modelica 2.1*. Wiley-IEEE Press.
- Fritzson, P., 2011. A cyber-physical modeling language and the OpenModelica environment. 7th International Wireless Communications and Mobile Computing Conference (IWCMC), Istanbul, Turkey, July 4-8, 2011.
- GIF, 2002. *A Technology Roadmap for Generation IV Nuclear Energy Systems*. Technical Report GIF-002-00.
- Grasso, G., Petrovich, C., Mikityuk, K., Mattioli, D., Manni, F., Gugiu, D., 2013. *Demonstrating the effectiveness of the European LFR concept: the ALFRED core design*. Proceedings of the International Conference on Fast Reactors and related Fuel Cycles: Safe Technologies and Sustainable Scenarios (FR 13), Paris, France, March 4-7, 2013.
- Guerrieri, C., Cammi, A., Luzzi, L., 2014. *A preliminary approach to the MSFR control issues*. Annals of Nuclear Energy, **64**, 472-484.
- Guidez, J., 2013. *Phenix, The feedback experience*. EDP sciences.
- Hetrick, D.L., 1971. *Dynamics of Nuclear Reactors*. University of Chicago Press,Chicago.
- Holcomb, D. E., 2013. *Advanced Small Modular Reactor R&D Program: Instrumentation, Controls, and Human-Machine Interface. Technical Meeting on Instrumentations and Control in Advanced SMRs*, IAEA, Vienna, Austria, May 21-24, 2013.
- Hopcroft, J. E., Motwani, R., Ullman, J. D., 2008. *Introduction to Automata Theory, Languages, and Computation.* Pearson Education, 3rd ed.
- IEEE Std 610.12-1990, 1990. *Standard Glossary of Software Engineering Terminology*.
- Jesionek, K. J., 2001. *Method of increasing steam turbine control stage efficiency*. In: Journal of Computational and Applied Mechanics, **2**, 37-43.
- Kozlowski, T., Downar, T.J., 2007. *PWR MOX/UO2 Core Transient Benchmark. Working Party on Scientific Issues of Reactor Systems*. Nuclear Science NEA/ NSC/DOC(2006)20, ISBN 92-64-02330-5.
- Kundur, P., 1994. *Power System Stability and Control*. McGraw-Hill Education.
- Laub, A.J., Heath, M.T., Paige, C.C., Ward, R.C., 1987. *Computation of System Balancing Transformations and Other Applications of Simultaneous Diagonalization Algorithms*. IEEE Transactions Automatic Control AC-32, 115-122.
- Levine, W. S., 1996. *The Control Handbook*. IEEE Press.
- Lyapunov, A.M., 1966. *The Stability of Motion*. Academic Press, New York and London.
- Lorenzi, S., 2011. *Development of a Control-oriented Simulator for a Lead-cooled Fast Reactor Demonstrator.* MSc. Thesis in Nuclear Engineering, Politecnico di Milano, Italy.
- Marconato, R., 2004. *Electric Power Systems, Volume 2, Steady State Behaviour, Controls, Short Circuits and Protection Systems. Second Edition,* CEI – Italian Electrotechnical Committee.
- MATLAB® and SIMULINK® software, 2005. The MathWorks, Inc.
- Measurement of the utility frequency, 2014. http://www.mainsfrequency.com/verlauf_en.htm.
- Miller, T., 2013. *DOE Strategic Vision for Small Modular Reactors.* IAEA Technical Working Group on Advanced Technologies for Light Water Reactors, IAEA, Vienna, Austria, 20 June 2013.
- Modelica, 2011. http://www.modelica.org.
- Moore, B.C., 1981. *Principal component analysis in linear systems: controllability, observability, and model reduction*. IEEE Transactions on Automatic Control AC-26 (1), 17-32.
- Na, M. G., Shin, S. H., Kim, W. C., 2003. *A model predictive controller for nuclear reactor power*. In: Journal of the Korean Nuclear Society, **35**, 399-411.

- OECD-NEA, 2007. *Handbook on Lead-bismuth Eutectic Alloy and Lead Properties, Materials Compatibility. Thermal Hydraulics and Technologies, No. 6195*.
- Papadourakis, A., Doherty, M.F., Douglas, J.M., 1987. *Relative gain array for units in plants with recycle*. Industrial & Engineering Chemistry Research 26 (6), 1259-1262.
- Peterson, J. L., 1981. *Petri Net Theory and the modelling of the systems*, Prentice Hall.
- Petzold, L.R., 1982. *A Description of DASSL: A Differential/Algebraic System Solver*. Proceedings of the 10th IMACS World Congress, Montreal, August 8-13, 1982.
- Schultz, M.A., 1961. *Nuclear reactor kinetics and control*. McGraw-Hill.
- Sciora, P., 2011. Private communication.
- Sciora, P., Blanchet, D., Buiron, L., Fontaine, B., Vanier, M., Varaine, F., Venard, C., 2013. *Low void effect core design applied on 2400MWth SFR reactor*. Proceedings of the International Conference on Fast Reactors and related Fuel Cycles: Safe Technologies and Sustainable Scenarios (FR 13), Paris, France, March 4-7, 2013.
- Seong, S. H., Kim, S. O,. *Performance evaluation of control strategies for power manoeuvring event of the KALIMER-600*. In: Annals of Nuclear Energy, **42**, 50-62, 2012.
- Skogestad, S., Postlethwaite, I., 2005. *Multivariable Feedback Control: Analysis and Design*. John Wiley and Sons, New York, USA.
- Souyri, A., Bouskela, D., Pentori, B., Kerkar, N., 2006. *Pressurized Water Reactor Modelling with Modelica*. Proceedings of the 5th International Modelica Conference, Vienna, Austria, September 4-5, 2006.
- Sterpu, S., 2009. *Power System Dynamic Performance: Primary Governing Frequency Response*. Proceedings of the IEEE Bucharest Power Tech Conference, June 28th - July 2nd, Bucharest, Romania.
- Todreas, N., Kazimi, M.S., 2012. *Nuclear Systems – Thermal Hydraulic Fundamentals, vol. 1*. CRC Press, 2nd edition.
- Tucek, K., Carlsson, J., Wider, H., 2006. *Comparison of sodium and lead-cooled fast reactors regarding reactor physics aspects, severe safety and economic issues*. In: Nuclear Engineering and Design, **236**,1589-1598.
- Van Dooren, P., 2000. *Gramian Based Model Reduction of Large-Scale Dynamical Systems*. In: Watson, G.A, Griffiths, D.F. (Eds.), Numerical Analysis 1999. Chapman & Hall/CRC Research Notes in Mathematics Series, London, 231-247.
- Vilim, R. B., 2013. Personal communication, Argonne National Laboratory (ANL).
- Wade, D.C., Fujita, E.K., 1988. *Trends Versus Reactor Size of Passive Reactivity Shutdown and Control Performance*. In: Nuclear Science and Engineering, **103**, 182.
- Waltar, A.E., Todd, D.R., Tsvetkov, P.V., 2011. *Fast Spectrum Reactors*. Springer, New York, ISBN 978-1-4419-9571-1.
- Wigeland, R., Cahalan, J., 2009. *Fast Reactor Fuel Type and Reactor Safety Performance*. Proceedings of Global 2009, Paris, France, September 6-11, 2009.